

# Other Contributions

# **American Meteorological Society**



## **2002 Annual Meeting**

**January 13-17**  
**Orlando, FL**

## **P1.6 MODIS RADIANCES AND REFLECTANCES FOR EARTH SYSTEM SCIENCE STUDIES AND ENVIRONMENTAL APPLICATIONS**

S. P. Ahmad \*, V. V. Salomonson, W. L. Barnes, X. Xiong, G. G. Leptoukh, and G. N. Serafino

NASA Goddard Space Flight Center, Greenbelt, Maryland

### **1. Introduction**

The Moderate Resolution Imaging Spectroradiometer (MODIS), a major component of NASA's Earth Observing System (EOS), was designed to provide improved long-term global observations of land, ocean and atmosphere features relative to "heritage sensors". MODIS was launched aboard the Terra satellite on December 18, 1999 (10:30 am equator crossing time, descending node, Sun-synchronous near polar orbit). MODIS with its 2330 km viewing swath width provides almost daily global coverage. It acquires data in 36 high spectral resolution bands between 0.415 and 14.235 microns with spatial resolutions of 250 m (2 bands), 500 m (5 bands), and 1000 m (29 bands). This year a similar instrument will be flown on the EOS-Aqua satellite (1:30 pm equator crossing time, ascending node). This will enable studies of the diurnal variation of rapidly varying systems. The radiance data measured by MODIS with some new channels (never used before for remote sensing from space) provides improved information about the physical structure of the Earth system. Measured raw sensor counts, radiometrically calibrated and geolocated radiances along with derived atmosphere and ocean data are archived (Ahmad et al. 2002) at the NASA Goddard Earth Sciences (GES) Distributed Active Archive Center (DAAC). These products and other MODIS derived products archived at other NASA centers are made freely available to the public and scientific community.

The purpose of this presentation is to provide key characteristics of the MODIS radiance and reflectance products (referred to as the Level 1B product) with some examples of applications of the MODIS radiances in detecting human impacts on the earth and its climate and how this data is used in improving the predictions and characterization of natural disasters such as wild fires, volcanoes, floods and drought.

### **2. MODIS Instrument**

MODIS, a cross-track scanning radiometer, provides high spectral resolution data from 36 bands with center wavelengths ranging from 0.412 to 14.235 microns (Barnes et al. 1998). MODIS spectral band passes are shown in Table 1. MODIS carries 490 detectors that are aligned in parallel rows on four separate focal planes (Visible, NIR, SWIR/MWIR, and LWIR).

The number of detectors per band are 10 for 1000 m, 20 for 500 m, and 40 for 250 m spatial resolution bands. In addition, 2 of the 1000 m spatial resolution bands

provide measurements for the same scenes at two gains, 13 L and 14L at low gains for measuring bright scenes and 13H and 14H at high gains for measuring dark ocean scenes.

The instrument's 110 degree field of view is swept over the focal planes by the double sided rotating scan mirror. Each mirror rotation provides two scans (one for each mirror side). The scan period is 1.477 sec. During each scan, 5 view sectors (solar diffuser, spectral radiometric calibration assembly, blackbody, space, and earth view) are observed. The 110 degree-wide instrument field of view sweeps out a ground swath approximately 2330 km wide during the 0.451 seconds of earth view. The ground swath ( $\pm 55$  deg viewing angles relative to nadir) exhibits significant earth curvature effects. The 55 degree scan angle increases to approximately 65 degree due to earth curvature. In addition, ground resolution increases with scan angle.

### **7. Summary**

The strengths of MODIS include its global coverage, high radiometric resolution, appropriate dynamic ranges, and accurate calibration in reflective and thermal infrared bands designed for retrievals of atmospheric, land and sea surface properties. Almost 40 higher level science standard products are being produced from MODIS Level 1B radiance data. Even though data validation activities are still in progress, the provisional radiometrically calibrated radiances and reflectances, and derived products (version-3) show very fine details and exceed the expectations when compared to in-situ observations. Almost one year of consistent data processed with an improved calibration algorithm (version-3), will soon be made available to the public and science user community. These high radiometric accuracy measurements can be used by the scientific community to detect subtle signatures of climate change, study regional and global phenomena, and for prediction and characterization of natural disasters such as wild fires, volcanoes, floods and drought. MODIS radiance counts, calibrated radiance and reflectance, geolocation products, and all derived geophysical atmospheric & ocean products are archived at the Goddard DAAC (<http://daac.gsfc.nasa.gov>). All land products are archived at Earth Resource Observation System (EROS) Data Center (EDC), and snow & ice products are archived at the National Snow and Ice Data Center (NSIDC). MODIS products, ancillary and related data, documents, and data analysis and visualization tools are freely made available to the public and science user community from these data archive centers via NASA EOS Data Gateway (EDG) at <http://eos.nasa.gov/imswelcome>.

\* Corresponding author address: Dr. Suraiya Ahmad,  
NASA/GSFC, Code 902, Greenbelt, MD 20771  
email: [ahmad@daac.gsfc.nasa.gov](mailto:ahmad@daac.gsfc.nasa.gov)

**NASA/TM-2002-210005**

## **SIMBIOS Project 2001 Annual Report**

Giulietta S. Fargion, Science Applications International Corporation, Maryland  
Charles R. McClain, Goddard Space Flight Center, Greenbelt, Maryland

National Aeronautics and  
Space Administration

**Goddard Space Flight Center**  
Greenbelt, Maryland 20771

March 2002



## Chapter 22

# Measurements and modeling of apparent optical properties of ocean waters in support to ocean color data calibration, validation, and merging

David Antoine, André Morel, Marcel Babin and Hervé Claustre

*Laboratoire d'Océanographie de Villefranche, CNRS-INSU, Villefranche sur Mer, France*

Stanford B. Hooker

*NASA/GSFC, Greenbelt, Maryland*

### 22.1 INTRODUCTION

This progress report does not show any results in terms of *in situ* data because the buoy' deployment is only planned for late January 2002. The advancement of the buoy development and testing, of the instrument integration and testing, and of all other preparatory activities (in particular monthly cruises to the deployment site) are succinctly described here. The objectives and the analyses that are planned thanks to the data to be collected are also reminded. This project is supported by the European Space Agency (ESA/ESTEC contract N° 14393/00/NL/DC), the French Space Agency "Centre National d'Etudes Spatiales (CNES)", the "Centre National de la Recherche Scientifique (CNRS-INSU)" and the "Observatoire Océanologique de Villefranche sur mer". A prerequisite to building long-term (over decades) archives of ocean color, in response to the need for assessing the response of the oceanic biota to climate changes, is to accurately calibrate the top-of-atmosphere satellite observations, then to validate the surface geophysical parameters derived from these observations. Ensuring coherence between these geophysical products, as derived from different sensors, is also an important aspect to consider. When ocean color observations from different sensors are considered in view of data merging, their cross-calibration and validation might be facilitated if it could be "anchored" on continuous long-term *in situ* stations (IOCCG, 1999). Deploying and maintaining moorings that operate in a continuous way is, however, a difficult task.

In response to these concerns, we propose to carry out match-up analyses and vicarious calibration experiments, based on a data set to be built from a permanent marine optical buoy. This new type of marine optical buoy has been specifically designed for the acquisition of radiometric quantities, and has been already deployed in the Mediterranean sea in July 2000 (a deployment of 3 months for validating the mooring concept), between France and Corsica.

The vicarious calibration experiments should allow the top-of-atmosphere total radiance to be simulated and compared to the satellite measurements, in particular for the European MERIS sensor. By this way, the need for a change of the pre-flight calibration coefficients for a given sensor might be evaluated, and its amount quantified. From this data set, match-up analyses shall be also possible for chlorophyll concentration and water-leaving radiances, as well as algorithm evaluation (atmospheric correction and pigment retrieval). Because of a certain commonality in the band sets of the new-generation ocean color sensors, the data acquired with the buoy might be used for several of these sensors, and then contribute to the international effort of cross-calibrating them and of cross-validating their products, which are amongst the basic goals of SIMBIOS. In addition, some protocol issues (measurements) are specifically linked to the use of buoys, while others, of general concern to marine optics measurements, may find specific answers in the case buoys are used. We propose to examine these aspects, which, to our knowledge, have not been thoroughly investigated up to now.

#### *Description of the planned analyses*

Two main "vicarious" calibration paths exist to produce ocean color products of the desired accuracy, *i.e.*, water-leaving radiances within an error of about 5% in the blue for an oligotrophic ocean (Gordon, 1997, Antoine and Morel, 1999). The first one is usually referred to as "vicarious calibration", and consists in forcing the satellite-derived water-leaving radiances to agree with a set of *in situ* water-leaving radiances ("match-up analyses"). A set of "vicarious calibration coefficients" is therefore obtained, which is applied to the Top-of-atmosphere (TOA) total radiances measured by the sensor. The second procedure, which is also an indirect ("vicarious") calibration is sometimes referred to as a "radiometric calibration", and consists in simulating the TOA signal that the sensor should measure under certain conditions, and to compare it to the measured signal.

# 2002 IEEE International Geoscience and Remote Sensing Symposium and the 24<sup>th</sup> Canadian Symposium on Remote Sensing



REMOTE SENSING:  
Integrating Our  
View of the Planet



June 24-28, 2002  
Toronto Canada

# IGARSS 2002

# Status of Terra MODIS and Aqua MODIS

William L. Barnes, X. (Jack) Xiong, and Vincent V. Salomonson

NASA/Goddard Space Flight Center

Greenbelt, Maryland

*Abstract-* Launched on December 18, 1999, the MODIS ProtoFlight Model on-board the EOS Terra spacecraft (near sun-synchronous polar orbit, 10:30 am equator crossing time) has been providing the science community global data sets for over two years. The instrument has been performing well on-orbit in terms of its spatial and spectral characterization and radiometric calibration. Many science products have been developed and validated using the MODIS Level 1B calibrated data. To be launched in April 2002, the MODIS Flight Model 1 on the EOS Aqua spacecraft (1:30 pm equator crossing time) will enhance the MODIS products by providing afternoon observations.

## I. Introduction

The MODerate Resolution Imaging Spectroradiometer (MODIS) is the key instrument on NASA's Earth Observing System (EOS) Terra and Aqua spacecraft. The MODIS ProtoFlight Model (PFM) was launched on-board the Terra spacecraft on December 18, 1999 in a near sun-synchronous polar orbit (descending southward, 10:30 am equator crossing time). The instrument nadir door was first opened on February 24, 2000. The instrument has been providing the science community global data sets for over two years. Overall, the instrument has been performing well in terms of its spatial and spectral characterization and radiometric calibration based on the on-orbit observations. Most of the land, oceans, and atmosphere science products developed from the Terra MODIS L1B calibrated data sets have been validated and put in use by a broad user community. In April 2002, MODIS Flight Model 1 (FM1) will be launched on the EOS Aqua spacecraft (ascending northward, 1:30 pm equator crossing time). This new mission will complement the Terra MODIS data sets by providing afternoon observations.

## II. Instrument Overview

MODIS has 36 spectral bands ranging from 0.4-14.5  $\mu\text{m}$ , distributed on four focal plane assemblies (VIS, NIR, SW/MWIR, and LWIR) with nadir spatial resolutions of 250m (bands 1-2), 500m (bands 3-7), and 1000m (bands 8-36). The operating temperature of the two cold FPAs (SW/MWIR, and LWIR) is

controlled by a passive radiative cooler. Using a two-sided scan mirror, the instrument provides a 10 km (nadir) along track by 2330 km cross-track swath every 1.478 seconds. The 20 reflective solar bands (RSB) are spectrally located between 0.4 and 2.1  $\mu\text{m}$ . The wavelengths of 16 thermal emissive bands (TEB) range from 3.75-14.5  $\mu\text{m}$ .

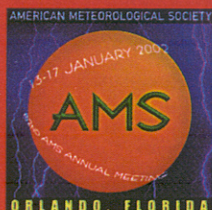
MODIS on-orbit calibrators include a solar diffuser (SD) and a solar diffuser stability monitor (SDSM) for the RSB radiometric calibration, a blackbody (BB) for the TEB radiometric calibration, and a Spectroradiometric Calibration Assembly (SRCA) for spatial and spectral characterization. A detailed description of the MODIS instrument characterization and pre-launch calibration results have been reported by Barnes, Pagano and Salomonson [1].

## V. Summary and Conclusions

In summary, the Terra MODIS is an excellent sensor that has already provided more than 400 terabytes of science data in over 40 global products spanning the period from November 2001 to the present. On-orbit performance has verified the pre-launch tests indicating that the sensor has met all but a very few of the large number of demanding specifications. Test data from the Aqua MODIS promises somewhat better performance than the Terra model. The Aqua satellite is slated for launch in April 2002. The combined data from the AM and PM MODIS should greatly enhance our ability to study the Earth as a system.



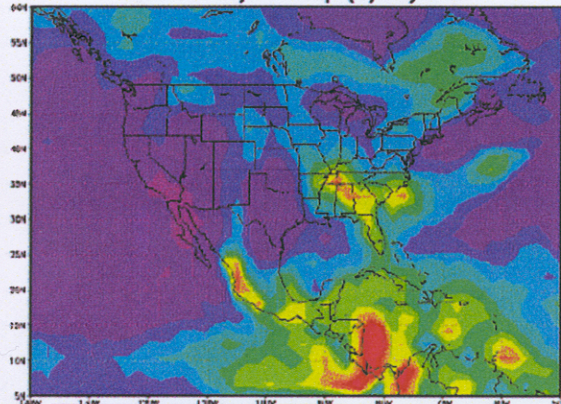
# 16th Conference on Hydrology



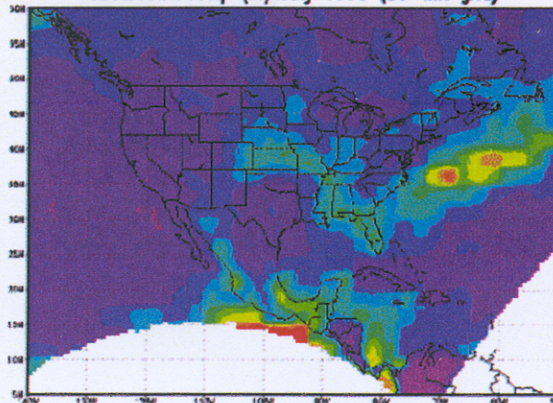
**13–17 January 2002**  
**Orlando, Florida**

## **NCEP Regional Reanalysis Result for July 1998**

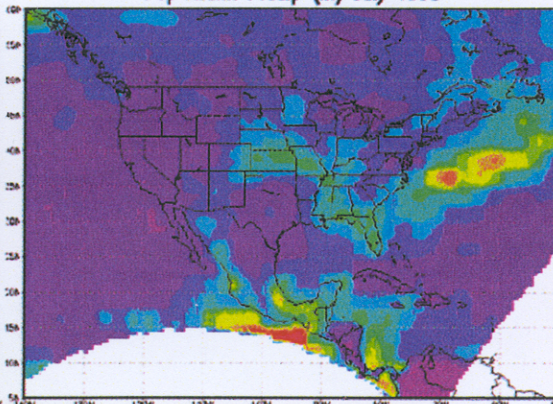
Global Reanalysis Precip (in) July 1998



Observed Precip (in) July 1998 (80-km grid)



Pop Assim Precip (in) July 1998



AMERICAN METEOROLOGICAL SOCIETY



## **J4.5 THE EFFECT OF ERRORS IN SNOW ASSIMILATION ON LAND SURFACE MODELING**

Brian A. Cosgrove<sup>1</sup> and Paul R. Houser<sup>2</sup>

<sup>1</sup>SAIC / Hydrological Sciences Branch & Data Assimilation Office

<sup>2</sup>Hydrological Sciences Branch & Data Assimilation Office  
NASA Goddard Space Flight Center

### **1. INTRODUCTION**

The accurate portrayal of the hydrological cycle is extremely important in land surface modeling. Central to this effort is the treatment of snow, as errors in the representation of this quantity can impact practically all other modeled quantities through alterations in the water and energy balances. Although land surface model (LSM) simulations can benefit from the assimilation of snow cover and snow depth observations, they can be negatively impacted if such observations contain errors or if a model bias exists in the simulation of surface or soil temperatures. Both cases may lead to excessive melting or growth of snow packs, and to large alterations in both the energy and water balances. Such problems in the snow assimilation process, made evident by the repeated melting and replenishing (without a snowfall event) of snow pack over significant areas of the United States, exists in the Eta Data Assimilation System (EDAS, Rogers et al., 1996) and is a product of the EDAS system's direct insertion assimilation of snow data (Figures 1a-c, 2). Occurring on a 24 hour cycle, the repeated melting infuses the soil column with a large quantity of water that upsets the hydrological cycle.

### **2. DISCUSSION**

In an effort to quantify the impacts of such errors in snow assimilation on water and energy budgets, a series of Mosaic LSM (Koster and Suarez, 1996) simulations were performed over the period covering October 1998 to September 1999. A control run was conducted to provide "perfect" snow observations that were then directly assimilated, once per day, into

experimental runs (Figure 3) which featured a range of warm and cold biases created by the manipulation of shortwave and surface temperature forcing data. These experimental simulations show that even a 0.5°C warm bias can interact with assimilated snow data to significantly impact the water budget. After one month of directly inserting snow data into an experimental Mosaic run characterized by this forcing bias, the total column soil moisture changed by up to 3.5%, and changed by up to 11% in a run featuring a 2°C warm bias (Figure 4). The error in the water budget is also substantial in both experimental runs, with the largest residuals of up to 250mm occurring over mountainous regions (Figure 5) in the 2°C bias run.

### **3. CONCLUSION**

These preliminary results demonstrate that while it might be expected that the assimilation of error-free snow observations would lead to improved LSM results, a small LSM temperature bias leads to large-scale errors in the water balance. Even if the snow assimilation system perfectly reconciled modeled and observed snowpack states, the law of mass conservation could still be violated if biases exist in the model. Complicating the issue is the fact that in practice, snow observations are not without error. As such, more research is needed to determine how best to reconcile imperfect snow observations with LSMs that may be characterized by model biases.

---

\*Corresponding Author: Brian A. Cosgrove  
NASA Goddard Space Flight Center  
Mail Code 974, Greenbelt, MD 20771  
Email: Brian.Cosgrove@gsfc.nasa.gov

# **American Meteorological Society**



## **2002 Annual Meeting**

**January 13-17**  
**Orlando, FL**

**P1.11**      **AN INTEGRATED AIRBORNE MEASUREMENT SYSTEM FOR THE DETERMINATION  
OF ATMOSPHERIC TURBULENCE AND OCEAN SURFACE WAVE FIELD PROPERTIES**

Gennaro H. Crescenti, Jeffrey R. French, and Timothy L. Crawford  
Air Resources Laboratory Field Research Division  
National Oceanic and Atmospheric Administration  
Idaho Falls, Idaho

Douglas C. Vandemark  
Laboratory for Hydrospheric Processes  
NASA / Goddard Space Flight Center  
Wallops Island, VA

## **1. INTRODUCTION**

A small single-engine research aircraft has been used in numerous air-sea interaction research studies to investigate the spatial variation of both the marine atmospheric boundary layer and the ocean surface wave field. The integrated instrument suite of *in situ* sensors carried by a LongEZ (registration N3R) airplane is used to measure mean properties of the atmosphere as well as turbulent fluxes of heat, moisture, and momentum. These data are coupled with remote sensor measurements of the ocean surface, such as sea surface temperature, wave height, length, slope, and phase. This integrated measurement platform is a powerful tool to directly examine mass, momentum and energy exchange processes occurring across the air-sea interface.

## **2. AIRCRAFT**

Over the last ten years, N3R (Fig. 1) has been used in a number of air-sea interaction research studies (Crawford et al. 1993, Crescenti et al. 1999; Vogel and Crawford 1999; French et al. 2000; Mourad et al. 2000; Vandemark et al. 2001). N3R is set apart from other airborne measurement platforms for a number of reasons.



**Fig. 1.** N3R in flight during a research mission.

---

*Corresponding author address:* Gennaro H. Crescenti,  
U.S. Dept. Commerce / NOAA, Air Resources Laboratory  
1750 Foote Drive, Idaho Falls, ID 83402; e-mail:  
jerry.crescenti@noaa.gov

The LongEZ was designed in the early 1980's as a high-performance sport aircraft. N3R is a custom-built aircraft licensed by the Federal Aviation Administration (FAA) under an experimental amateur-built airworthiness category. It is a safe and reliable aircraft with exceptional performance characteristics. The differences of N3R from that of other single-engine aircraft are visually apparent. Unlike most aircraft that are constructed with metal, N3R is fabricated from a lighter and stronger fiberglass and foam composite. Another important difference is that the engine is mounted on the rear of the airframe. The large main laminar-flow wing is set back further than that of conventional aircraft. Vertical winglets found on either end of the main wing enhance aircraft lift. A smaller second wing (canard) is found near the nose of the aircraft. This forward lifting surface is designed to increase aircraft stability and to prevent the main wing from stalling.

An important characteristic of an aircraft with a pusher engine and a canard is that it responds to turbulence far less than conventional aircraft with the same wing loading (weight per unit area). Since the canard contributes to both lift and stability, it can be heavily loaded relative to the main wing. For conventional aircraft with a rear-mounted elevator, an upward wind gust will tend to make the aircraft pitch up. This increases the lift generated by the wings and amplifies the aircraft response to an upward wind gust. In contrast, canard aircraft have their elevators forward of their center of gravity. The same upward wind gust will push the canard elevator up which results in a compensating downward pitch response. Aircraft pitch response to either upward or downward wind gusts is opposed to the gust direction, thus giving canard-type aircraft their superior turbulent response characteristics.

A canard aircraft is also stall-resistant. As the angle of attack on the airplane is increased, the canard loses lift before the main wing. This causes the nose to drop, which decreases the angle of attack, thereby providing automatic stall recovery without allowing the main wing to stall.

## **8. SUMMARY**

The N3R integrated airborne measurement system is capable of acquiring high-fidelity atmospheric turbulence and ocean surface wave field data. N3R is a high-utility aircraft that is an ideal platform to carry state-of-the-science *in situ* and remote sensors. These data are being used to advance our understanding of air-sea interaction.

**NASA/TM-2002-210005**

## **SIMBIOS Project 2001 Annual Report**

Giulietta S. Fargion, Science Applications International Corporation, Maryland  
Charles R. McClain, Goddard Space Flight Center, Greenbelt, Maryland

National Aeronautics and  
Space Administration

**Goddard Space Flight Center**  
Greenbelt, Maryland 20771

March 2002



## Chapter 2

# SIMBIOS: Science Team and Contracts

Giulietta S. Fargion

*Science Applications International Corporation (SAIC), Beltsville, Maryland*

## 2.1 SCIENCE TEAM

The Science Team is selected through a NASA Research Announcement (NRA). Presently, NASA has had two NRA's, in 1996 and 1999. NASA HQ manages the process of team selection, but the Goddard Space Flight Center (GSFC) NASA Procurement Office handles the team contracts, work statements and, if necessary, budget negotiations. The Project funds numerous US investigators and collaborates with several international investigators, space agencies (e.g., NASDA, CNES, KARI, etc.) and international organizations (e.g., IOCCG, JRC). US investigators under contract provide *in situ* atmospheric and bio-optical data sets, and develop algorithms and methodologies for data merger schemes. NASA GSFC Procurement requires formal evaluations for all contracts at the end of each contract year. These evaluations are to go into a database and are shared with the PI's institution or upper management.

The locations of specific SIMBIOS team investigations (i.e., NRA-99) are shown in Figures 2.1. The international ocean color community response for the NRA-99 was overwhelming, with a total of 75 PI's attempting to collaborate with the Project group in twelve proposals. The twelve international proposals cover topics ranging from protocols, calibration-validation activities, atmospheric-biological algorithms, and data merging.

The SIMBIOS Science Team (NRA-96) meetings were held in August 1997 at Solomons Island (Maryland), in September 1998 at La Jolla (California) and in September 1999 at Annapolis (Maryland). Meanwhile, the SIMBIOS Science Team's (NRA-99) meeting will be held in January 2001 at GSFC in Greenbelt, Maryland and in January 2002 at the Mariott (BWI), Baltimore, Maryland.

In general, all Science Team members, US and international, were in attendance or were represented by one of their staff. Also, the IOCCG and MODIS Teams are invited, and most attended or sent representatives. During each year the Project Office has fostered international collaborations by hosting visiting scientists at GSFC. These visits lasted from one week to several months. For international participants, the Project provided partial or as-needed travel support to team meetings or to collaborate with the project on specific topics such as calibration, and product evaluations.

The fifth science team meeting (January 2002) was the most attended, participation reached over 90 scientists (Figure 2.2). The team had a substantial US (SIMBIOS and MODIS PIs) and international participation, with official representation from OCTS, POLDER-I and II, MOS, MERIS, GLI, and VIIRS missions. During the meeting the team addressed atmospheric correction and bio-optical algorithms, a MODIS data merging plan for 2002, uncertainty budget and sources from *in situ* observation, SeaWiFS re-processing, protocols updates and international collaborations. The agenda, presentations, minutes and recommendations are posted at <http://simbios.gsfc.nasa.gov/Info/>

Chapters 4 to 21 contain the individual PI's contributions and describe the funded research topics, field studies activities, and results of concluded research. These chapters are reproduced as submitted with minimal editing by the Project Office.

## 2.2 CONTRACT OVERVIEW

The second-year of the SIMBIOS NRA-99 contracts ended on November 30, 2000. The SIMBIOS Project scheduled a telephone conference (telecon), of about 30-45 minutes, with each PI and other appropriate staff during the month of October. Prior to the telecon, the SIMBIOS Project reviewed each contract, the statement of work, and the agreed to deliveries. The Project Office followed the same procedure used in 1999 and coordinated an inside panel with key contract and project personnel to perform an across-the-board evaluation of all funded contracts (Table 2.1).

Table 2.1 Contract evaluation key personnel

Contracting Officer:	Lynne Hoppel
Contracting Assistant:	Kathy Lingerfelt
Resource/Financial Officer:	Patty Clow
Manager, SIMBIOS Project:	Giulietta Fargion
Manager, Office for Global Carbon Studies:	Charles McClain

The four categories to be evaluated are suggested in the "Evaluation of Performance" from the Federal Acquisition Regulation (FAR) 42.15 and NASA FAR Supplement (NSF) 1842.15 or NASA form 1680 used by GSFC.

**NASA/TM-2002-210005**

## **SIMBIOS Project 2001 Annual Report**

Giulietta S. Fargion, Science Applications International Corporation, Maryland  
Charles R. McClain, Goddard Space Flight Center, Greenbelt, Maryland

National Aeronautics and  
Space Administration

**Goddard Space Flight Center**  
Greenbelt, Maryland 20771

March 2002

## Chapter 3

# SIMBIOS Project Data Processing and Analysis Results

Giulietta Fargion, Bryan Franz, Ewa Kwiatkowska-Ainsworth, Christophe Pietras and Paul Smith  
*Science Applications International Corporation (SAIC), Beltsville, Maryland*

Sean Bailey, Joel Gales and Gerhard Meister  
*FutureTech Corporation, Greenbelt, Maryland*

Kirk Knobelspiesse and Jeremy Werdell  
*Science Systems and Applications Inc., Greenbelt, Maryland*

Charles McClain and Gene Feldman  
*NASA Goddard Space Flight Center, Greenbelt, Maryland*

### 3.1 INTRODUCTION

The SIMBIOS Project is concerned with ocean color satellite sensor data intercomparison and merger for biological and interdisciplinary studies of the global oceans (Barnes et al., 2000). Imagery from different ocean color sensors (OCTS, POLDER, SeaWiFS, MOS and OSMI) can now be processed by a single software package using the same algorithms, adjusted by different sensor spectral characteristics, and the same ancillary meteorological and environmental data. This enables cross-comparison and validation of the data derived from satellite sensors and, consequently, creates continuity in ocean color information on both the temporal and spatial scale. The next step in this process is the integration of *in situ* ocean and atmospheric parameters to enable cross-validation and further refinement of the ocean color methodology. The SIMBIOS Project Office accomplishments during 2001 year are summarized under (a) satellite data processing, (b) data merging (c) SeaBASS database, (d) supporting services, (e) sun photometers and calibration activities and (f) calibration round robins. These accomplishments are described below.

### 3.2 SATELLITE DATA PROCESSING

#### 3.2.1 Satellite Characterization

The SIMBIOS Project has worked closely with our colleagues in the OSMI Program and with the instrument manufacturer to define and assemble the instrument performance characteristics required for the lookup tables for the algorithms that determine OSMI top-of-the-atmosphere radiances. Of special importance in this regard are the spectral responses of the OSMI bands and the spatial co-registration of

the detectors. In addition, the Project has opened a collaboration with the GLI Program. GLI is scheduled for launch not sooner than November 2002. The GLI/SIMBIOS collaboration has centered on the characteristics of the GLI scan mirror as a function of scan angle and the normalization of detector-to-detector gain differences in the GLI bands. Plans are underway for a cross-calibration of the GLI and SeaWiFS near infrared bands, which are used for the determination of the aerosol type and amount for the atmospheric correction algorithms.

#### 3.2.2 MOS Data Collection, Processing, and Distribution

Since February of 1999, the SIMBIOS project has been operating a receiving station at NASA's Wallops Flight Facility (WFF) to acquire data from the German Modular Optoelectronic Scanner (MOS) onboard the Indian IRS-P3 spacecraft. When a pass is acquired at Wallops, the raw files are transferred to the SIMBIOS project at NASA's Goddard Space Flight Center via an automated FTP process. The raw files are then converted to Level-0 format through a software package provided by the Indian Space Research Organization (ISRO). The resulting Level-0 files are made available to the German Remote Sensing Data Centre (DLR-DFD) for archive and distribution. In addition, the SIMBIOS project is processing the data through Level-1B using the standard software provided by the German Institute for Space Sensor Technology (DLR-ISST) (Neumann et al., 1995). All data processed by the SIMBIOS project is made available through the MOS browse system at <http://simbios.gsfc.nasa.gov/oceancolor.html>. The Level-1B data can be processed to Level-2 using SIMBIOS-developed software tools distributed through SeaDAS.

**NASA/TM-2002-210005**

## **SIMBIOS Project 2001 Annual Report**

Giulietta S. Fargion, Science Applications International Corporation, Maryland  
Charles R. McClain, Goddard Space Flight Center, Greenbelt, Maryland

National Aeronautics and  
Space Administration

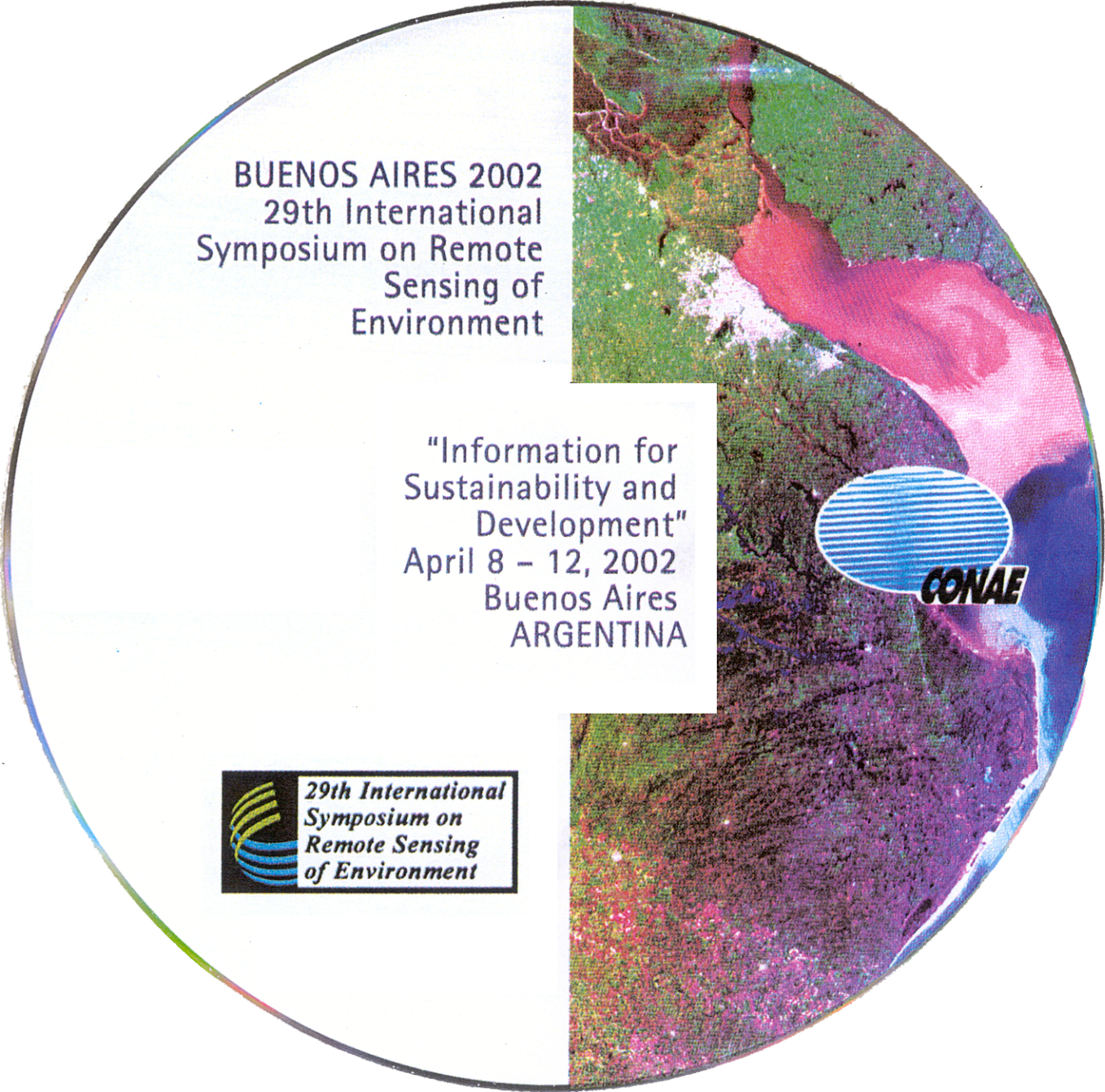
**Goddard Space Flight Center**  
Greenbelt, Maryland 20771

March 2002

## *Preface*

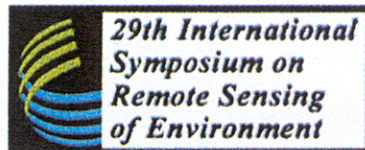
The purpose of this technical report is to provide current documentation of the the Sensor Intercomparison and Merger for Biological and Interdisciplinary Oceanic Studies (SIMBIOS) Project activities, NASA Research Announcement (NRA) research status, satellite data processing, data product validation, and field calibration. This documentation is necessary to ensure that critical information is related to the scientific community and NASA management. This critical information includes the technical difficulties and challenges of validating and combining ocean color data from an array of independent satellite systems to form consistent and accurate global bio-optical time series products. This technical report is not meant as a substitute for scientific literature. Instead, it will provide a ready and responsive vehicle for the multitude of technical reports issued by an operational project.

The SIMBIOS Science Team Principal Investigators (PIs) original contributions to this report are in chapters four and above. The purpose of these contributions is to describe the current research status of the SIMBIOS-NRA-96 funded research. The contributions are published as submitted, with the exception of minor edits to correct obvious grammatical or clerical errors.



BUENOS AIRES 2002  
29th International  
Symposium on Remote  
Sensing of  
Environment

"Information for  
Sustainability and  
Development"  
April 8 – 12, 2002  
Buenos Aires  
ARGENTINA



# Seasonal Snow Extent and Snow Mass from 1988 - 2001 in the Patagonia Region of South America Using SSM/I Passive Microwave Data

J. L. Foster, A. T. C. Chang, D. K. Hall, and R. Kelly  
NASA/Goddard Space Flight Center  
Hydrological Sciences Branch  
Greenbelt, MD USA 20771

[jfoster@glacier.gsfc.nasa.gov](mailto:jfoster@glacier.gsfc.nasa.gov)

**ABSTRACT** - Seasonal snow cover in South America was examined in this study using passive microwave satellite data from the Special Sensor Microwave Imagers (SSM/I) on board Defense Meteorological Satellite Program (DMSP) satellites. For the period from 1988-2001, both snow cover extent and snow depth (snow mass) were investigated during the winter months (May-August) in the Patagonia region of Argentina. Since above normal temperatures in this region are typically above freezing, the coldest winter month was found to be not only the month having the most extensive snow cover but also the month having the deepest snows. For the fourteen-year period of this study, the average snow cover extent (May-August) was about 0.46 million km<sup>2</sup> and the average monthly snow mass was about  $1.18 \times 10^{13}$  kg. July 2000 was the month having the greatest snow extent (8.1 million km<sup>2</sup>) and snow mass (approximately  $2.8 \times 10^{13}$  kg).

## I. INTRODUCTION

Using data from the SSM/I on board DMSP satellites, seasonal snow extent and snow depth (snow mass) have been calculated for the period from 1988-2001 in the middle latitudes of South America. It should be noted that in mid winter approximately 99% of the snow cover in the Southern Hemisphere is confined to Antarctica. The data record shows that South America is the only continent in the Southern Hemisphere (other than Antarctica) where an extensive, non-mountainous, winter snow cover may occur. Therefore, the emphasis in this study is on South America. The objectives of this study are to map the seasonal snow cover during the cold months of the year using passive microwave satellite data and to generate a snow record comparable to the record for North America and Eurasia.

## II. STUDY AREA

In southern Argentina, snow may accumulate as early as May and as late as October. Each winter, snow is a regular feature south of about 45 degrees latitude, and in the snowiest years, over 1 million square km of snow has been measured (Dewey and Heim, 1983). A single storm may cover the ground with several hundred thousand km<sup>2</sup> of snow. Snow can fall at locations much further north than expected, and it can even lay on the ground for a few days as far north as 27 degrees south latitude. Snow here is usually confined to elevations greater than 1,000 meters above sea level, where as much as 30 cm of snow has been observed in southern Brazil. In July 2000, freezing temperatures and snowfall in southern Brazil and Paraguay damaged coffee crops (Prohaska, 1976).

Typically, snow cover in southern South America results from disturbances embedded in the westerly air streams. East winds and heavy precipitation during the winter in southern South America are caused by quasi-stationary, high-pressure systems at high latitudes over the western South Atlantic Ocean (Kidson, 1988). These anticyclones block the normally zonal air flow in such a way that normal sea level cyclonic systems are steered around the "high" toward Patagonia (the South American states of Rio Negro, Chubut, Santa Cruz and Tierra Del Fuego). In southeastern Brazil, snow can fall when incursions of polar air from the south push northward, coincident with a weakening of the normally dominant sub-tropical high-pressure belt.

Although snow cover may be significant in South America in terms of its effects on weather, especially temperature and agriculture, it is variable from year-to-year. This is to be expected when accumulations generally are shallow. According to Dewey and Heim (1983), over a 7-year period from 1974-1980, snow cover reached a maximum extent of about  $1 \times 10^6$  million km<sup>2</sup> in 1980, but in 1979, the maximum extent was only about 70% of this amount. For comparison, during the 1980 snow season, snow covered an area about the size of the country of Bolivia.

## VI CONCLUSIONS

Exclusive of Antarctica, seasonal snow in the Southern Hemisphere is, for the most part, confined to South America. Though snow may fall and even persist on the ground for several days in Africa and Australia, on those continents, however, snow is basically a novelty. This study demonstrates that passive microwave radiometry is especially useful in estimating the snow cover extent and snow mass in areas where clouds are a near-constant problem and where the snow is typically ephemeral. The passive microwave observations show that there are sharp year-to-year differences that exist in the seasonal snow extent over the Patagonia region of South America. This agrees with earlier findings in the work of Dewey and Heim (1983).

# **SPIE Conference on Remote Sensing for Agriculture, Ecosystems, and Hydrology – 2002**



**September 17-22, 2002  
Capsis Sofitel Conference Center  
Agia Pelagia  
Crete, Greece**



# **Comparison of Relative Errors in Snow Maps in North America and Eurasia in 2001-02**

J. L. Foster\*, D. K. Hall\*, R. E. J. Kelly\*\*, A. T. C. Chang\*, J.Y.L. Chien\*\*\*

\*Code 974, NASA/Goddard Space Flight Center  
Greenbelt, MD 20771 U.S.A.  
email: jfoster@glacier.gsfc.nasa.gov  
phone: 301-614-5769, fax: 301-614-5808

\*\*Goddard Earth Sciences and Technology Center  
University of Maryland, Baltimore County  
Baltimore, MD 21250 U.S.A.

\*\*\*General Sciences Corporation, Laurel, MD 20707 U.S.A.

## **ABSTRACT**

Results of this investigation confirm previous results by several authors (see Armstrong and Brodzik, 1999; Hall et al., in press ) that correspondence between the MODIS and SSM/I-derived snow maps improves as the winter progresses. Early in the season, the SSM/I snow mapping algorithms are unable to identify shallow and wet snow as snow cover, while the MODIS snow maps perform well under those circumstances, but cannot map snow through clouds and cannot provide estimates of SWE. By mid winter when the snowpack is deeper, temperatures are colder, and liquid water in the snowpack is minimal, the agreement between MODIS- and SSM/I-derived snow maps improves. For North America, the difference averaged about 5% for maps examined in February of 2002, and for Eurasia (eastern Asia), the difference was less than 10% in January of 2001.

## **1. INTRODUCTION**

Accurate snow maps are required for hydrological and climatological applications and by operational agencies to monitor snow conditions, and to predict spring water supply and flood conditions. Visible/near-infrared-based snow maps have the advantage of high spatial and temporal resolution (tens of meters and daily coverage) and the ability to measure albedo, while passive-microwave snow maps have a high temporal resolution, the spatial resolution is poor (on the order of tens of km). However, passive microwave data are indifferent to clouds and darkness, but visible data are limited to daytime operation, and clouds limit their mapping efficacy. In this study, Moderate Resolution Imaging Spectroradiometer (MODIS) and Special Sensor Microwave Imager (SSM/I) snow data are examined and compared during the winter season in North America and Eurasia.

Since November 1978, the Scanning Multichannel Microwave Radiometer (SMMR) instrument on the Nimbus-7 satellite, and the SSM/I on the Defense Meteorological Satellite Program (DMSP) series of satellites have been acquiring passive microwave data that can be used to estimate both snow extent and snow water equivalent (snow depth). In addition, passive-microwave sensors have the capability to estimate snow depth and snow-water equivalent (SWE) as well as snow extent.

NASA's MODIS sensor on-board the Terra and Aqua satellites, and the Advanced Microwave Scanning Radiometer (AMSR) currently all produce snow maps. The Terra satellite, launched in December of 1999, has the MODIS as part of its payload of five instruments, while the Aqua satellite, launched in May of 2002, contains a second MODIS instrument, the AMSR-E and four other instruments. Snow maps have

# **NASA/TM-2002-210004/Rev3-Vol2**

**James L. Mueller<sup>1</sup> and Giulietta S. Fargion<sup>2</sup>**  
**Editors**

<sup>1</sup> *CHORS, San Diego State University, San Diego, California*

<sup>2</sup> *Science Applications International Corporation, Beltsville, Maryland*

## **Ocean Optics Protocols For Satellite Ocean Color Sensor Validation, Revision 3, Volume 2**

J. L. Mueller, C. Pietras, S. B. Hooker, D. K. Clark, A. Morel, R. Frouin, B.G. Mitchell,  
R. R. Bidigare, C. Trees, J. Werdell, G. S. Fargion, R. Arnone, R. W. Austin, S. Bailey,  
W. Broenkow, S. W. Brown, K. Carder, C. Davis, J. Dore, M. Feinholz, S. Flora, Z.P.  
Lee, B. Holben, B. C. Johnson, M. Kahru, D. M. Karl, Y. S Kim, K. D. Knobelspiesse, C.  
R. McClain, S. McLean, M. Miller, C. D. Mobley, J. Porter, R.G. Steward, M. Stramska,  
L. Van Heukelem, K. Voss, J. Wieland, M. A. Yarbrough and M. Yuen.

National Aeronautical and  
Space administration

**Goddard Space Flight Space Center**  
Greenbelt, Maryland 20771

**February 2002**

## Chapter 14

# Sun and Sky Radiance Measurements and Data Analysis Protocols

Robert Frouin<sup>1</sup>, Brent Holben<sup>2</sup>, Mark Miller<sup>3</sup>, Christophe Pietras<sup>4</sup>, Kirk D. Knobelspiesse<sup>5</sup>, Giulietta S. Fargion<sup>4</sup>, John Porter<sup>6</sup> and Ken Voss<sup>7</sup>

<sup>1</sup>*Scripps Institution of Oceanography, University of California, San Diego, California*

<sup>2</sup>*Biospheric Sciences Branch, NASA Goddard Space Flight Center, Greenbelt, Maryland*

<sup>3</sup>*Department of Applied Science, Brookhaven National Laboratory, Upton, New York*

<sup>4</sup>*SAIC General Sciences Corporation, Beltsville, Maryland*

<sup>5</sup>*Science Systems and Applications, Inc., Greenbelt Maryland*

<sup>6</sup>*School of Ocean & Earth Science & Technology, University of Hawaii, Hawaii*

<sup>7</sup>*Physics Department, University of Miami, Florida*

## 14.0 INTRODUCTION

This chapter is concerned with two types of radiometric measurements that are required to verify atmospheric correction algorithms and to calibrate vicariously satellite ocean color sensors. The first type is a photometric measurement of the direct solar beam to determine the optical thickness of the atmosphere. The intensity of the solar beam can be measured directly, or obtained indirectly from measurements of diffuse global upper hemispheric irradiance. The second type is a measurement of the solar aureole and sky radiance distribution using a CCD camera, or a scanning radiometer viewing in and perpendicular to the solar principal plane.

From the two types of measurements, the optical properties of aerosols, highly variable in space and time, can be derived. Because of the high variability, the aerosol properties should be known at the time of satellite overpass. Atmospheric optics measurements, however, are not easy to perform at sea, from a ship or any platform. This complicates the measurement protocols and data analysis. Some instrumentation cannot be deployed at sea, and is limited to island and coastal sites. In the following, measurement protocols are described for radiometers commonly used to measure direct atmospheric transmittance and sky radiance, namely standard sun photometers, fast-rotating shadow-band radiometers, automated sky scanning systems, and CCD cameras. Also discussed are methods of data analysis and quality control, as well as proper measurement strategies for evaluating atmospheric correction algorithms and atmospheric parameters derived from satellite ocean color measurements.

## 14.1 AUTOMATIC SUN PHOTOMETER AND SKY RADIANCE SCANNING SYSTEMS

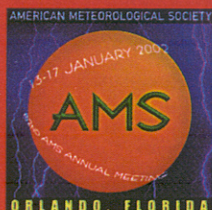
The technology of ground-based atmospheric aerosol measurements using sun photometry has changed substantially since Volz (1959) introduced the first hand-held analog instrument almost four decades ago. Modern digital units of laboratory quality and field hardness collect data more accurately and quickly and are often equipped for onboard processing (Schmid et al. 1997; Ehsani 1998, Forgan 1994; and Morys et al. 1998). The method used remains the same, i.e., a detector measures through a spectral filter the extinction of direct beam solar radiation according to the Beer-Lambert-Bouguer law:

$$V(\lambda) = V_o(\lambda) \left( \frac{d}{d_o} \right)^2 \exp[-(\tau(\lambda)M)] t_g(\lambda), \quad (14.1)$$

where  $V(\lambda)$  is the measured digital voltage,  $V_o(\lambda)$  is the extra-terrestrial voltage,  $M$  is the optical air mass,  $\tau(\lambda)$  is the total optical depth,  $\lambda$  is wavelength,  $d$  and  $d_o$  are respectively the actual and average earth-sun distances, and  $t_g(\lambda)$  is the transmission of absorbing gases. The total optical depth is the sum of the Rayleigh and aerosol optical depth.



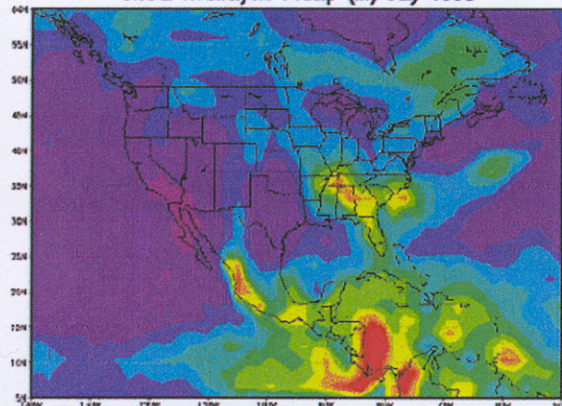
# 16th Conference on Hydrology



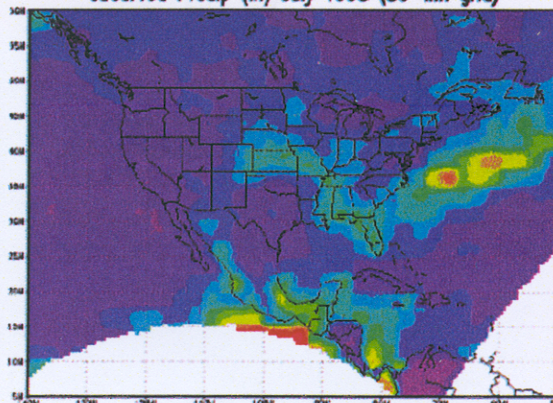
**13–17 January 2002**  
**Orlando, Florida**

## **NCEP Regional Reanalysis Result for July 1998**

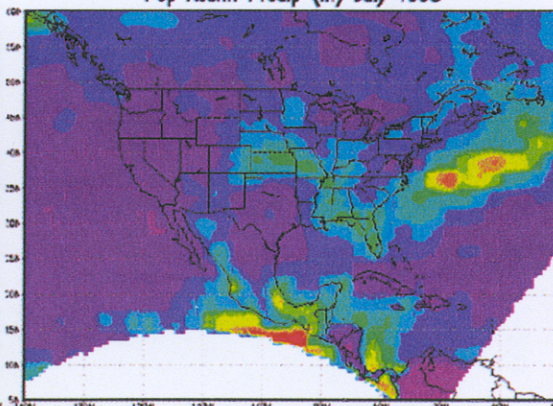
Global Reanalysis Precip (in) July 1998



Observed Precip (in) July 1998 (80-km grid)



Pop Assim Precip (in) July 1998



AMERICAN METEOROLOGICAL SOCIETY



Jon C. Gottschalk<sup>\*1</sup>, Paul R. Houser<sup>1</sup>, and Xubin Zeng<sup>2</sup><sup>1</sup> NASA / GSFC – UMBC / GEST, Greenbelt, Maryland<sup>2</sup> University of Arizona, Tucson, Arizona

## 1. INTRODUCTION

The parameterization of vegetation in land surface models plays a major role in the simulation of the surface energy balance and therefore weather and climate prediction. Historically, parameters in land surface process models have been assigned based on generalized land surface classifications that do not account for local anomalies in phenology. More recently, however, there have been studies that have incorporated satellite remote sensing data in the parameterization of the vegetation used in land surface models (Sellers et al. 1996; Los et al. 2000; Zeng et al. 2001). Satellite data provides better spatial and temporal resolution and so improved sampling of the seasonal variability of critical vegetation parameters such as leaf area index (LAI) and fractional vegetation cover. Our hypothesis is that using these improved remotely-sensed parameters may produce improved land surface simulations and our group is actively working on incorporating satellite remote sensing data into the Global Land Data Assimilation System (GLDAS, <http://ldas.gsfc.nasa.gov>) currently being developed at NASA's Goddard Space Flight Center and at NOAA's National Center for Environmental Prediction. This paper presents the current state of this work -- our initial methodology and preliminary findings.

## 3. RESULTS AND DISCUSSION

Differences in the assignment of LAI impact a number of processes and variables in CLM2. In this paper we focus on canopy transpiration, soil surface temperature, and total column soil moisture and focus on North America for the sake of clarity. Figure 2 illustrates the difference in canopy transpiration (original LAI – AVHRR LAI) between the two model simulations after one month. There are some substantial differences mainly over the central and western areas of North America (transpiration lower with the AVHRR LAI) caused by the assignment of much higher values of LAI in the original CLM2 (Figure 1). The vegetation types in these areas include grassland and shrubland that equate to lower LAI values

using the radiative transfer algorithm then what other datasets have shown (Sellers et al. 1996; Los et al. 2000). In addition, large areas of cropland in this region are impacted by weather and agricultural changes. The absolute magnitudes in canopy transpiration for the model runs ranged up to  $350 \text{ Wm}^{-2}$ .

Less canopy transpiration alters the surface energy balance through lower total latent heat flux. Figure 3 illustrates the difference in soil surface temperature and shows a signature very similar to that of Figure 2 with warmer soil surface

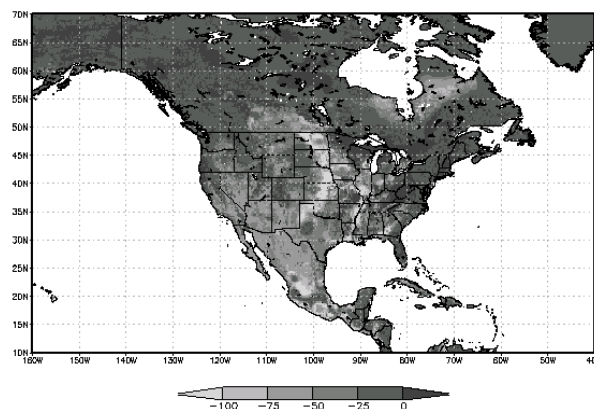


Figure 2: Difference in canopy transpiration (original LAI – AVHRR LAI) in  $\text{Wm}^{-2}$  valid on 30 June 2001.

temperatures in western North America and in parts of the southeast US and Mississippi River valley where the AVHRR dataset indicates areas of lower LAI. In addition, greater solar radiation enters the soil and allows higher temperatures. The differences are substantial and are range up to and over  $10^\circ \text{C}$  warmer for the AVHRR simulation in parts of the central and western US and Mexico. The AVHRR simulation also shows that the soil surface temperature across the whole continent for the most part is warmer than with the original LAI designation. The absolute temperatures in both model runs generally ranged from  $260 - 330^\circ \text{K}$  globally.

The lower transpiration in these areas limits the loss of total soil moisture content for the AVHRR simulation (Figure 4). The soil is significantly moister across Mexico for instance.

\* Corresponding author address: Jon C. Gottschalk, Hydrological Sciences Branch – Code 974, NASA / Goddard Space Flight Center, Greenbelt, MD 20771; e-mail: [jgotts@hsb.gsfc.nasa.gov](mailto:jgotts@hsb.gsfc.nasa.gov).

**NASA/TM-2002-210005**

## **SIMBIOS Project 2001 Annual Report**

Giulietta S. Fargion, Science Applications International Corporation, Maryland  
Charles R. McClain, Goddard Space Flight Center, Greenbelt, Maryland

National Aeronautics and  
Space Administration

**Goddard Space Flight Center**  
Greenbelt, Maryland 20771

March 2002

## Chapter 7

# Merging Ocean Color Data From Multiple Missions

Watson W. Gregg

*NASA Goddard Space Flight Center, Greenbelt, Maryland*

## 7.1 INTRODUCTION

We propose to investigate, develop, and test algorithms for merging ocean color data from multiple missions. We seek general algorithms that are applicable to any retrieved Level-3 (derived geophysical products mapped to an Earth grid) ocean color data products, and that maximize the amount of information available in the combination of data from multiple missions. Most importantly, we will investigate merging methods that produce the most complete coverage in the smallest amount of time, nominally, global daily coverage. We will emphasize 4 primary methods: 1) averaging, 2) subjective analysis, 3) blending, and 4) statistical (optimal) interpolation. We will also assess the ability to produce fuller coverage in larger time increments, including 4-day, 8-day (weekly), monthly, and seasonal. Secondly, we will investigate the ability of the missions to produce coverage at different times of day, for diel variability and dynamical evaluations, and develop algorithms to produce this information, again on as full a spatial coverage as possible. We intend to develop methods that are not mission-specific, but take advantage of the unique characteristics of the missions as much as possible. However, given the peculiarities of sensor design and performance, and mission characteristics, we acknowledge that individual merging methods may be required to take full advantage of the unique characteristics of the missions as much as possible, and produce the highest quality data set.

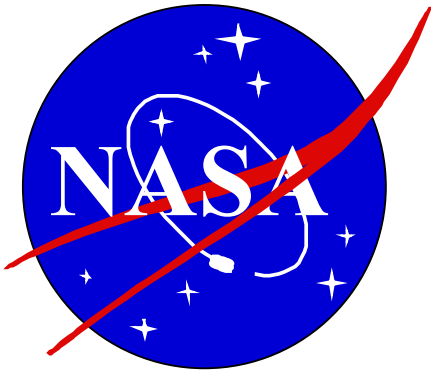
## 7.2 RESEARCH ACTIVITIES

Work has focused on analysis, development, and testing of candidate merger algorithms. We began investigating four possible approaches for merging ocean color satellite data: (1) simple splicing/averaging, where data from two or more satellites are averaged where they coexist at grid points, and use of a single satellite in gaps where only one exists; (2) subjective analysis, where specific dependences and deficiencies are identified using knowledge about sensor environmental conditions and co-located observations are merged using different weighting functions for the sensors;

(3) the Conditional Relaxation Analysis Method (CRAM), where the best data are selected as interior boundary conditions into a merged set using Poisson's equation; and (4) optimal interpolation, where merging occurs by weighting individual sensor data to minimize spatial covariance function. The latter two algorithms were developed under separate funding. The algorithms have been characterized and implemented in software; their capabilities and limitations are known, as well as their ability to be modified. The application of algorithms and potential modifications depends on a characterization of the merged data sets.

Significant progress has been made on each of these techniques with the majority of analysis this year focusing on blending. The blended analysis has traditionally been applied to merging satellite and in situ data. Also known as the Conditional Relaxation Analysis Method (CRAM), this analysis assumes that in situ data are valid and uses these data directly in the final product. To blend multiple satellite ocean color data sets, one sensor's data would replace the role of the in situ data as the internal boundary condition (IBC). In January 2001, initial results of the application of blended analysis using SeaWiFS and early MODIS data were presented at the SIMBIOS Science Team Meeting in Greenbelt, Maryland. SeaWiFS chlorophyll data were used as the IBC. The radiometric calibration of the MODIS data was insufficient for scientific use but served the purpose of algorithm investigation. For this preliminary analysis, six weeks of daily Level-3 globally mapped MODIS and SeaWiFS data were obtained from the Goddard DAAC. Routines were written in IDL (Interactive Data Language) to extract the MODIS and SeaWiFS chlorophyll images from their native HDF (Hierarchical Data Format), to scale and orient the images properly, to retrieve the accompanying quality flags for MODIS, and to save the resulting images as FORTRAN binary. Global equal-area mapped MODIS data is available at 4-km, 36-km, and 1-degree; SeaWiFS standard mapped images are at 9-km resolution. Both are available daily, weekly, monthly and yearly. For testing, the blend code was modified to run at different spatial resolutions and several weeks of blended results were obtained using daily 36-km and 1-degree data. Running the blend code at a higher spatial resolution on a global data set is possible, but time consuming.

**NASA/TM---2002-104606, Vol. 22**



**Technical Report Series on Global  
Modeling and Data Assimilation**

*Max Suarez, Editor*

**Volume 22**

**A Coupled Ocean-Atmosphere Radiative  
Model for Global Ocean Biogeochemical  
Models**

*Watson W. Gregg  
Goddard Space Flight Center, Greenbelt, Maryland*

National Aeronautics and Space Administration

**Goddard Space Flight Center**  
Greenbelt, Maryland 20771

---

**August 2002**



**Abstract.** An ocean-atmosphere radiative model (OARM) evaluates irradiance availability and quality in the water column to support phytoplankton growth and drive ocean thermodynamics. An atmospheric component incorporates spectral and directional effects of clear and cloudy skies as a function of atmospheric optical constituents, and spectral reflectance across the air-sea interface. An oceanic component evaluates the propagation of spectral and directional irradiance through the water column as a function of water, five phytoplankton groups, and chromophoric dissolved organic matter. It tracks the direct and diffuse streams from the atmospheric component, and a third stream, upwelling diffuse irradiance. The atmospheric component of OARM was compared to data sources at the ocean surface with a coefficient of determination ( $r^2$ ) of 0.97 and a root mean square of 12.1%.

## 1 Introduction

Knowledge of oceanic irradiance is critical for realistic simulation of ocean biogeochemistry. Since irradiance affects ocean thermodynamics and physiological processes of biota in the oceans, it may affect the abundances and distributions of phytoplankton, and potentially affect the uptake of carbon dioxide.

In order to understand the effects of irradiance on phytoplankton abundances and primary production in the global oceans, we require a reasonably realistic simulation of the irradiance reaching the ocean surface, and propagating through the water column. The simulation must explicitly include the effects of atmospheric optical constituents on surface irradiance, processes occurring at the air-sea interface, and the results of these effects in the water column taking into account the optical properties of the water, phytoplankton, and dissolved detrital materials. In this paper we describe atmospheric and oceanic radiative transfer models, combined as the Ocean-Atmosphere Radiative Model (OARM) that provide a reasonably complex and realistic representation of atmospheric radiative processes and the irradiance availability in the oceans.

## 2 Ocean-Atmosphere Radiative Model (OARM)

### 2.1 *Atmospheric Component.*

The atmospheric radiative model is based on the Gregg and Carder (1990) spectral model for clear skies, and relies on Slingo (1989) for spectral cloud transmittance. The clear sky model of Gregg and Carder (1990) was derived from Bird and Riordan (1986), but was limited to the spectral range of photosynthetically available radiation (PAR), defined as 350-700 nm. It also contained increased spectral resolution and marine atmospheric and surface reflectance conditions. It compared within  $\pm 6.6\%$  root mean square (RMS) with surface observations of spectral irradiance and  $\pm 5.1\%$  RMS with integrated PAR (Gregg and Carder, 1990). This model is extended for OARM from the PAR spectral domain to the entire solar spectrum, from 200 nm to 4  $\mu\text{m}$ , representing  $>99\%$  of the total solar irradiance impinging on the top of the atmosphere. For computational efficiency, the spectral resolution is degraded from 1 nm used in Gregg and Carder (1990) to a variable resolution appropriate for the spectral absorbing properties of the major atmospheric optically active gases, specifically ozone, water vapor, oxygen, and carbon dioxide (Table 1). The spectral resolution is fixed at 25 nm for the PAR range, which is the region of interest for phytoplankton photosynthesis.

# 2002 IEEE International Geoscience and Remote Sensing Symposium and the 24<sup>th</sup> Canadian Symposium on Remote Sensing



REMOTE SENSING:  
Integrating Our  
View of the Planet



June 24-28, 2002  
Toronto Canada

# IGARSS 2002

# Frequency Dependence of Scattering by Dense Media of Small Particles

## Based on Monte Carlo Simulation of Maxwell's Equations

Jianjun Guo\*, Leung Tsang\*, Alfred T.C. Chang\*\*, Kung-Hau Ding<sup>+</sup>, Chi-Te Chen\*

\*Department of Electrical Engineering, University of Washington, Box 352500, Seattle, WA 98195-2500  
Tel: (206)221-6513 Fax: (206)543-3842

<sup>§</sup>Department of Electronic Engineering, City University of Hong Kong, Hong Kong

<sup>+</sup> Air Force Research Lab, Sensors Directorate/SNHE, 80 Scott Road, Hanscom AFB, MA 01731-2909

\*\* Hydrological Sciences Branch, NASA/Goddard Space Flight Center, Greenbelt, MD 20771-0001  
Email: jguo@u.washington.edu

**Abstract** The frequency dependence of scattering by geophysical media at microwave frequencies is an important issue because multi-frequency measurements are useful for remote sensing applications. Classically, the independent scattering theory states that if the particles are small, scattering is proportional to the fourth power in 3-D scattering and the third power in 2-D scattering. In this paper, we study rigorously the frequency dependence of scattering by dense media by Monte Carlo simulations of the solutions of both 2- and 3-dimensional Maxwell's equations. The particle positions are generated by deposition and bonding techniques. The Sparse-Matrix Canonical-Grid method has been applied to speed up the simulation of scattering by 2D small particles. Numerical solutions of Maxwell's equations indicate that the frequency dependence of densely packed sticky small particles is much weaker than that of independent scattering. The results are illustrated using parameters of snow in microwave remote sensing.

### I Introduction

Wave propagation and scattering in the densely packed media are important issues in the volume scattering problem of geophysical media [1][2]. The frequency dependence of emission and scattering of snow at microwave remote sensing frequencies (e.g. 19GHz, and 37GHz) is a quantity that must be studied rigorously because multi-frequency measurements are useful for remote sensing applications. When the particles are much smaller than a wavelength, the frequency dependence is to the fourth power for 3-D particles and the third power for the 2-D particles, based on the conventional independent scattering model. Physically, in densely packed media, the particles can adhere to form aggregates. The correlation between particles has to be taken into account. To better understand such a scattering property, we study the frequency dependence of scattering by sticky and non-sticky particles rigorously. In this rigorous approach, we generate the positions of particles rigorously using bonding technique; and

then solve the Maxwell's equations that include all the multiple scattering based on Monte Carlo simulation. For the sticky particles, the frequency variation is dependent on a "sticky" parameter representing the degree of adhesiveness of the cylinders. The extinction, scattering and absorption properties of dense media are calculated for dense media of sticky and non-sticky particles. The T-matrix method is used. It has been shown that the internal field formulation of Foldy-Lax equations have much better condition numbers for the matrix equations [2]. Thus the use of internal field formulation is advantageous for iterative solution of the Foldy-Lax matrix equation. Various numerical parameters are tested to show that the results are accurate. Convergence tests are performed for these numerical parameters. A sufficient number of realizations of the Monte Carlo simulations is performed to ensure the convergence. Up to 50 realizations are used in this paper. For most of the cases, the results converge within 20 to 30 realizations. The number of particles used in this study is between 100 and 2000 depending on the fractional volume and frequency.

### IV Simulation Results and Discussions

We use the internal field formulation and conjugate gradient (CG) method in computing the numerical results. In the following, we present results for dielectric cylinders with  $\epsilon_p=3.2$  based on Monte Carlo simulations for non-sticky and sticky cylinders (2D problem) and spherical particles (3D problem). In Table 1, we tabulate the results of normalized scattering coefficients  $\kappa_s/k$  for the 2-D scattering problem.

For 3D scattering problem, we tabulate the frequency dependence of scattering rates in Table II. The scattering rate at 18 GHz is used as reference. Assuming the scattering rates and frequencies has the relationship of

$$\frac{\kappa_s(at f_2)}{\kappa_s(at f_1)} = \left(\frac{f_2}{f_1}\right)^n \quad (9)$$

where  $f_1$  and  $f_2$  are the frequencies,  $\kappa_s$  is the scattering rate at a specific frequency, and  $n$  is the index of frequency dependence.

# **NASA/TM-2002-210004/Rev3-Vol1**

**James L. Mueller<sup>1</sup> and Giulietta S. Fargion<sup>2</sup>**  
**Editors**

<sup>1</sup> *CHORS, San Diego State University, San Diego, California*

<sup>2</sup> *Science Applications International Corporation, Beltsville, Maryland*

## **Ocean Optics Protocols For Satellite Ocean Color Sensor Validation, Revision 3, Volume 1**

J. L. Mueller, C. Pietras, S. B. Hooker, D. K. Clark, A. Morel, R. Frouin, B.G. Mitchell,  
R. R. Bidigare, C. Trees, J. Werdell, G. S. Fargion, R. Arnone, R. W. Austin, S. Bailey,  
W. Broenkow, S. W. Brown, K. Carder, C. Davis, J. Dore, M. Feinholz, S. Flora, Z.P.  
Lee, B. Holben, B. C. Johnson, M. Kahru, D. M. Karl, Y. S Kim, K. D. Knobelspiesse, C.  
R. McClain, S. McLean, M. Miller, C. D. Mobley, J. Porter, R.G. Steward, M. Stramska,  
L. Van Heukelem, K. Voss, J. Wieland, M. A. Yarbrough and M. Yuen.

National Aeronautical and  
Space administration

**Goddard Space Flight Space Center**  
Greenbelt, Maryland 20771

**February 2002**

## *Chapter 8*

# **Stability Monitoring of Field Radiometers Using Portable Sources**

Stanford B. Hooker

*NASA Goddard Space Flight Center, Greenbelt, Maryland*

## **8.1 INTRODUCTION**

Mueller and Austin (1995) included a discussion on tracking instrument performance in between calibration activities with stable lamp sources in rugged, fixed geometric configurations. The recommended specifications of the device included the stability of the lamp output and the repeatability of measurement must be sufficient to detect 2 % variations in an instrument's performance. In terms of the protocols for using the source, it was recommended that an instrument should be connected to the portable standard and its response recorded daily, keeping a record of instrument responsivity throughout an experiment. Furthermore, these sources would provide an essential warning of problems if they appear.

One of the more important requirements in the use of the portable source was it must be available when the complete radiometric calibrations are performed, so a baseline may be established and maintained for each sensor channel, but recognizing that the source cannot be a substitute for complete calibrations. The temporal record they provide will, however, be invaluable in cases where the pre-and post-cruise calibrations disagree or if the instrument is disturbed, e.g., opened between calibrations, subjected to harsh treatment during deployment or transport, or if the data quality are otherwise suspect. These portable standards are an important part of the recommended instrument package.

## **8.2 The SQM**

Although Mueller and Austin (1995) specified the need for, and described some of the requirements of, a portable source, no such device was then commercially available. In response to the need for a portable source, NASA and NIST developed the SQM. The engineering design and characteristics of the SQM are described by Johnson et al. (1998), so only a brief description is given here. A separate rack of electronic equipment, composed principally of two computer controlled power supplies and a multiplexed, digital voltmeter (DVM), are an essential part of producing the stable light field. All of the external components are controlled by a computer program over a general purpose interface bus (GPIB).

The SQM has two sets of halogen lamps with eight lamps in each set; both lamp sets are arranged symmetrically on a ring and operate in series, so if one lamp fails, the entire set goes off. The lamps in one set are rated for 1.05 A (4.2 V) and are operated at 0.95 A, and the lamps in the other set are rated for 3.45 A (5.0 V) and are operated at 3.1 A; the lamp sets are hereafter referred to as the 1 A and 3 A lamps, respectively. The lamps are operated at approximately 95 % of their full amperage rating to maximize the lifetime of the lamps.

A low, medium, and high intensity flux level is provided when the 1 A, 3 A, and both lamp sets are used, respectively. Each lamp set was aged for approximately 50 hours before deploying the SQM to the field. The interior light chamber has bead-blasted aluminum walls, so the diffuse component of the reflectance is significant. The lamps illuminate a circular plastic diffuser protected by safety glass and sealed from the environment by o-rings. The diffuser is resilient to ultraviolet yellowing, but can age nonetheless. The exit aperture is 20 cm in diameter and has a spatial uniformity of 98 % or more over the interior 15 cm circle. The SQM does not have, nor does it require, an absolute calibration, but it has design objectives of better than 2 % stability during field deployments.

A faceplate or *shadow collar* provides a mounting assembly, so the device under test (DUT), usually a radiance or irradiance sensor, can be positioned in the shadow collar. The DUT has a D-shaped collar fitted to it at a set distance, 3.81 cm (1.5 inch), from the front of the DUT. This distance was chosen based on the most restrictive clearance requirement of the radiometers used in the different deployment rigs. The D-shaped collar ensures the DUT can be mounted to the SQM at a reproducible location and orientation with respect to the exit aperture each time the DUT is used.

## SeaWiFS Postlaunch Technical Report Series

Stanford B. Hooker, Editor

*NASA Goddard Space Flight Center  
Greenbelt, Maryland*

Elaine R. Firestone, Senior Scientific Technical Editor

*Science Applications International Corporation  
Beltsville, Maryland*

## Volume 19, Coastal Atmosphere and Sea Time Series (CoASTS), Part 1: A Tower-Based, Long-Term Measurement Program

Giuseppe Zibordi

Jean-François Berthon

John P. Doyle

Stefania Grossi

Dirk van der Linde

Cristina Targa

*JRC Space Applications Institute  
Ispra, Italy*

Luigi Alberotanza

*CNR Institute for the Study of Dynamics of Large Masses  
Venice, Italy*



## ABSTRACT

The Coastal Atmosphere and Sea Time Series (CoASTS) Project, aimed at supporting ocean color research and applications, from 1995 up to the time of publication of this document, has ensured the collection of a comprehensive atmospheric and marine data set from an oceanographic tower located in the northern Adriatic Sea. The instruments and the measurement methodologies used to gather quantities relevant for bio-optical modeling and for the calibration and validation of ocean color sensors, are described. Particular emphasis is placed on four items: 1) the evaluation of perturbation effects in radiometric data (i.e., tower-shading, instrument self-shading, and bottom effects); 2) the intercomparison of seawater absorption coefficients from *in situ* measurements and from laboratory spectrometric analysis on discrete samples; 3) the intercomparison of two filter techniques for *in vivo* measurement of particulate absorption coefficients; and 4) the analysis of repeatability and reproducibility of the most relevant laboratory measurements carried out on seawater samples (i.e., particulate and yellow substance absorption coefficients, and pigment and total suspended matter concentrations). Sample data are also presented and discussed to illustrate the typical features characterizing the CoASTS measurement site in view of supporting the suitability of the CoASTS data set for bio-optical modeling and ocean color calibration and validation.

## 1. INTRODUCTION

Optical measurements from space enable estimates of the concentration of materials suspended or dissolved in seawater (i.e., pigment, sediment, and colored dissolved organic matter) which are of great relevance in environmental and climate-related studies. Because of this, a number of new advanced ocean color sensors were designed to support oceanographic studies and applications including the Modular Opto-electronic Sensor (MOS), the Ocean Color and Temperature Scanner (OCTS), the Polarization and Directionality of the Earth's Reflectance (POLDER) sensor, the Sea-viewing Wide Field-of-view Sensor (SeaWiFS), the Moderate Resolution Imaging Spectroradiometer (MODIS), and the Medium Resolution Imaging Spectrometer (MERIS). All of these sensors were successfully launched and have contributed significantly to the general problem of inverting optical measurements to derive concentration estimates of biogeochemical parameters; several continue to provide regular coverage of the global biosphere.

To ensure a better exploitation of the data supplied by spaceborne sensors, national and international calibration and validation projects have been started. Their major objectives are the development of the bio-optical algorithms required for extracting quantitative information from space data; the validation of products obtained from satellite imagery; and the indirect absolute calibration (i.e., vicarious calibration) of the radiometers in space. All of these activities require comprehensive *in situ* atmospheric and marine measurements. In agreement with this requirement, the Coastal Atmosphere and Sea Time Series (CoASTS) Project was set up at the Joint Research Centre (JRC) in Ispra, Italy to support bio-optical modeling and ocean color calibration and validation exercises at a coastal site in the northern Adriatic Sea.

In order to provide a comprehensive overview of the CoASTS measurement activities, this report has three primary objectives:

- 1) Present the instrumentation and the measurement methodologies,
- 2) Assess the accuracy of the most relevant measurements needed for bio-optical modeling as well as ocean color vicarious calibration and algorithm validation activities; and
- 3) Discuss sample data that display the relevant features of the measurement site.

## 10. CONCLUSIONS

This report presented the measurement program used within the CoASTS Project (at the AAOT site) and extensively discussed the applied methods with a particular emphasis on those more relevant for bio-optical modeling and the calibration and validation of ocean color sensors. The methods discussed for the analysis of radiometric measurements highlighted the importance of correcting in-water radiance and irradiance data from superstructure (tower-shading) effects, instrument self-shading, and bottom effects. These perturbations for the specific measurement conditions analyzed in this study, may induce an overall spectral uncertainty in  $L_u(0^-\lambda)$  ranging from 4–18% at 412 nm, –2 to +10% at 490 nm, –9 to +10% at 555 nm, and 6–16% at 665 nm.

The intercomparison of seawater absorption coefficients from AC-9 *in situ* measurements and from laboratory spectrometric analysis of discrete seawater samples, showed the best agreement when the scattering correction—for perturbation effects induced in AC-9 data by the finite acceptance angle of the optics and the non-ideal reflective surface of the absorption chamber—is performed removing a variable percentage of the scattering coefficient. In this case, the scatterplots of the absorption coefficients from spectrometric analysis of seawater samples and AC-9 measurements showed average absolute percentage differences of –2, –19, –18, and –18% at 412, 488, 555, and 676 nm, respectively.

## SeaWiFS Postlaunch Technical Report Series

Stanford B. Hooker, Editor

*NASA Goddard Space Flight Center  
Greenbelt, Maryland*

Elaine R. Firestone, Senior Scientific Technical Editor

*Science Applications International Corporation  
Beltsville, Maryland*

## Volume 20, Coastal Atmosphere and Sea Time Series (CoASTS), Part 2: Data Analysis

Jean-François Berthon

Giuseppe Zibordi

John P. Doyle

Stefania Grossi

Dirk van der Linde

Cristina Targa

*JRC Space Applications Institute  
Ispira, Italy*



## ABSTRACT

In this document, the first three years of a time series of bio-optical marine and atmospheric measurements are presented and analyzed. These measurements were performed from an oceanographic tower in the northern Adriatic Sea within the framework of the Coastal Atmosphere and Sea Time Series (CoASTS) project, an ocean color calibration and validation activity. The data set collected includes spectral measurements of the in-water apparent (diffuse attenuation coefficient, reflectance,  $Q$ -factor, etc.) and inherent (absorption and scattering coefficients) optical properties, as well as the concentrations of the main optical components (pigment and suspended matter concentrations). Clear seasonal patterns are exhibited by the marine quantities on which an appreciable short-term variability (on the order of a half day to one day) is superimposed. This short-term variability is well correlated with the changes in salinity at the surface resulting from the southward transport of freshwater coming from the northern rivers. Concentrations of chlorophyll  $a$  and total suspended matter span more than two orders of magnitude. The bio-optical characteristics of the measurement site pertain to both Case-1 (about 64%) and Case-2 (about 36%) waters, based on a relationship between the beam attenuation coefficient at 660 nm and the chlorophyll  $a$  concentration. Empirical algorithms relating in-water remote sensing reflectance ratios and optical components or properties of interest (chlorophyll  $a$ , total suspended matter, and the diffuse attenuation coefficient) are presented.

## 1. INTRODUCTION

The use of remotely-sensed ocean color data has increased considerably over the last years, since several new sensors were put in orbit more than 10 years after the Coastal Zone Color Scanner (CZCS) ceased its activity. These sensors, specifically, the Sea-viewing Wide Field-of-view Sensor (SeaWiFS), the Ocean Color and Temperature Scanner (OCTS), the Marine Optical Spectroradiometer (MOS), the Moderate Resolution Imaging Spectroradiometer (MODIS), and the Medium Resolution Imaging Spectrometer (MERIS), present advanced characteristics compared to CZCS, in the addition of a certain number of channels, and an increased signal-to-noise ratio and dynamic range (IOCCG 1998). These increased capacities are intended, in particular, to improve the retrieval of chlorophyll  $a$  concentration in the open ocean (Hooker et al. 1992 and O'Reilly et al. 1998), as well as eventually allowing the retrieval of additional marine quantities such as total suspended matter or colored dissolved organic matter (Carder et al. 1999).

For the open ocean, the possibility of retrieving chlorophyll  $a$  and additional water components from remotely-sensed data is presumably simplified, because in most cases, they all co-vary (but see Carder et al. 1991). In coastal waters (where most of the so-called optical "Case-2" waters can be found), however, this retrieval is less successful. In effect, because of the diversity of the sources (rivers, atmospheric input, bottom resuspension, etc.) the simplifying assumption of co-variation may not be verified. Consequently, by contributing—often antagonistically—to the total marine signal, the occurrence of these different components makes their separation much more difficult on an optical basis.

As a consequence of the number of sensors now operational, there is an increasing demand for *in situ* bio-optical data (water and atmosphere) in order to address two main topics:

- 1) The development of models and algorithms allowing the retrieval of marine and atmospheric quantities from the signal at the top of the atmosphere; and
- 2) The vicarious calibration of the sensors, and the validation of their different products.

Programs including time-series of measurements on specific sites such as the Marine Optical Buoy (MOBY, Clark et al. 1997), the Yamato Bank Optical Mooring (YBOM, Kishino et al. 1997), and the Plymouth Marine Bio-Optical Data Buoy (PlyMBODY, Pinkerton and Aiken 1999), or repetitive ship cruises such as the Atlantic Meridional Transect (AMT) program (Aiken et al. 2000) were developed considerably in the past years. Basing the investigation of the environment on a long time or space scale, one of their objectives was, in particular, to encompass a wide range of optical properties and concentration of optically significant components.

In this context, a program of extensive *in situ* measurements called the Coastal Atmosphere and Sea Time Series (CoASTS), was set up (Zibordi et al. 2002). Within this program, a series of marine and atmospheric measurements are performed from an oceanographic tower located in the northern Adriatic Sea, off the Venice Lagoon. As of this writing, the project has provided more than six years of data (with a frequency of 1–2 campaigns per month) including water apparent and inherent optical properties and the corresponding optically significant components, as well as atmospheric measurements, which allows for the estimation of aerosol properties. The resulting data set was

NASA Technical Memorandum 2002–206892, Volume 17

## SeaWiFS Postlaunch Technical Report Series

Stanford B. Hooker, Editor

*NASA/Goddard Space Flight Center  
Greenbelt, Maryland*

Elaine R. Firestone, Senior Scientific Technical Editor

*Science Applications International Corporation  
Beltsville, Maryland*

## Volume 17, The Seventh SeaWiFS Intercalibration Round-Robin Experiment (SIRREX-7), March 1999

Stanford B. Hooker

*NASA/Goddard Space Flight Center  
Greenbelt, Maryland*

Scott McLean

Jennifer Sherman

Mark Small

Gordana Lazin

*Satlantic, Inc.  
Halifax, Canada*

Giuseppe Zibordi

*JRC/SAI/Marine Environment Unit  
Ispra, Italy*

James W. Brown

*RSMAS/University of Miami  
Miami, Florida*

## ABSTRACT

This report documents the scientific activities during the seventh SeaWiFS Intercalibration Round-Robin Experiment (SIRREX-7) held at Satlantic, Inc. (Halifax, Canada). The overall objective of SIRREX-7 was to determine the uncertainties of radiometric calibrations and measurements at a single calibration facility. Specifically, this involved the estimation of the uncertainties in a) lamp standards, b) plaque standards (including the uncertainties associated with plaque illumination non-uniformity), c) radiance calibrations, and d) irradiance calibrations. The investigation of the uncertainties in lamp standards included a comparison between a calibration of a new FEL by the National Institute of Standards and Technology (NIST) and Optronic Laboratories, Inc. In addition, the rotation and polarization sensitivity of radiometers were determined, and a procedure for transferring an absolute calibration to portable light sources was defined and executed.

## Prologue

The Sea-viewing Wide Field-of-view Sensor (SeaWiFS) Project at the National Aeronautics and Space Administration (NASA) Goddard Space Flight Center (GSFC) has two important goals with respect to the spaceborne radiance measurements (Hooker and Esaias 1993): a) normalized water-leaving radiance with an uncertainty to within 5%, and b) chlorophyll *a* concentration with an uncertainty to within 35%. These goals are very ambitious, and can only be achieved by augmenting the SeaWiFS measurements with a program of ongoing validation measurements to a) verify the radiometric uncertainty and long-term stability of the SeaWiFS instrument's radiance responsivities, and b) validate the atmospheric correction models and algorithms used to convert SeaWiFS radiances to water-leaving radiances,  $L_W(\lambda)$ . One of the principal approaches to this critical aspect of the SeaWiFS mission are frequent direct comparisons between spaceborne and *in situ* measurements of  $L_W(\lambda)$ . Because there are many sources of uncertainty contributing to the final uncertainty objective (5%), each source must be minimized and kept at the lowest level possible. The goal for the calibration of the field instruments has always been to have reproducible calibrations from 400–850 nm as close to 1% as possible (with 2% as a hoped for upper limit).

The calibration goal for SeaWiFS field instruments is not only driven by a simple argument of sums. Given the myriad objectives associated with SeaWiFS validation, the only economically feasible approach for acquiring a large and globally distributed database of *in situ* radiometric measurements, is to solicit contributions of data from the oceanographic community at large. Such an approach demands an assurance that the aggregate data set will be of uniform quality, and one of the first points of quality control is maintaining a high standard for instrument calibration (Hooker and McClain 2000).

The entire process is more complicated than a careful scrutiny of calibration facilities, and the SeaWiFS Project is addressing this problem through the SeaWiFS Calibration and Validation Program (McClain et al. 1992). At

the outset, the Project sponsored a workshop to draft protocols for ocean optics measurements to support SeaWiFS validation (Mueller and Austin 1992), which included instrument performance specifications, and requirements for instrument characterization and calibration. The importance of the protocols to the community was established by the considerable expansion of the original document to accommodate a broader range of measurements, techniques, and sampling considerations (Mueller and Austin 1995).

The strategy adopted for the validation of the SeaWiFS remote sensing data is to calibrate all of the field instruments within a network consisting of the instrument manufacturers plus a few additional laboratories that have recurrently provided instrument calibrations. In recognition of the need to maintain internal consistency between calibrations of *in situ* instruments and that of the SeaWiFS instrument itself, the SeaWiFS Project, under the Calibration and Validation Program, implemented an ongoing series of SeaWiFS Intercalibration Round-Robin Experiments (SIRREXs). The objectives of the SIRREX activity, at each separate event and over time, are to accomplish the following:

1. Intercalibrate FEL lamp working standards of spectral irradiance and to reference each to the National Institute of Standards and Technology (NIST) scale of spectral irradiance via a secondary or tertiary standard;
2. Intercalibrate the integrating sphere sources of spectral radiance;
3. Intercompare the plaques used to transfer the scale of spectral irradiance from an FEL lamp to a scale of spectral radiance, as well as the support electronics involved (most critically shunts and voltmeters);
4. Evaluate the suitability of the equipment and laboratory methods being employed for radiometric calibrations at each institution; and
5. Intercompare radiometers in the field while evaluating the measurement protocols being used.

NASA Technical Memorandum 2002–206892, Volume 17

## SeaWiFS Postlaunch Technical Report Series

Stanford B. Hooker, Editor

*NASA/Goddard Space Flight Center  
Greenbelt, Maryland*

Elaine R. Firestone, Senior Scientific Technical Editor

*Science Applications International Corporation  
Beltsville, Maryland*

## Volume 17, The Seventh SeaWiFS Intercalibration Round-Robin Experiment (SIRREX-7), March 1999

Stanford B. Hooker

*NASA/Goddard Space Flight Center  
Greenbelt, Maryland*

Scott McLean

Jennifer Sherman

Mark Small

Gordana Lazin

*Satlantic, Inc.  
Halifax, Canada*

Giuseppe Zibordi

*JRC/SAI/Marine Environment Unit  
Ispra, Italy*

James W. Brown

*RSMAS/University of Miami  
Miami, Florida*

---

## Chapter 2

---

### SIRREX-7 Instrumentation

STANFORD B. HOOKER  
*NASA/Goddard Space Flight Center*  
*Greenbelt, Maryland*

SCOTT MCLEAN  
*Satlantic, Inc.*  
*Halifax, Canada*

#### ABSTRACT

The highest priority for the instrumentation used for SIRREX-7 was to bring together as wide a diversity of equipment used in the laboratory calibration and field measurement process as possible, so the agreed upon minimum number of replicates for a particular equipment type was three. Each participating group contributed more than one example of a particular equipment type, which ensured equipment with a wide range of ages, calibration histories, sensitivities, flux levels, etc. Equipment that was used as part of the digitization or control process, like voltmeters and shunts, were calibrated as close to the SIRREX-7 activity as possible; all other types of equipment were reviewed to ensure their calibration histories were within the guidelines prescribed by the manufacturer or the protocols governing their use (like lamps and plaques). In some cases, equipment that did not meet the recency of calibration requirements were used, so the effect of ignoring this practice (regardless of the reason) could be quantified. In addition, some equipment with known problems were included to see if the outer range of variance in the results was defined by substandard equipment or if other factors (like operator error) were more important.

---

## 2.1 INTRODUCTION

The equipment used during SIRREX-7 was representative of the instrumentation used on a regular basis by the ocean color community either for laboratory calibration or field measurements. Although several manufacturers were not represented in the suite of instruments used, the functionality of the missing devices was represented, so individual groups using nonrepresentative equipment can still derive lessons and conclusions from SIRREX-7. With a small number of participants, it was not feasible to accept the added complexity of differing instruments; by using predominantly one manufacturer, it was possible to maximize the number of experiments or the number of replicate samplings within an experiment over the relatively short time period of the activity.

## 2.2 LAMPS

Many laboratories base their absolute calibrations of irradiance and radiance responsivities on the NIST scale of spectral irradiance, which is available to the wider community through calibrated tungsten-halogen FEL lamps (Walker et al. 1987). Some laboratories acquire a calibrated FEL lamp standard of spectral irradiance directly

from NIST, but more typically, a laboratory bases its irradiance scale on a lamp which was calibrated and certified as traceable to the NIST scale by a commercial standardizing laboratory. The former are usually referred to as *secondary* standards, and the latter as *tertiary* standards. In some cases, a laboratory will purchase additional seasoned, but uncalibrated lamps, and transfer the spectral irradiance scale from their primary calibrated lamp using a transfer radiometer (the JRC was experimenting with this approach using L005). The use of less expensive standards for calibration experiments is a common practice in most cases, because it avoids a shortening in the useful lifetime of the primary reference lamp. One of the questions addressed here is what extra uncertainty is associated with this cost-effective practice.

Another type of lamp is the so-called *working lamp*. This lamp is used for illumination requirements in keeping with FEL light levels wherein it would not be prudent or cost effective to reduce the lifetime of a standard lamp. Detailed information about the standard and working lamps used during SIRREX-7 is presented in Table 5. The former are indicated by the “L” codes and the latter by the “W” codes.



NASA Technical Memorandum 2002–206892, Volume 17

## SeaWiFS Postlaunch Technical Report Series

Stanford B. Hooker, Editor

*NASA/Goddard Space Flight Center  
Greenbelt, Maryland*

Elaine R. Firestone, Senior Scientific Technical Editor

*Science Applications International Corporation  
Beltsville, Maryland*

## Volume 17, The Seventh SeaWiFS Intercalibration Round-Robin Experiment (SIRREX-7), March 1999

Stanford B. Hooker

*NASA/Goddard Space Flight Center  
Greenbelt, Maryland*

Scott McLean

Jennifer Sherman

Mark Small

Gordana Lazin

*Satlantic, Inc.  
Halifax, Canada*

Giuseppe Zibordi

*JRC/SAI/Marine Environment Unit  
Ispra, Italy*

James W. Brown

*RSMAS/University of Miami  
Miami, Florida*

---

# Chapter 1

---

## SIRREX-7 Overview

STANFORD B. HOOKER  
*NASA/Goddard Space Flight Center*  
*Greenbelt, Maryland*

SCOTT MCLEAN  
*Satlantic, Inc.*  
*Halifax, Canada*

### ABSTRACT

The primary objective of SIRREX-7 was a thorough inquiry into the absolute capability of a single calibration facility. A small team of investigators was assembled to address this question at Satlantic, Inc. The experimental group was kept small, because the entire activity had to take place in a single room with a small number of experimental stations. Because this required a substantial commitment in time and resources, there was a strong desire to learn as much as possible about the equipment and methods normally used in the calibration process. Consequently, a wide diversity of each equipment type was assembled: 10 FEL lamps, 7 reflectance plaques, 10 fixed wavelength radiometers, 1 hyperspectral radiometer, the SXR, 1 single-channel mapping (narrow field-of-view) radiometer, plus the original SQM and 4 SQM-IIs. The instrumentation came from three different organizations with differing calibration and measurement objectives, so the assembled equipment had a diverse range of calibration histories, ages, sizes, intended uses, sensitivities, flux levels, etc. Although SIRREX-7 was conducted at only one facility, the diversity in equipment ensures that a significant subset of the results achieved will have a wider applicability to the larger community.

---

## 1.1 INTRODUCTION

The determination of the absolute radiometric response of an irradiance or radiance sensor requires a properly staffed and equipped calibration facility. For SeaWiFS calibration and validation activities, the latter must include stable sources and sensors with defined spectral radiometric characteristics traceable to NIST. The calibration facility must also have a variety of specialized radiometric and electronic equipment, including reflectance plaques, spectral filters, integrating spheres, and highly regulated power supplies for the operation of the lamps. Precision electronic measurement capabilities are also required, both for setting and monitoring lamp current and voltage, and for measuring the output of the radiometer.

Although there have been six previous SIRREXs and significant progress was made at each one, in terms of understanding the sources of uncertainties in radiometric calibrations, a thorough inquiry into the absolute capability of a calibration facility regularly used by the ocean color community was not investigated. This was an important task, because, as already mentioned, the goal of a calibration facility used for SeaWiFS validation is to provide reproducible calibrations from 400–850 nm to within  $\pm 1\%$ .

SIRREX-7 was convened with a small team of investigators to estimate calibration uncertainties at Satlantic, Inc. The experimental group was kept small, because the entire activity had to take place in a single room. Satlantic agreed to be the hosting organization, because:

1. Many SeaWiFS and SIMBIOS investigators rely on Satlantic equipment and calibrations;
2. They have a state-of-the-art facility (all calibrations are done in a clean room with exceptional baffling and optical alignment equipment);
3. They commercialized the original SQM (so several units were available for an absolute intercomparison experiment); and
4. They have the interest and commitment (having participated in all of the previous SIRREXs) to underwrite the significant financial requirements for the hosting organization.

A final uncertainty budget for any instrument requires a thorough understanding of laboratory and field performance. The SeaWiFS Project participated to provide expertise and unique equipment (the original SQM and SXR), a variety of sources and targets (plaques, FEL lamps, etc.),

NASA Technical Memorandum 2002–206892, Volume 17

## SeaWiFS Postlaunch Technical Report Series

Stanford B. Hooker, Editor

*NASA/Goddard Space Flight Center  
Greenbelt, Maryland*

Elaine R. Firestone, Senior Scientific Technical Editor

*Science Applications International Corporation  
Beltsville, Maryland*

## Volume 17, The Seventh SeaWiFS Intercalibration Round-Robin Experiment (SIRREX-7), March 1999

Stanford B. Hooker

*NASA/Goddard Space Flight Center  
Greenbelt, Maryland*

Scott McLean

Jennifer Sherman

Mark Small

Gordana Lazin

*Satlantic, Inc.  
Halifax, Canada*

Giuseppe Zibordi

*JRC/SAI/Marine Environment Unit  
Ispra, Italy*

James W. Brown

*RSMAS/University of Miami  
Miami, Florida*

---

## Chapter 8

---

### Absolute Calibration of the SQM and SQM-II

STANFORD B. HOOKER  
*NASA/Goddard Space Flight Center*  
*Greenbelt, Maryland*

SCOTT MCLEAN  
GORDANA LAZIN  
*Satlantic, Inc.*  
*Halifax, Canada*

#### ABSTRACT

To better understand the capability of portable sources, a series of experiments were conducted to transfer an absolute calibration to the original SQM and four SQM-IIs, and to map the homogeneity of an SQM-II exit aperture. Approximately 25% of the central portion of the exit aperture was within 2% of the maximum signal, and about 40% was to within 5%. The decay in SQM flux over a 500 day time period, which included one shipping event, was estimated to be approximately 0.9% every 100 days. The decay for an SQM-II (S/N 004) over the same time period, but encompassing four shipping events, was approximately 2.2% every 100 days. The average and standard deviations in the coefficient of variation was used as a stability parameter for the SQM and SQM-II. Both sources showed a spectral dependence with the greatest stability in the red part of the spectrum, and the least stability in the blue. The standard deviation in the coefficient of variation was independent of wavelength for the SQM, but the SQM-II had a noticeable spectral dependence—the reddest wavelength (775 nm) had a standard deviation approximately half that of the blue wavelengths. Using the overall averages as generalized metrics for stability, the SQM was more stable than the SQM-II: the overall average was a factor of three smaller, and the overall standard deviation was an order of magnitude smaller.

---

## 8.1 INTRODUCTION

Most SeaWiFS validation campaigns have been on Atlantic Meridional Transect (AMT) cruises (Aiken et al. 2000), which occur twice a year and involve a transit of the Atlantic Ocean between Grimsby (UK) and Stanley (Falkland Islands) with a port call in Montevideo (Uruguay). In all of the AMT cruises the SQM was a part of, it was shipped long distances between the US, the UK, and the Falkland Islands or Uruguay (also once to South Africa) with no negative effects on performance both during the cruise time period and between cruises.

The SQM lamps were changed after its commissioning to produce a flux level more in keeping with the radiometers being deployed on AMT cruises, but the same lamp set was used during AMT-5 through AMT-7 (another lamp change was made after AMT-7 to fine tune the flux levels). During the design stage of the SQM, there was some controversy about running the lamps below their rated current (approximately 95% of rating), but there has been no observable degradation in the performance of the lamps as a

result of this—indeed, they have survived long shipment routes using a variety of transportation vehicles (trucks, planes, etc.) on repeated occasions, as well as, the high vibration environment of a ship.

Figure 30 is a summary of SQM performance during the AMT-5 through AMT-7 time period (spanning 460 days). It shows the internal blue monitor signal, measured with the glass fiducial, as a function of time, but presented as the percent difference with respect to the mean value for the entire time period. A confirmation of the signal is given by the R035 radiometer for the 443 nm channel (which is very similar to the blue internal monitor), and it very nearly mirrors the internal monitor signal. The two detectors yield similar decay rates of approximately 0.007% per day, or approximately 0.25% for a 35-day cruise. This is an underestimate, however, because the degradation is due mostly to lamp usage, and this is most significant during use, and not during shipping and storage. This is best seen by looking at the individual cruises, and comparing them to the laboratory work after AMT-7.

NASA Technical Memorandum 2002–206892, Volume 17

## SeaWiFS Postlaunch Technical Report Series

Stanford B. Hooker, Editor

*NASA/Goddard Space Flight Center  
Greenbelt, Maryland*

Elaine R. Firestone, Senior Scientific Technical Editor

*Science Applications International Corporation  
Beltsville, Maryland*

## Volume 17, The Seventh SeaWiFS Intercalibration Round-Robin Experiment (SIRREX-7), March 1999

Stanford B. Hooker

*NASA/Goddard Space Flight Center  
Greenbelt, Maryland*

Scott McLean

Jennifer Sherman

Mark Small

Gordana Lazin

*Satlantic, Inc.  
Halifax, Canada*

Giuseppe Zibordi

*JRC/SAI/Marine Environment Unit  
Ispra, Italy*

James W. Brown

*RSMAS/University of Miami  
Miami, Florida*



---

## Chapter 5

---

### Uncertainties in Radiance Calibrations

STANFORD B. HOOKER  
NASA/Goddard Space Flight Center  
Greenbelt, Maryland

SCOTT MCLEAN  
JENNIFER SHERMAN  
Satlantic, Inc.  
Halifax, Canada

#### ABSTRACT

Three types of experiments were conducted to estimate the uncertainties in radiance calibrations using a plaque and FEL lamp: a) The average repeatability uncertainty (based on one plaque and one FEL used with 11 trials for three different radiometers) was less than 0.1% (0.06% in the blue-green part of the spectrum and 0.09% in the red); b) the uncertainty that can be removed from radiance calibrations if ambient rather than dark measurements are used was 0.13% (0.11% in the blue-green and 0.17% in the red); and c) the overall uncertainty from secondary reflections, (for example, originating from an alignment laser) was 0.11% (0.06% in the blue-green wavelength domain and 0.19% in the red).

---

## 5.1 INTRODUCTION

The calibration coefficient for a radiance sensor (identified by  $S_{ID}$ ) is computed using a plaque (identified by  $T_{ID}$ ) with a calibrated reflectance,  $R_{T_{ID}}^{\text{cal}}$ , plus a standard lamp (identified by  $L_{ID}$ ) with a calibrated irradiance,  $E_{L_{ID}}^{\text{cal}}$ . The general procedures require the lamp to be positioned a distance  $d$  on axis and normal to the center of the plaque (specific details for each step are given in Sect. 1.5). The radiance sensor is capped, and dark voltage levels for the sensor are recorded. An average dark level for each channel,  $\bar{D}_{S_{ID}}(\lambda)$ , is calculated from the dark samples.

The radiance sensor is positioned to view the plaque at  $45^\circ$  with respect to the lamp illumination axis<sup>†</sup>. The lamp is powered on, and the voltage levels of the individual sensor channels are recorded, from which an average calibration voltage for each channel,  $\bar{V}_{S_{ID}}(\lambda)$ , is obtained. The calibration coefficient is calculated as:

$$C_{S_{ID}}^{\text{Rad}}(\lambda) = \frac{\frac{1}{\pi} R_{T_{ID}}^{\text{cal}}(\lambda) E_{L_{ID}}^{\text{cal}}(\lambda, 50)}{\bar{V}_{S_{ID}}(\lambda) - \bar{D}_{S_{ID}}(\lambda)} \left[ \frac{50 \text{ cm}}{d} \right]^2, \quad (10)$$

where  $d$  is given in centimeters.

---

<sup>†</sup> An alternative angle for which the reflectance of the plaque is known is also acceptable, but for all of the SIRREX-7 experiments,  $45^\circ$  was the calibrated reflectance angle of the plaque and the corresponding sensor viewing angle.

Three types of experiments were conducted to explore the uncertainties associated with radiance calibrations: a) one plaque and one FEL were used with three OCR-200 radiometers to estimate the repeatability uncertainty in radiance calibrations (based on 11 trials for each sensor); b) three OCR-200 sensors and the SXR were used to explore the uncertainties in ambient versus dark measurements; and c) the uncertainty from secondary reflections used in the calibration process (in this case, an alignment laser) was measured with the SXR and three OCR-200 sensors.

## 5.2 RADIANCE REPEATABILITY

The uncertainties in radiance calibrations were estimated by independently calibrating three OCR-200 sensors (R035, R036, and R067) 11 times each (following the usual procedures). The trials were all with the same plaque and FEL, but the lamp was not powered on and off each time; it was left on to minimize lamp usage time (standard FEL lamps are too expensive to include the warm-up time for each trial in the experiment).

### 5.2.1 Equipment

The equipment used for the radiance repeatability trials was as follows:

- Satlantic Optronics lamp F-547 (L008);
- Satlantic white (18 in) plaque 05816 (T001);

NASA Technical Memorandum 2002–206892, Volume 17

## SeaWiFS Postlaunch Technical Report Series

Stanford B. Hooker, Editor

*NASA/Goddard Space Flight Center  
Greenbelt, Maryland*

Elaine R. Firestone, Senior Scientific Technical Editor

*Science Applications International Corporation  
Beltsville, Maryland*

## Volume 17, The Seventh SeaWiFS Intercalibration Round-Robin Experiment (SIRREX-7), March 1999

Stanford B. Hooker

*NASA/Goddard Space Flight Center  
Greenbelt, Maryland*

Scott McLean

Jennifer Sherman

Mark Small

Gordana Lazin

*Satlantic, Inc.  
Halifax, Canada*

Giuseppe Zibordi

*JRC/SAI/Marine Environment Unit  
Ispra, Italy*

James W. Brown

*RSMAS/University of Miami  
Miami, Florida*

---

## Chapter 7

---

### Rotation and Polarization Uncertainties

STANFORD B. HOOKER  
*NASA/Goddard Space Flight Center*  
*Greenbelt, Maryland*

SCOTT MCLEAN  
 MARK SMALL  
*Satlantic, Inc.*  
*Halifax, Canada*

#### ABSTRACT

Separate experiments were conducted during SIRREX-7 to estimate the rotation and polarization uncertainties of radiometers during the calibration process. Rotational uncertainties for radiance sensors were usually less than 1%, with single and multiple aperture systems having average rotational uncertainties of 0.2–0.3% and 0.4–0.9%, respectively. Rotational uncertainties for a multiple aperture irradiance sensor was 0.7% on average, which was in close agreement with multiple aperture radiance sensors. The only significant spectral dependence was with an OCR-2000 (hyperspectral) sensor which had maximal effects in the bluest and reddest wavelengths and minimal effects in the green domain. The average polarization parameter, in percent, varied between 0.6–4.6%. The Satlantic instruments had an average polarization below 2.0%, but the OCR-200 sensors showed maximum polarization sensitivity in the blue part of the spectrum (1.4–2.4%), while the OCR-2000 instrument had maximum sensitivity in the red wavelength domain (2.1–2.6%).

---

## 7.1 INTRODUCTION

Two different experiments were designed to estimate the rotation and polarization effects on the calibration process. Although the former can be considered as a mechanical positioning problem, there are practical aspects of the problem which are more associated with the usual methods used during instrument calibration. For example, the angular positioning of the sensor during the calibration process is usually not maintained from one calibration to the next (in fact, many commercial radiometers are cylindrical and are not explicitly indexed), and the mounting hardware used is not always the best for reproducing an indexing scheme. The D-shaped collar was designed to overcome this limitation, and when used with a V-block is much easier to use for repositioning requirements than a ring carrier. In comparison, polarization is mostly an instrument design problem, with a design objective that is set by the optical protocols being used.

## 7.2 ROTATION EFFECTS

Two experiments were conducted to estimate the rotation sensitivity of radiance and irradiance sensors during the calibration process. Most Satlantic radiometers (e.g.,

the OCR-200 and OCR-1000 series of instruments) have separate apertures for each channel organized in one or more circular arrays around a central channel (Fig. 3), so changes in the orientation of the sensor in a V-block or ring mount will necessarily cause a change in what part of the plaque is viewed during the calibration process. The objective of the rotation experiments was to determine the level of uncertainty that can be associated with this part of the sensor positioning process.

Custom rotator mount adapters, which took advantage of the D-shaped collars, were built for the OCI-200 and OCR-200 series of radiometers. Separate custom adapters were also built for the SXR and the OCR-2000 instruments. The latter two also required a mechanical support (a V-block) to stabilize the large housings of these instruments during the rotation process. Although this helped maintain the stability of the large mass of these instruments during rotation, it did not ensure an axial symmetry for all trials, and some data were not used, because of unbalanced rotation.

### 7.2.1 Rotation of Radiance Sensors

Four types of radiance sensors were used for the rotation sensitivity experiments: R035, R064, P002, and X001.

NASA Technical Memorandum 2002–206892, Volume 21

## SeaWiFS Postlaunch Technical Report Series

Stanford B. Hooker, Editor

*NASA Goddard Space Flight Center  
Greenbelt, Maryland*

Elaine R. Firestone, Senior Scientific Technical Editor

*Science Applications International Corporation  
Beltsville, Maryland*

## Volume 21, The Eighth SeaWiFS Intercalibration Round-Robin Experiment (SIRREX-8), September–December 2001

Giuseppe Zibordi

Davide D’Alimonte

Dirk van der Linde

Jean-François Berthon

*JRC/Institute for Environment and Sustainability  
Ispra, Italy*

Stanford B. Hooker

*NASA/Goddard Space Flight Center  
Greenbelt, Maryland*

James L. Mueller

*SDSU/Center for Hydro-Optics and Remote Sensing  
San Diego, California*

Gordana Lazin

Scott McLean

*Satlantic, Inc.  
Halifax, Canada*

---

## Chapter 2

---

### The CHORS Immersion Factor Method

STANFORD B. HOOKER

*NASA/Goddard Space Flight Center  
Greenbelt, Maryland*

JAMES L. MUELLER

*SDSU/Center for Hydro-Optics and Remote Sensing  
San Diego, California*

GIUSEPPE ZIBORDI

*JRC/IES/Inland and Marine Waters Unit  
Ispra, Italy*

#### ABSTRACT

The CHORS method for experimentally determining the immersion factor for irradiance sensors is based on the method developed at the Visibility Laboratory for this measurement. It uses tap water and has the following major features: a) it uses a large covered tank with a sensor support system, which places the radiometer well above the turbulence associated with filling and emptying the tank (the volume of water below the sensor is greater than the amount above the sensor) or any perturbations from the bottom of the tank, so the interior of the tank (when covered) is especially *black*; b) it uses a 400 W lamp with a very small filament, so the light source very nearly approximates a point source; and c) it uses an adjustable final baffle to ensure the cone of light illuminating the in-water sensor is as small as possible.

---

## 2.1 INTRODUCTION

The CHORS laboratory procedure for characterizing immersion coefficients for an irradiance sensor was first described in Petzold and Austin (1988). The apparatus used was designed to accept a large variety of sensor types, both large and small, from different manufacturers. Although measurement accuracy was an important objective of the method, another priority was to be able to execute the measurement process in a time-efficient manner.

## 2.2 LABORATORY SETUP

The characterization of immersion factors at CHORS took place in a *high-bay* facility adjacent to the room used for radiometric calibrations. The walls and ceiling of the facility were painted flat black to remove any significant sources of reflected or secondary illumination.

A schematic of the CHORS measurement system for measuring  $I_f(\lambda)$  for cosine collectors, is shown in Fig. 2. It consisted primarily of a large fiberglass tank in which the radiometer to be characterized could be immersed, a screened 400 W tungsten-halogen lamp with a power supply (PS) and multiple baffles, a reference radiometer to monitor the lamp, and a ducted fan to keep the lamp and

reference cooled. The in-water sensor was placed in a support frame on top of a grated platform. The platform was covered with a fine black mesh and provided two functions:

1. It significantly reduced any water turbulence during the filling (and, to a lesser extent, the draining) of the tank; and
2. It provided a horizontal surface which allowed the sensor support frame to be accurately leveled and positioned within the baffled light field.

To reduce light reflections within the tank, the interior was painted with an exterior flat black paint, and the metal surfaces of the grated platform plus the sensor support frame were covered with black tape or black paint. The inside of the tank lid was painted black, and a large opening in the lid was fitted with a black curtain which could be drawn back to permit easy access to the inside of the tank.

The sensor support frame was composed primarily of a tube with an inner diameter just a little larger than the outer diameter of the in-water radiometer. A D-shaped collar was fitted to each in-water sensor which leveled the radiometer against the top of the tube. The flat side of the D-shaped collar (Fig. 1) was used as a coarse alignment reference to ensure the radiometer was positioned in a reproducible fashion within the light field.



**NASA/TM-2002-210005**

## **SIMBIOS Project 2001 Annual Report**

Giulietta S. Fargion, Science Applications International Corporation, Maryland  
Charles R. McClain, Goddard Space Flight Center, Greenbelt, Maryland

National Aeronautics and  
Space Administration

**Goddard Space Flight Center**  
Greenbelt, Maryland 20771

March 2002

## Chapter 9

# Refinement of Protocols for Measuring the Apparent Optical Properties of Seawater

Stanford B. Hooker

*NASA/GSFC/SeaWiFS Project, Greenbelt, Maryland*

Giuseppe Zibordi and Jean-François Berthon

*JRC/IES/Inland and Marine Waters, Ispra, Italy*

André Morel and David Antoine

*CNRS/UPMC/Laboratoire d'Océanographie de Villefranche, Villefranche-sur-Mer, France*

## 9.1 INTRODUCTION

Ocean color satellite missions, like the Sea-viewing Wide Field-of-view Sensor (SeaWiFS) or the Moderate Resolution Imaging Spectroradiometer (MODIS) projects, are tasked with acquiring a global ocean color data set, validating and monitoring the accuracy and quality of the data, processing the radiometric data into geophysical units using a set of atmospheric and bio-optical algorithms, and distributing the final products to the scientific community. The long-standing objective of the SeaWiFS Project, for example, is to produce water-leaving radiances to within 5% absolute (Hooker and Esaias 1993). The accurate determination of upper ocean apparent optical properties (AOPs) is essential for the vicarious calibration of ocean color data and the validation of the derived data products, because the sea-truth measurements are the reference data to which the satellite are compared (Hooker and McClain 2000). The uncertainties associated with *in situ* AOP measurements have various sources, such as, the deployment and measurement protocols used in the field, the absolute calibration of the radiometers, the environmental conditions encountered during data collection, the conversion of the light signals to geophysical units in a data processing scheme, and the stability of the radiometers in the harsh environment they are subjected to during transport and use.

In recent years, progress has been made in estimating the magnitude of some of these uncertainties and in defining procedures for minimizing them. For the SeaWiFS Project, the first step was to convene a workshop to draft the SeaWiFS Ocean Optics Protocols. The protocols adhere to the Joint Global Ocean Flux Study (JGOFS) sampling procedures (Joint Global Ocean Flux Study 1991) and define the standards for

optical measurements to be used in SeaWiFS radiometric validation and algorithm development (Mueller and Austin 1992). The protocols are periodically updated as deficiencies are identified and outstanding issues are resolved (Mueller and Austin 1995, and Mueller 2000). The follow-on inquiries into controlling uncertainties investigated a variety of topics. The SeaWiFS Intercalibration Round-Robin Experiment (SIRREX) activity demonstrated that the uncertainties in the traceability between the spectral irradiance of calibration lamps were approximately 1.0%, and the intercomparisons of sphere radiance was approximately 1.5% in absolute spectral radiance and 0.3% in stability (Mueller et al. 1996). The first SeaWiFS Data Analysis Round Robin (DARR-94) showed differences in commonly used data processing methods were about 3–4% of the aggregate mean estimate (Siegel et al. 1995). Hooker and Aiken (1998) made estimates of radiometer stability using the SeaWiFS Quality Monitor (SQM), a portable and stable light source, and showed the stability of radiometers in the field during a 36-day deployment was on average to within 1.0% (although some channels occasionally performed much worse). More recently, Hooker and Maritorena (2000) quantified differences in the in-water methods and techniques employed for making radiometric measurements and demonstrated a total uncertainty in the measurement of in-water AOPs at approximately the 3% level.

## 9.2 RESULTS

### *Open Ocean*

The SeaWiFS Field Team has combined the collection of ground-truth observations with specific experiments to investigate the sources of uncertainties in AOP measurements.

NASA Technical Memorandum 2002–206892, Volume 21

## SeaWiFS Postlaunch Technical Report Series

Stanford B. Hooker, Editor

*NASA Goddard Space Flight Center  
Greenbelt, Maryland*

Elaine R. Firestone, Senior Scientific Technical Editor

*Science Applications International Corporation  
Beltsville, Maryland*

## Volume 21, The Eighth SeaWiFS Intercalibration Round-Robin Experiment (SIRREX-8), September–December 2001

Giuseppe Zibordi

Davide D’Alimonte

Dirk van der Linde

Jean-François Berthon

*JRC/Institute for Environment and Sustainability  
Ispra, Italy*

Stanford B. Hooker

*NASA/Goddard Space Flight Center  
Greenbelt, Maryland*

James L. Mueller

*SDSU/Center for Hydro-Optics and Remote Sensing  
San Diego, California*

Gordana Lazin

Scott McLean

*Satlantic, Inc.  
Halifax, Canada*

---

# Chapter 1

---

## SIRREX-8 Overview

STANFORD B. HOOKER

*NASA/Goddard Space Flight Center  
Greenbelt, Maryland*

GIUSEPPE ZIBORDI

*JRC/IES/Inland and Marine Waters Unit  
Ispra, Italy*

### ABSTRACT

The primary objective of SIRREX-8 was a thorough inquiry into the uncertainties associated with the general problem of determining the immersion factors for marine radiometers, and restricting the analysis to Atlantic in-water Ocean Color Irradiance 200-series sensors (the so-called OCI-200 instruments). A small team of investigators was assembled to address these points at three different facilities (the diversity in participants assured no one peculiarity in one of the methods could bias the results). The secondary SIRREX-8 objective was to measure the cosine response of one sensor at two of the participating facilities. Although up to 12 sensors were measured, 9 were rotated through all three facilities. The instrumentation came primarily from two different organizations with differing measurement objectives, so the assembled sensors had a diverse range of calibration histories, ages, intended uses, sensitivities, saturation levels, etc. The diversity in sensors means a significant subset of the results will have a wider applicability to the larger community.

---

## 1.1 INTRODUCTION

When a cosine collector is immersed in water, its light transmissivity is less than it was in air. Irradiance sensors are calibrated in air, however, so a correction for this change in collector transmissivity must be applied when the in-water raw data are converted to physical units. The correction term is called the immersion factor, and it must be determined experimentally, using a laboratory protocol, for each sensor wavelength,  $\lambda$ .

When the sensor is illuminated, the raw optical data samples at each wavelength are recorded as digitized voltages,  $V(\lambda)$ , usually in counts. Each sample is recorded at a particular time,  $t_i$ , which also sets the depth,  $z$ . Raw irradiance data are typically converted to physical units using a calibration equation of the following form:

$$E(\lambda, t_i) = C_c(\lambda) I_f(\lambda) [V(\lambda, t_i) - \bar{D}(\lambda)], \quad (1)$$

where  $E(\lambda, t_i)$  is the calibrated irradiance,  $C_c(\lambda)$  is the calibration coefficient (determined during the radiometric calibration of the sensor),  $I_f(\lambda)$  is the immersion factor<sup>†</sup>,

and  $\bar{D}(\lambda)$  is the average bias or dark voltage measured during a special *dark cast* with the caps on the radiometer. The difference between  $V(\lambda, t_i)$  and  $\bar{D}(\lambda)$  is the net signal level detected by the radiometer while exposed to light.

In some cases, dark voltages are replaced by so-called *background* or *ambient* measurements, so illumination biases can be removed along with the dark correction. For the purposes of SIRREX-8, background data were collected with the direct illumination of the target by the source occluded by an intervening *on-axis baffle*, so only indirect light (from the source and any other light emissions from equipment in the room) reached the sensor aperture. Ambient data were collected with the source off, so only illumination from other light-emitting devices in the room reached the sensor aperture.

In the formulation given in (1), the irradiances measured during ocean color field campaigns are usually the in-water downward irradiance,  $E_d(z, \lambda)$ , the in-water upwelled irradiance,  $E_u(z, \lambda)$ , and the above-water total solar irradiance,  $E_d(0^+, \lambda)$ . In some data processing schemes (Hooker et al. 2001), there is an explicit attempt to try and get the extrapolated in-water downward irradiance to agree with the measured above-water total solar irradiance over the time period associated with the extrapolation interval, so the application of the immersion factor to the former must be accurate.

---

<sup>†</sup> For the purposes of the calibration equation, the immersion factor for an above-water irradiance sensor is always equal to unity.

NASA Technical Memorandum 2002–206892, Volume 17

## SeaWiFS Postlaunch Technical Report Series

Stanford B. Hooker, Editor

*NASA/Goddard Space Flight Center  
Greenbelt, Maryland*

Elaine R. Firestone, Senior Scientific Technical Editor

*Science Applications International Corporation  
Beltsville, Maryland*

## Volume 17, The Seventh SeaWiFS Intercalibration Round-Robin Experiment (SIRREX-7), March 1999

Stanford B. Hooker

*NASA/Goddard Space Flight Center  
Greenbelt, Maryland*

Scott McLean

Jennifer Sherman

Mark Small

Gordana Lazin

*Satlantic, Inc.  
Halifax, Canada*

Giuseppe Zibordi

*JRC/SAI/Marine Environment Unit  
Ispra, Italy*

James W. Brown

*RSMAS/University of Miami  
Miami, Florida*



---

## Chapter 9

---

### SIRREX-7 Synthesis, Discussion, and Conclusions

STANFORD B. HOOKER  
*NASA/Goddard Space Flight Center*  
*Greenbelt, Maryland*

GIUSEPPE ZIBORDI  
*JRC/SAI/Marine Environment Unit*  
*Ispira, Italy*

SCOTT MCLEAN  
*Satlantic, Inc.*  
*Halifax, Canada*

#### ABSTRACT

A combined uncertainty budget for radiometric calibrations can be constructed from the SIRREX-7 data set. Although it is comprehensive, it does not address every source of uncertainty at the same level of detail and some must be considered as approximate. Nonetheless, the care taken in each experiment ensures the uncertainty estimates are representative of what can be expected if careful metrology and practices are used. Perhaps just as importantly, the consequences of discrepancies are also well estimated. To provide a range of possible outcomes in the calibration process, minimum, typical, and maximum uncertainties are computed from the various entries, which range from 1.1–3.4% and 1.5–6.7% for irradiance and radiance calibrations, respectively. The Satlantic facility falls somewhere between the minimum and typical values. If an additional (average) 1.0% is included to account for an unknown bias detected with the lamp and plaque uncertainty experiments (described in Sects. 3.2 and 4.2, and discussed in Sects. 9.2 and 9.5), the uncertainty for Satlantic irradiance calibrations is 1.8%, and the uncertainty for radiance calibrations is 2.3%.

---

## 9.1 INTRODUCTION

This chapter synthesizes the results from the various SIRREX-7 experiments and discusses the conclusions that can be drawn from them. The lessons learned are separated according to irradiance or radiance calibrations, and those applicable to both. Not all types of Satlantic sensor were included in SIRREX-7, in fact, the most common instrument was the model 200 series of radiance and irradiance sensors (Table 7). Most Satlantic instruments share design commonalities, however, so the results have some applicability to most instrument classes. An obvious exception is the difference between single- and multiple-aperture sensors: the latter have more complicated alignment effects, because they have multiple viewing axes.

A summary of the various experiments executed during SIRREX-7 is presented in Table 13. Although it was not possible to replicate all the experiments the same number of times, the primary experiments were executed as many times as economically feasible to ensure statistical reliability. Most of the experiments involved the use of all

three principle components of radiometry, source, target, and detector, so most have results applicable to other objectives. The material presented here is organized primarily according to the order the experiments were presented in Chapters 3–8 (some information originally presented in different chapters was combined into one section).

## 9.2 LAMP UNCERTAINTIES

The results from the investigations into lamp uncertainties (Sect. 3.2.3) showed a deterministic bias when the irradiance of the lamps calculated from the SXR measurements of the NIST plaque were compared to the values supplied with the lamp (Fig. 5). Each component of the experiment has an uncertainty on the order of 1%, and given another (maximum) 1% from mechanical setup uncertainties, the range of uncertainty seen with the so-called *trusted* lamps is within the quadrature sum of these components, that is, the approximately 2% uncertainty in the blue part of the spectrum is very close to  $\sqrt{4}$ .

The spectral dependence in SXR uncertainties is approximately 0.5% (Johnson et al. 1998a), with maximal un-

NASA Technical Memorandum 2002–206892, Volume 17

## SeaWiFS Postlaunch Technical Report Series

Stanford B. Hooker, Editor

*NASA/Goddard Space Flight Center  
Greenbelt, Maryland*

Elaine R. Firestone, Senior Scientific Technical Editor

*Science Applications International Corporation  
Beltsville, Maryland*

## Volume 17, The Seventh SeaWiFS Intercalibration Round-Robin Experiment (SIRREX-7), March 1999

Stanford B. Hooker

*NASA/Goddard Space Flight Center  
Greenbelt, Maryland*

Scott McLean

Jennifer Sherman

Mark Small

Gordana Lazin

*Satlantic, Inc.  
Halifax, Canada*

Giuseppe Zibordi

*JRC/SAI/Marine Environment Unit  
Ispra, Italy*

James W. Brown

*RSMAS/University of Miami  
Miami, Florida*

---

## Chapter 6

---

### Uncertainties in Irradiance Calibrations

STANFORD B. HOOKER  
NASA/Goddard Space Flight Center  
Greenbelt, Maryland

GIUSEPPE ZIBORDI  
JRC/SAI/Marine Environment Unit  
Ispra, Italy

SCOTT MCLEAN  
JENNIFER SHERMAN  
Satlantic, Inc.  
Halifax, Canada

#### ABSTRACT

Three types of experiments were conducted to estimate the uncertainties associated with irradiance calibrations using an FEL standard lamp: a) the repeatability uncertainty (based on one FEL standard lamp used during 11 trials with three different irradiance sensors) was less than 0.5% (0.2% on average, with usually larger uncertainties in the blue part of the spectrum and smaller uncertainties in the red); b) the additional uncertainty that can be removed from radiance calibrations if ambient rather than dark measurements are used was 0.05% (0.05% in the blue, 0.04% in the green, and 0.06% in the red); and c) the overall uncertainty from secondary reflections, originating from ancillary equipment used during the calibration process (in this case, an alignment laser) was 0.06% (0.03% in the blue-green wavelength domain and 0.12% in the red).

---

## 6.1 INTRODUCTION

Typically, the calibration coefficients for an irradiance sensor (identified by  $S_{ID}$ ) are computed using an FEL standard lamp ( $L_{ID}$ ) with a calibrated irradiance,  $E_{L_{ID}}^{cal}(\lambda, 50)$ . The general procedures require the lamp to be positioned a distance  $d$  on axis and normal to the faceplate of the irradiance sensor (Sect. 1.5.7). The irradiance sensor is capped, and dark (digital voltage) levels for the sensor are recorded from which average dark levels,  $\bar{D}_{S_{ID}}(\lambda)$ , are calculated.

The lamp is powered on, and the voltage levels of the individual sensor channels are recorded, from which an average calibration voltage for each channel,  $\bar{V}_{S_{ID}}(\lambda)$ , is obtained. The calibration coefficient is calculated using:

$$C_{S_{ID}}^{Irr}(\lambda) = \frac{E_{L_{ID}}^{cal}(\lambda, 50)}{\bar{V}_{S_{ID}}(\lambda) - \bar{D}_{S_{ID}}(\lambda)} \left[ \frac{50 \text{ cm}}{d} \right]^2, \quad (14)$$

where  $d$  is given in centimeters.

Three types of experiments were conducted to explore the uncertainties associated with irradiance calibrations:

- a) The same FEL standard lamp was used with three OCI-200 radiometers to estimate the repeatability

uncertainty in irradiance calibrations (based on 11 trials for each sensor);

- b) The importance of ambient versus dark measurements was explored with three OCI-200 sensors; and
- c) The uncertainty associated with reflections from improperly baffled ancillary equipment used in the calibration process (in this case, an alignment laser) was measured with three OCI-200 sensors.

## 6.2 IRRADIANCE REPEATABILITY

This experiment was designed to estimate the uncertainties in irradiance calibrations (set up and executed following the usual procedures). Three OCI-200 sensors (I040, I050, and I097) were calibrated independently 11 times each. Although the trials were all executed with the same FEL standard lamp, the lamp was not powered on and off for each trial; it was left on to minimize the amount of time used with the lamp (standard FEL lamps are too expensive to include the warm-up time for each trial in the experiment).

NASA Technical Memorandum 2002–206892, Volume 17

## SeaWiFS Postlaunch Technical Report Series

Stanford B. Hooker, Editor

*NASA/Goddard Space Flight Center  
Greenbelt, Maryland*

Elaine R. Firestone, Senior Scientific Technical Editor

*Science Applications International Corporation  
Beltsville, Maryland*

## Volume 17, The Seventh SeaWiFS Intercalibration Round-Robin Experiment (SIRREX-7), March 1999

Stanford B. Hooker

*NASA/Goddard Space Flight Center  
Greenbelt, Maryland*

Scott McLean

Jennifer Sherman

Mark Small

Gordana Lazin

*Satlantic, Inc.  
Halifax, Canada*

Giuseppe Zibordi

*JRC/SAI/Marine Environment Unit  
Ispra, Italy*

James W. Brown

*RSMAS/University of Miami  
Miami, Florida*

---

## Chapter 3

---

### Uncertainties in Lamp Standards

STANFORD B. HOOKER  
*NASA/Goddard Space Flight Center  
Greenbelt, Maryland*

GIUSEPPE ZIBORDI  
*JRC/SAI/Marine Environment Unit  
Ispira, Italy*

SCOTT MCLEAN  
JENNIFER SHERMAN  
*Satlantic, Inc.  
Halifax, Canada*

#### ABSTRACT

The uncertainties associated with the use of lamp standards was estimated by using several lamps with different calibration histories to illuminate a NIST reflectance standard (T005), and then comparing the calibrated radiance from the plaque (calculated from the calibrated reflectance of the plaque and the calibrated irradiance from the lamp), with that measured by the SXR. The average uncertainty of the most *trusted* lamps, those with no known problems and established good performance capabilities, was approximately 1.2%. All of the lamps had a calibration repeatability less than 0.5%, and all of the lamps except one had a repeatability less than 0.2%. A comparison of an Optronic calibration of an FEL lamp with a NIST calibration of the same lamp showed an overall average agreement to within approximately 1.3%. A similar comparison exercise executed as a part of SIRREX-5 showed the Optronic calibration of FEL F-409 differed from the NIST calibration by an average of approximately 2.6%, whereas a second calibration by Optronic differed from the NIST calibration by about 0.8%.

---

### 3.1 INTRODUCTION

Three experiments were conducted to examine the uncertainties associated with using lamps during calibrations. The first involved using a NIST reflectance standard and the SXR to estimate the uncertainties in using Labsphere (Spectralon) plaques, the second quantified how much of the variability in calibrations is due to changes in the lamp from one calibration session to the next, and the third compared the NIST and Optronic calibrations for a newly purchased lamp.

### 3.2 LAMP UNCERTAINTIES

The uncertainties associated with the use of lamp standards was estimated by using several lamps with different calibration histories to illuminate a NIST reflectance standard (T005), and then comparing the calibrated radiance from the plaque (calculated from the calibrated reflectance of the plaque and the calibrated irradiance from the lamp), with that measured by the SXR. A monitoring

sensor (R035) was mounted on the rail opposite the SXR to provide an independent measure of the illumination stability of the plaque.

#### 3.2.1 Equipment

The equipment used for determining the uncertainties in lamp standards involved the following:

- Satlantic NIST lamp F-409 (L007), and SeaWiFS NIST lamps F-182 (L002) and F-137 (L001);
- JRC Hoffman Lamps H97505 (L004) and H96551 (L005);
- Satlantic Optronic lamps F-539, F-536, and F-516 (L003, L006, and L000, respectively), plus two new Satlantic Optronic lamps F-547 (L008) and F-548 (L009);
- NIST plaque K299 (T005);
- The SXR (X001) with custom mount and digital voltmeter (V003);

NASA Technical Memorandum 2002–206892, Volume 17

## SeaWiFS Postlaunch Technical Report Series

Stanford B. Hooker, Editor

*NASA/Goddard Space Flight Center  
Greenbelt, Maryland*

Elaine R. Firestone, Senior Scientific Technical Editor

*Science Applications International Corporation  
Beltsville, Maryland*

## Volume 17, The Seventh SeaWiFS Intercalibration Round-Robin Experiment (SIRREX-7), March 1999

Stanford B. Hooker

*NASA/Goddard Space Flight Center  
Greenbelt, Maryland*

Scott McLean

Jennifer Sherman

Mark Small

Gordana Lazin

*Satlantic, Inc.  
Halifax, Canada*

Giuseppe Zibordi

*JRC/SAI/Marine Environment Unit  
Ispra, Italy*

James W. Brown

*RSMAS/University of Miami  
Miami, Florida*



---

## Chapter 4

---

### Uncertainties in Plaque Standards

STANFORD B. HOOKER

*NASA/Goddard Space Flight Center  
Greenbelt, Maryland*

GIUSEPPE ZIBORDI

*JRC/SAI/Marine Environment Unit  
Ispra, Italy*

SCOTT MCLEAN

JENNIFER SHERMAN

GORDANA LAZIN  
*Satlantic, Inc.  
Halifax, Canada*

#### ABSTRACT

The experiments conducted to estimate the uncertainties associated with the use of plaque standards involved calculating the reflectances of seven plaques using SXR measurements and the calibrated irradiance provided with the lamp standard, which were then compared to the reflectances provided with each plaque. The average uncertainties between the calculated and calibrated reflectances showed a range of 1.0–3.2%. With the exception of the gray plaque (T007), maximum uncertainties occurred in the blue part of the spectrum, and minimum uncertainties in the red. The importance of bidirectional effects was determined by comparing the SXR plaque measurements made from two different sides of a plaque, but with the same viewing geometry. The smallest uncertainties were associated with T005 (the NIST PTFE plaque), and the largest with T007 (the gray plaque), 0.3 and 2.1%, respectively. All of the other plaques had RPD values which fell into a narrow range with the same spectral dependence and an overall average RPD of approximately 1.0%. Plaque uniformity improved with all increases in the lamp-to-plaque distance. Regardless of the lamp-to-plaque distance, there was a constant offset of approximately 20 mm in the vertical ( $z$ ) direction between the maximum signal and the center of the plaque for all the lamps; some of the lamps also showed offsets in the horizontal ( $x$ ) direction.

---

#### 4.1 INTRODUCTION

Three experiments were conducted to examine the uncertainties associated with using plaques during calibrations. The first involved using a NIST reflectance standard and the SXR to estimate the uncertainties in using Labsphere (Spectralon) plaques, the second estimated the importance of bidirectional effects by comparing calibrations from two different sides of a plaque, but with the same viewing geometry, and the third used a mapping radiometer to estimate the uniformity of Labsphere plaques illuminated with the same FEL lamp.

#### 4.2 PLAQUE UNCERTAINTIES

This experiment was designed to estimate the uncertainties in plaque standards by comparing the calculated reflectance of a number of different plaques illuminated

with a single NIST standard lamp. The reflectance of each plaque was calculated using the SXR measurements and the calibrated irradiance provided with the lamp. The calculated reflectances were then compared to the reflectances provided with each plaque.

##### 4.2.1 Equipment

The equipment used for determining the uncertainties in plaque standards involved the following:

- Satlantic Optronics Lamp F-539 (L003);
- NIST plaque K299 (T005);
- The SeaWiFS gray (10 in) plaque 24328 (T007), the JRC white (18 in) plaque 22463 (T004), the new Satlantic white (18 in) plaque 05816 (T001), and the two old Satlantic white (18 in) plaques 13172 (T002) and 01873 (T003);

## GLDAS: AN IMPORTANT CONTRIBUTION TO CEOP

Paul R. Houser and Matthew Rodell

Hydrological Sciences Branch  
NASA Goddard Space Flight Center

Scientists at NASA's Goddard Space Flight Center (GSFC) have developed a high-resolution Global Land Data Assimilation System (GLDAS) in cooperation with researchers at NOAA's National Centers for Environmental Prediction (NCEP). The goal of GLDAS is to produce optimal output fields of land surface states and fluxes by making use of data from advanced observing systems (See figure on back page). Errors in land surface forcing and parameterization tend to accumulate in modeled land stores of water and energy, leading to incorrect surface water and energy partitioning. GLDAS aims to minimize this effect by constraining the models in two ways. First, by forcing the land surface, primarily by observations (such as precipitation and radiation), the biases in atmospheric model-derived forcing are avoided. Second, by employing land surface data assimilation techniques, observations of land surface storages (soil temperature, soil moisture, and snow depth/cover) can be used to steer unrealistic simulated storages towards reality. These techniques also enable identification and mitigation of observational errors and minimization of the impact of simplified land parameterizations. **The value-added data produced by GLDAS will improve land surface, weather, and climate predictions by providing global fields of land surface energy and moisture stores for initialization.**

Drivers have been installed in GLDAS for three land surface models (LSMs): Mosaic; the Community Land Model (CLM); and the NCEP, Oregon State University, United States Air Force, and Office of Hydrology model (NOAH). GLDAS runs globally with a 15-minute time step at 0.25° (soon to be 0.125°) and coarser resolutions. A vegetation-based "tiling" approach is used to simulate sub-grid scale variability, with the University of Maryland's 1 km global vegetation data set as its basis. Soil parameters are derived from 5-minute global soils information produced by USDA Agricultural Research Service. GLDAS uses the GTOPO30 global digital elevation model as its standard and corrects input fields accordingly. In addition to an operational, near-real time simulation using the standard parameterization and forcing data, several parallel simulations run with varying combinations of models, forcing data, and advanced options. Forcing options include the global atmospheric forecast model output (from GSFC's Data Assimilation Office, NCEP, and the Euro-

observation-based precipitation and radiation fields. Advanced options, which are in various stages of planning, implementation, and testing, include a routine for satellite-based updates of leaf area index, canopy greenness and albedo, soil moisture and temperature data assimilation, observation-based snow corrections, simulation of the atmospheric boundary layer, and runoff routing.

The Coordinated Enhanced Observation Period (CEOP) was initiated by the international efforts of GEWEX and is focused on the measurement, understanding and modeling of water and energy cycles within the climate system. It is motivated by the synchronism of the new generation of Earth observing satellites and GEWEX Continental Scale Experiments (CSEs). Its primary goal is to develop a consistent data set for 2003-2004 to support research objectives in climate prediction and monsoon system studies. The requirements of the international climate research community at large have been taken fully into account in planning the assembly of the data set. CEOP also will assist studies of global atmospheric circulation and water resources availability. CEOP has gained the interest of a broad range of international organizations, as evidenced by the proposal for an Integrated Global Water Cycle Observations (IGWCO) theme within the framework of the International Global Observing Strategy Partnership (IGOS-P), which has re-affirmed CEOP as "the first element of the IGWCO." The CEOP implementation plan can be viewed at: [http://www.gewex.org/ceop/ceop\\_ip.pdf](http://www.gewex.org/ceop/ceop_ip.pdf).

**CEOP aims to integrate the many streams of data coming from new space-based observation systems into a coherent database relevant to CEOP science issues, which will facilitate analytical investigations.**

**GLDAS is a valuable tool for CEOP because it assimilates the information from multiple models and observation platforms to provide the best available assessment of the current state of the land surface.** The international GEWEX and CEOP communities have recognized that GLDAS can be leveraged and further developed to address the needs of CEOP. CEOP is specifically interested in the generation and application of GLDAS results in regional climate analysis, model initialization, and comparison with results from field campaigns and modeling experiments. The use of GLDAS model location time series (MOLTS), which are time series of land surface model output for points of interest, will be one of the primary tools to enable this globally-consistent intercomparison. Each GLDAS MOLTS will be particularly relevant because it will be generated based on a GLDAS subgrid "tile" with a vegetation class that matches that of the observation. Furthermore,

land surface models that GLDAS drives (currently three; five planned). These comparison exercises and the data produced by the continental scale experiments also will provide much-needed validation for the GLDAS project.

CEOP has requested that NASA further develop GLDAS as a central "CEOP data integration center", including the following aspects:

- A test bed for evaluating multiple land surface models.
- Long term land model baseline experiments and intercomparisons.
- Linking and inclusion of reference site observations with globally consistent observation and modeling to enable GEWEX-CSE land transferability studies.
- Land initialization for seasonal-to-interannual coupled predictions.
- Evaluation of numerical weather and climate predictions for land.
- Integration of remotely sensed land observations in land/atmospheric modeling for use in CEOP and higher level understanding.
- A quality control check on observations.
- 4DDA "value-added" GLDAS-CEOP data sets.

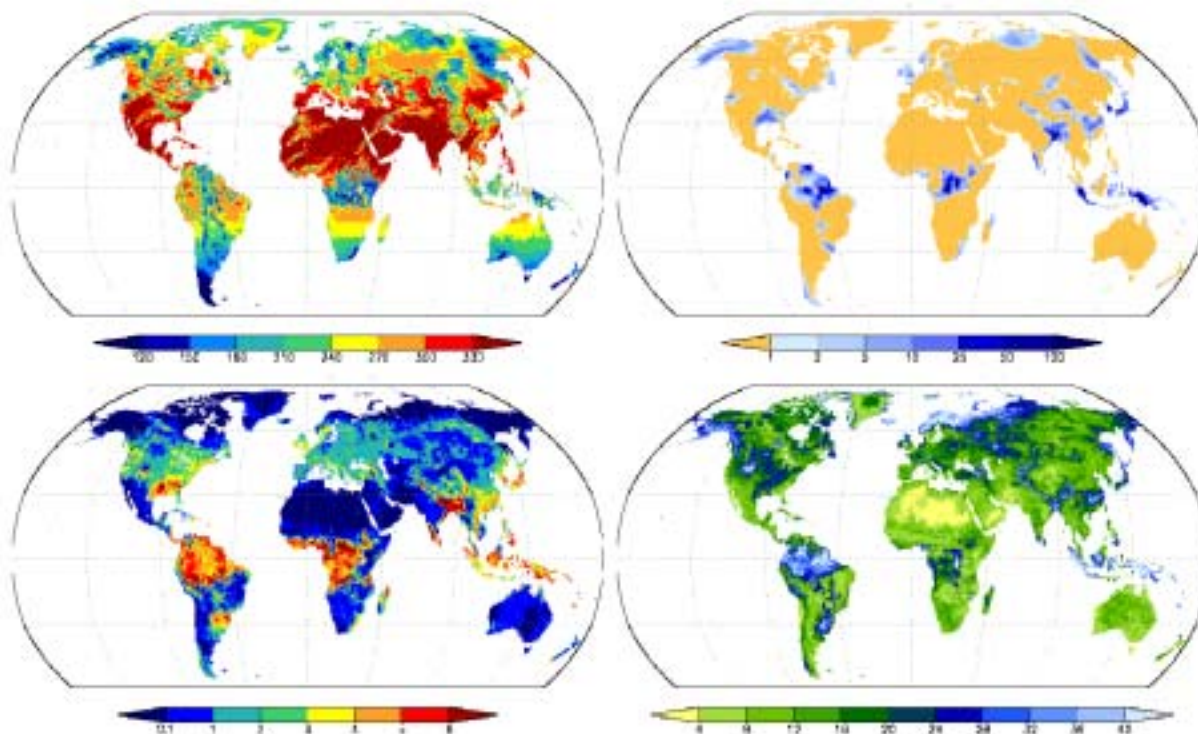
- The production of GLDAS MOLTS.
- The expansion of GLDAS to include selected atmosphere and ocean observations.
- The development of a long-term archive function.

The GLDAS contribution to CEOP is expected to have the following timeline:

- Data Integration Period (2002-2005): Compile the forcing data (observations and analyses) and assimilation data including radiance observations (level 1), high-level satellite data products, *in situ* observations, and NWP land analyses into a long term archive. Produce MLDAS (Molts LDAS) by reconfiguring GLDAS to run only MOLTS points for explicit linkages to CEOP reference sites.
- Reanalysis Period (2006-2007 work activity): Reprocess CEOP data in a globally consistent 1/8 degree resolution; global land reanalysis including multiple land model products (NOAH, CLM, VIC, etc.) and data assimilated value-added analysis.

For more information on GLDAS, please visit <http://ldas.gsfc.nasa.gov>.

### GLDAS: AN IMPORTANT CONTRIBUTION TO CEOP



*GLDAS forcing and output, 30 April 2002. Mean observation-based downward shortwave radiation [ $W/m^2$ ] (top left); total precipitation [mm] (top right); total evapotranspiration [mm] (bottom left); mean observation-based upward longwave radiation [ $W/m^2$ ] (bottom right).*



# 2002 IEEE International Geoscience and Remote Sensing Symposium and the 24<sup>th</sup> Canadian Symposium on Remote Sensing



REMOTE SENSING:  
Integrating Our  
View of the Planet



June 24-28, 2002  
Toronto Canada

# IGARSS 2002

# Remotely Sensed Forcing Data and the Global Land Data Assimilation System

U. Jambor<sup>1</sup>, P. R. Houser<sup>2</sup>, M. Rodell<sup>2</sup>, J. Gottschalck<sup>1</sup>, C.-J. Meng<sup>1,3</sup>, B. Cosgrove<sup>4</sup>, and J. K. Entin<sup>5</sup>

<sup>1</sup>Goddard Earth Science and Technology Center, University of Maryland, Baltimore County / NASA GSFC  
Hydrological Sciences Branch, Greenbelt, MD 20771

<sup>2</sup>NASA GSFC Hydrological Sciences Branch, Greenbelt, MD 20771

<sup>3</sup>NOAA National Centers for Environmental Prediction, Camp Springs, MD 20746

<sup>4</sup>SAIC / NASA GSFC Hydrological Sciences Branch, Greenbelt, MD 20771

<sup>5</sup>Now at NASA Headquarters, Washington, DC 20546

**Abstract**—A high-resolution, near-real-time Global Land Data Assimilation System (GLDAS) that integrates information from relevant satellite- and ground-based observations within a land data assimilation framework is being developed at NASA's Goddard Space Flight Center and NOAA's National Centers for Environmental Prediction (NCEP). The GLDAS framework enables it to serve as a powerful tool for various types of research and applications. Here, we examine the impact of replacing model-based forcing fields with observation-derived fields on Mosaic land surface model (LSM) simulations. Due to a paucity of recent land surface state observations over large domains, GLDAS-forced Mosaic LSM simulations will be evaluated against finer-resolution North American LDAS-forced results.

## I. INTRODUCTION

Accurate initialization of land surface moisture and energy stores is critical in weather and climate prediction because of their regulation of surface water and energy fluxes between the surface and atmosphere over a variety of time scales. Since these are integrated states, errors in land surface forcing and parameterization accumulate in land stores, leading to incorrect surface water and energy partitioning. The purpose of the Global Land Data Assimilation System (GLDAS) is to integrate satellite- and ground-based observational data products, using advanced land surface modeling and data assimilation techniques, in order to produce optimal fields of land surface states and fluxes [1]. GLDAS drives multiple land surface models (LSMs) globally at 0.25° and lower spatial resolutions on a sub-hourly timestep. A vegetation-based “tiling” approach is used to simulate sub-grid scale variability, with a 1 km global vegetation dataset as its basis. Soil and elevation parameters are based on high-resolution global information. The system runs in near-real time using a combination of observation-based precipitation and radiation fields and the best available global coupled weather forecast model output (Fig. 1). The global land surface fields that GLDAS provides will be used for initialization of coupled weather and climate prediction models and subsequent research and applications. Furthermore, the 2001-forward GLDAS archive of modeled and observed, global, surface meteorological data will be unparalleled in scope.

The GLDAS project has its basis in the North American Land Data Assimilation System (NLDAS) project [2]. The study region for the NLDAS encompasses the continental United States and parts of Mexico and Canada, and LSMs are run at 0.125° resolution. By choosing to compare the GLDAS forcing and output fields with those of the NLDAS over a concurrent, common domain, the underlying

assumption is that the NLDAS simulation is a better representation of the true atmospheric and land surface states. This study is a step towards understanding the GLDAS product over the global domain by first focusing on a region that is heavily observed and modeled.

## II. METHODOLOGY

Three types of operational Mosaic LSM [3] runs were performed over July 2001. The two GLDAS simulations were run at 0.25° resolution, with each vegetation-based tile included per grid cell accounting for at least 10% of the grid cell area. The NLDAS simulation was run at 0.125° resolution, allowing for up to 10 vegetation-based tiles per grid cell, each accounting for at least 5% of the grid area.

For both GLDAS experiments the baseline forcing was 1° global grid output from the Goddard Earth Observing System Data Assimilation System (GEOS) model [4]. The second

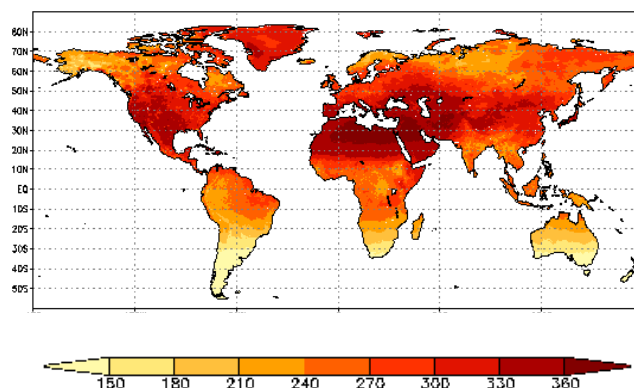


Fig. 1. Mean downward shortwave flux ( $\text{W m}^{-2}$ ) for July 2001. This forcing field was assembled by GLDAS, using satellite-derived radiation data to replace baseline model forcing values whenever possible.

## IV. CONCLUSION

Accurate representation of atmospheric forcing inputs in land surface simulations is fundamental. As such, it is important to identify which types of forcing data are most appropriate for such use, and the limitations associated with them. The GLDAS and NLDAS frameworks are well suited to perform such evaluations.

Recognizing the differences in model resolution, land surface parameters, and initial conditions among these discussed GLDAS and NLDAS simulations, we plan to minimize their effect on an LSM outcome by constraining such differences in future experiments.



# 2002 IEEE International Geoscience and Remote Sensing Symposium and the 24<sup>th</sup> Canadian Symposium on Remote Sensing



REMOTE SENSING:  
Integrating Our  
View of the Planet



June 24-28, 2002  
Toronto Canada

# IGARSS 2002



# Parameterization of snowpack grain size for global satellite microwave estimates of snow depth

R.E.J. Kelly<sup>1</sup>, A.T.C. Chang<sup>2</sup>, L. Tsang<sup>3</sup>, and C.T. Chen<sup>3</sup>

<sup>1</sup>Goddard Earth Sciences and Technology Center, University of Maryland Baltimore County, MD 21250 USA

<sup>2</sup>Hydrological Sciences Branch/Code 974, NASA/Goddard Space Flight Center, Greenbelt, MD 20771, USA

<sup>3</sup>Department of Electrical Engineering, University of Seattle, Washington, WA 98195-2500

**Abstract-** For accurate estimation of global snow depth or snow water equivalent on the Earth's surface using passive microwave instruments, knowledge of the snow pack's physical properties is important. It is known that the bulk snow grain size distribution exerts an important control over the microwave response from snow between 3mm and 300 mm wavelengths. In the absence of high quality snowpack data at a global scale, we show how the grain size distribution can be estimated using a general empirical model of grain growth. This information is used to parameterize a dense media radiative transfer model (DMRT) to estimate the radiometric response from a snow pack as a function of changing grain size distribution. The DMRT equations are based on the quasi-crystalline approximation (QCA) for densely distributed moderate sized particles in a medium such as a snow pack. The model snow depth estimates from the DMRT are used to calibrate a Special Sensor Microwave Imager (SSM/I) snow depth retrieval algorithm which is based on the brightness temperature difference between 19 and 37 GHz with the SWE. The method is tested using meteorological data from the WMO global network. Results show that using the DMRT model coupled with a grain size model improved estimates of snow depth are obtained.

## I. INTRODUCTION

Remote sensing has been used to monitor continental-scale snow cover area in the northern hemisphere for almost 25 years [1]. With the improvement in satellite microwave instrumentation, regional and local scales can now be mapped effectively. However, passive microwave (PM) retrieval methods of snow water equivalent (SWE) and/or snow depth (SD) are less mature with large errors often resulting from retrievals at the global scale. One of the key reasons for these large errors is because instantaneous parameterization of snowpack properties at the global scale is not straightforward. Studies have shown that snowpack models can be used successfully to quantify changes in properties of the pack (e.g. average grain size) [2]. These models often require intensive-scale observations of meteorological surface conditions that are usually not available in a high quality globally distributed form. Thus, to overcome this problem, we implement a simple statistical model of snow pack grain growth and couple it to a microwave emission model and passive microwave observations to estimate snow depth.

## III. TESTING OF THE MODEL AND CONCLUSIONS

The model is tested on snow depth time series (1992-1993, 1993-1994 and 1994-1995) for two locations, one in

north Sweden (67° 13' N, 23° 24' E) and the other in north America (56° 39' N, 111° 13' W). The original algorithm of

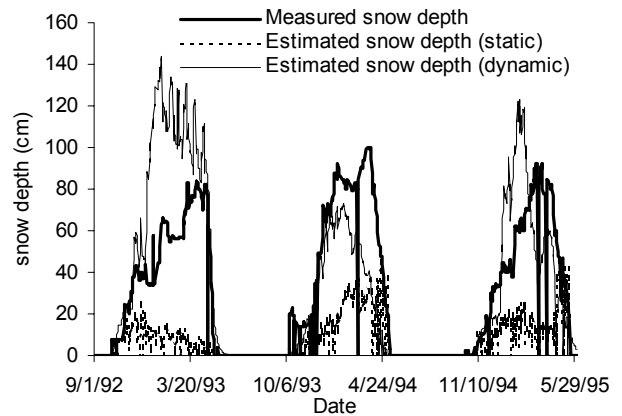


Fig. 2 Comparison of measured snow depth with estimated snow depth from the static and dynamic algorithms for north Sweden.

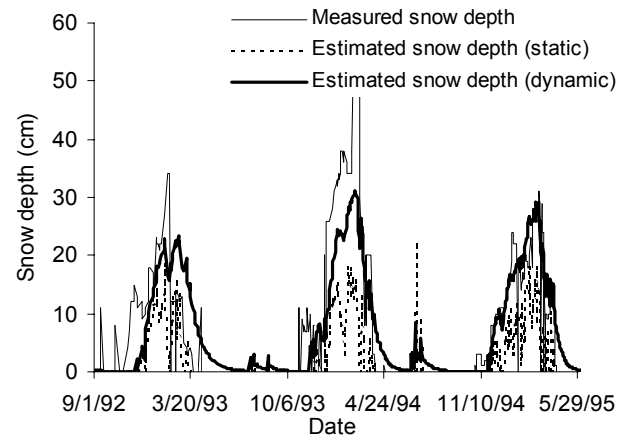


Fig. 3 Comparison of measured snow depth with estimated snow depth from the static and dynamic algorithms for north America.

[1] is compared with the newer algorithm and the results are shown in Figs. 2 and 3 for Sweden and north America respectively. Generally, the original static algorithm underestimates snow depth systematically for both sites. For the north Sweden site, however, there is overestimation in the 1992-1993 winter season but for the other two years the results are good. Overall, the correlation between the static algorithm and measured snow depth over the accumulated three winter seasons for north Sweden is 0.61 and for the dynamic model it is 0.77. For the north American site, the correlation for the static model is 0.71 while for the dynamic model it is 0.87. Thus, the dynamic model shows improvement over the original static algorithm.

## Special Report

# CEOP Satellite Data Integration



Figure 1. 500Tera-byte data archive system at the Institute Industrial Sciences, University of Tokyo

**Toshio Koike**, University of Tokyo  
**Paul Houser and Matthew Rodell**, NASA GSFC

## Special Report

# CEOP Satellite Data Integration



Figure 1. 500Tera-byte data archive system at the Institute of Industrial Sciences, University of Tokyo

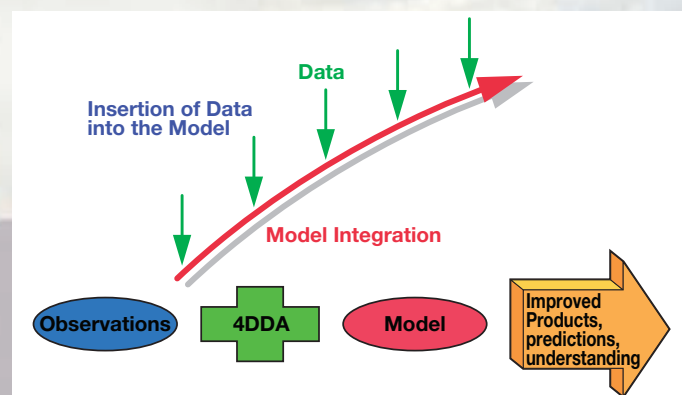
To provide satellite data integration products including 4DDA “value-added” Global Land Data Assimilation System (GLDAS) datasets, of water cycle variables, two CEOP Satellite Data Integration Centers (CSDICs) are to be established, one at the University of Tokyo (UT) in cooperation with NASDA and the other at NASA's Goddard Space Flight Center (GSFC).

The CSDIC at UT will receive CEOP customized levels 1b and 2 and standard level 3 earth observation satellite data from space agencies and archive them by using a 500 tera-byte data archival system at the Institute of Industrial Sciences of UT as shown in Figure 1. The Committee on Earth Observation Satellite (CEOS) Working Group on Information Systems and Services (WGISS) Test Facility for CEOP (CEOP-WTF) advanced by NASDA and NASA will be developed for providing catalogue interoperability with CEOS agencies' systems by using CEOS' protocols and exchanging data and information with CEOS agencies and affiliates as well as users through automated links. Integrated CEOP satellite products overlaid with in-situ data and model output will be delivered to users by Web Mapping Technology and other visual technologies through networks. UT and NASDA propose a three phased approach for production and archiving of satellite data products; Phase I, for all reference sites, started in June, 2002, Phase II, for the monsoonal regions, begin in June, 2003, and Phase III, fully operational, beginning in September, 2005. To support phenomena detection, knowledge discovery and coincident search capabilities across a huge amount of very heterogeneous datasets, “Visual Data Mining” combined with the artificial intelligence approach in the computer sciences is now being developed as an important function of the CSDIC at UT.

Scientists at GSFC have developed a high-resolution GLDAS in cooperation with researchers at NOAA's National Centers for

**Toshio Koike**, University of Tokyo  
**Paul Houser and Matthew Rodell**, NASA GSFC

Environmental Prediction (NCEP). The goal of GLDAS is to produce optimal output fields of land surface states and fluxes by making use of data from advanced observing systems (see GEWEX News May 2002 and <http://ldas.gsfc.nasa.gov/> for further details). GLDAS uses various new satellite and ground based observation systems within a land data assimilation framework to produce optimal output fields of land surface states and fluxes. GLDAS includes four components implemented globally at 1/4 degree resolution (higher resolutions are planned) in near real time: land modeling, land surface observation, land surface data assimilation and calibration and validation. The core advantage of GLDAS is its use of satellite-derived observations (including precipitation, solar radiation, snow cover, surface temperature, and soil moisture) to realistically constrain the system dynamics. This allows it to avoid the biases that exist in near-surface atmosphere fields produced by atmospheric forecast models, minimize the impact of simplified land parameterizations, and to identify and mitigate errors satellite observations used in data assimilation procedures (Figure 2 shows the GLDAS system). These value-added GLDAS data will improve land surface, weather, and climate predictions by providing global fields of land surface energy and moisture stores for initialization. GLDAS is a valuable tool for CEOP because it assimilates the information from multiple models and observation platforms to provide the best available assessment of the current state of the land surface. In addition, an interface to access data from the near-real time GLDAS operational model runs is provided through the web site (<http://ldas.gsfc.nasa.gov/map/webout.html>). A region can be specified by either manually entering the coordinates in the text boxes or automatically by creating a rectangle on the map. Users can subset the data by time period as well as parameter type. The international GEWEX and CEOP communities have recognized that GLDAS can be leveraged and further developed to address the needs of CEOP. The CSDIC at NASA GSFC is working with the CEOP-GLDAS products in cooperation with NASA Data Assimilation Office (DAO).



Concept of the Land Data Assimilation System

**Genetic and Evolutionary  
Computation  
COnference 2002** **GECCO**

**New York**

**July 9-13, 2002**

---

# Comparison of Multiobjective Optimization Evolutionary Algorithms for a Three-objective Problem

---

**Sujay V. Kumar**

Goddard Earth Science Technology Center  
UMBC, NASA GSFC  
Greenbelt, MD 20771

**Ranji Ranjithan**

Department of Civil Engineering,  
North Carolina State University  
Raleigh, NC 27695.

## Abstract

This paper presents a systematic comparative study of CMEA (constraint method-based evolutionary algorithm) with several other commonly reported multiobjective evolutionary algorithms (MOEAs) in solving a three-objective optimization problem. The best estimate of the noninferior space was also obtained by solving this MO problem using a binary linear programming procedure. Several quantitative metrics are used in this study to compare the noninferior solutions with respect to relative accuracy, as well as spread and distribution of solutions in the noninferior space. Results based on multiple random trials of the MOEAs indicate that overall CMEA performs better than the other MOEAs for this three-objective problem.

## 1 Introduction

With the recent emergence of interest in solving realistic multiobjective (MO) problems, numerous multiobjective evolutionary algorithms (MOEAs) have been reported in the literature. While most of them have been successfully tested and evaluated for an array of two-objective test problems, little work is reported on solving MO problems with more than two objectives. Building upon the study reported by Zitzler et al. (2001) for a three-objective problem, this paper reports a comparison of performance of the constraint method-based evolutionary algorithm (CMEA) (Ranjithan et al. 2001, Kumar 2002) with those of SPEA-II (Zitzler et al. 2001), NSGA-II (Deb et al. 2000), and PESA (Corne et al. 2000). These results are also compared with the noninferior set obtained using a MO analysis with a binary linear programming procedure. An array of quantitative metrics is used to conduct a systematic performance comparison among the solutions generated by these MOEAs. In addition to several existing metrics that are extended from the original definitions for two objectives, a new one is defined to evaluate the relative degree of dominance of one set of noninferior solutions over another. As computational needs associated with

each MOEA scale up differently with the increase in the number of objectives, the total number of evaluations required to generate the noninferior sets used in this comparative study are kept to be similar. Thus the comparisons represent the quality of the noninferior solutions obtained with similar computational effort.

The next section provides a brief background on CMEA. The subsequent section describes the performance metrics used in this study. Section 4 defines the test problem and a comparison of the results, followed by conclusions.

## 5 Conclusions

Comparing the noninferior solutions obtained using the MOEAs with those obtained using BLP (which is the best estimate available), CMEA performs relatively well in finding noninferior solutions that are close to the best available estimation, as well as in covering most of the noninferior surface for the three-objective extended knapsack problem. When comparing the solutions obtained by the different MOEAs tested in this study, CMEA performs better than all others with respect to the spread of solutions in the noninferior space. While CMEA is able to generate a good distribution of solutions in a wider range of the noninferior space, the other MOEAs generate a high density of solutions in the central portion of the noninferior space. In the context of accuracy or degree of dominance, the CMEA solutions dominate those generated by the other MOEAs relatively more frequently. As the total number of function evaluations were kept similar for the different MOEAs, all the comparisons reflect the quality of the resulting noninferior solutions obtained using each MOEA.

While this study provides a systematic comparison of several MOEAs for a three-objective MO problem, further testing and evaluation studies are needed. Similar to the large array of test problems used in two-objective MO optimization, additional three-objective test problems reflecting different problem complexities need to be defined and be used in further comparative studies of these MOEAs. Also, the implications of MO problem scale up on the computational needs of the different MOEAs need to be investigated.



# 2002 IEEE International Geoscience and Remote Sensing Symposium and the 24<sup>th</sup> Canadian Symposium on Remote Sensing



REMOTE SENSING:  
Integrating Our  
View of the Planet



June 24-28, 2002  
Toronto Canada

# IGARSS 2002



# ESTAR Experience with RFI at L-band and Implications for Future Passive Microwave Remote Sensing from Space

David M. Le Vine

Code 975 Goddard Space Flight Center, Greenbelt, MD 20771  
Tel: 301-614-5640; FAX: 301-614-5558; email: dmlevine@priam.gsfc.nasa.gov

**Abstract**—Although the spectral window at 1.413 GHz (L-band) is protected for passive use, radiometers for remote sensing commonly encounter problems with RFI. Experience with the synthetic aperture radiometer, ESTAR, suggests that airports are one source of this RFI. The existence of RFI at L-band could be a problem for future remote sensing from space.

## 1. INTRODUCTION

The spectral window at 1.413 GHz (L-band), set aside for passive use only, is critical for remote sensing from space [1]. It is the largest spectral window available at the long wavelength end of the microwave spectrum, and long wavelengths are needed for monitoring parameters such as soil moisture and sea surface salinity. The importance of soil moisture and sea surface salinity for understanding the global hydrologic cycle and ocean circulation, is reflected in the new sensors and remote sensing missions that recently have been proposed to make measurements at L-band from space (e.g. Aquarius [2], Hydros [3] and SMOS [4,5]).

Although the window at 1.413 GHz is protected for passive use, RFI is a common problem. For example, during the Southern Great Plains experiments [6,7], the ESTAR radiometer [5,8] experienced RFI significant enough to warrant changes in flight lines. Noise levels frequently were sufficient to saturate the total power channel. RFI has been a sufficiently common problem for ESTAR, that the first step in processing data is to screen for RFI (a filter is used in data processing to detect rapid changes in brightness temperature).

RFI is a serious concern for future passive remote sensing missions in space. This is especially true for synthetic aperture radiometers because they employ small antennas with a wide field-of-view. The measurement of salinity is particularly vulnerable to RFI because of the extreme radiometric sensitivity (better than 0.2 K) needed to detect small changes in salinity in the open ocean [2]. Studies done during the design of the synthetic aperture radiometer, HYDROSTAR [5], suggest that spurious radiation from air traffic control radar can not be ignored by future L-band sensors in space. (See Section III below.)

## II. EXPERIENCE WITH ESTAR

ESTAR is a hybrid synthetic-and-real aperture radiometer. It employs long, “stick” antennas to achieve resolution along track and uses aperture synthesis to achieve resolution across track [8,9]. The use of aperture synthesis across track permits substantial thinning of the array, reducing the number of sticks needed. Thinning could also be done in the along track dimension to further reduce the real aperture. This is being

done in Europe for the SMOS mission to measure soil moisture and ocean salinity [5]. Aperture synthesis works well with antennas that have broad beams in the dimension where resolution is to be synthesized. However, broad antennas are particularly sensitive to RFI since radiation is received from a wide field-of-view. In the case of ESTAR, the field-of-view is restricted (about  $\pm 8$  degrees) in the along track dimension by the antenna aperture. However, in the across track dimension incoming signals from all angles are received.

Fig. 1 is an ESTAR image made in 1997 in the vicinity of Richmond, VA. The image has been superimposed on a map of land-water boundaries to help identify features. At the far right is the Chesapeake Bay, and the York and James Rivers are visible in the image. This image is the composite of several east-west lines flown at 25 kft with ESTAR aboard the Orion P-3B aircraft based at NASA’s Wallops Flight Facility. In this image, the RFI filtering normally done in software was not performed in order to illustrate the problem. The small, vertical, white dashes are strong signals associated with RFI. To get an idea of the temporal structure of these signals, the raw data from the zero spacing channel (total power radiometer) is shown in Fig. 2. The data shown is the uncalibrated output from a noise injection radiometer. This data was collected at about 77 WLong at the location of the arrow in Fig. 1. The periodic spikes are RFI. The undulating signal on which they ride is the slow variation in total power one normally associates with changes in surface features (e.g. soil moisture and vegetation canopy) at L-band. The period (10 s) is reasonable for air traffic control radar (e.g. with a rotation rate of about 5 rpm).

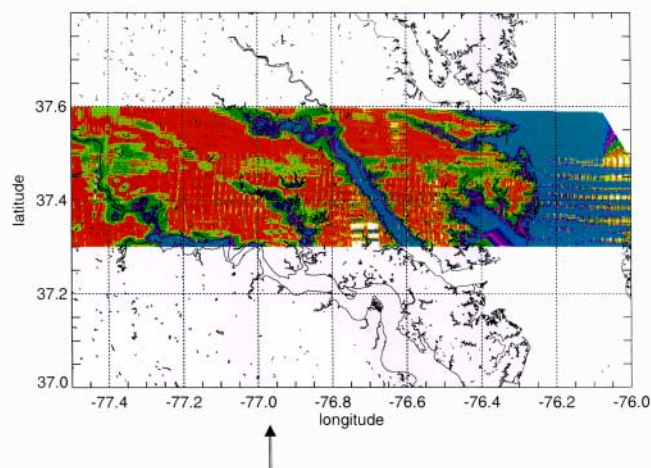


Fig. 1. ESTAR image showing the effects of RFI in the vicinity of Richmond, VA. The small vertical stripes are artifacts in the image due to large RFI.

# 2002 IEEE International Geoscience and Remote Sensing Symposium and the 24<sup>th</sup> Canadian Symposium on Remote Sensing



REMOTE SENSING:  
Integrating Our  
View of the Planet



June 24-28, 2002  
Toronto Canada

# IGARSS 2002



# Bright-Band Modeling of Air/Space-Borne Microwave Radars

Liang Liao<sup>1</sup>, Robert Meneghini<sup>2</sup> and Toshio Iguchi<sup>3</sup>

<sup>1</sup>Caelum Research Corp., Code 975, NASA/GSFC, Greenbelt, MD 20771

<sup>2</sup>Code 975, NASA/GSFC, Greenbelt, MD 20771

<sup>3</sup>Applied Research and Standards Division, CRL, Tokyo, 184-8795, Japan

**Abstract-** In simulating the radar echo in the melting layer of stratiform rain, a melting snowflake is modeled as a spherical non-uniform mixture, prescribed as a stratified-sphere in that the fractional water content is given as a function of the radius of sphere. Combined with the melting layer model that depicts the melting fractions and fall velocities of hydrometeors, the radar profiles are produced and then compared with the measurements of TRMM PR and the dual-wavelength airborne radar.

## I. INTRODUCTION

The bright band of enhanced radar reflectivity is often observed in the layer where the melting of snow takes place. Understanding the effect of melting hydrometeors on the electric wave propagation is important for algorithms that are used to retrieve rain rates from spaceborne sensors, such as the Tropical Rainfall Measuring Mission (TRMM) Precipitation Radar (PR) and the TRMM Microwave Imager (TMI). Aside from the bright band model needed for simulations of the radar profiles in the melting region, correctly modeling snowflake melting process is also important in the simulation of the radar bright-band profile. The bright band, or melting layer model that describes the complex dynamical and thermodynamical processes within the melting layer, provides the data of the water fractions and fall velocities of the melting snow as a function of the particle size and the distance from the 0°C isotherm. The melting snow model, on the other hand, describes how the melting process takes place. Two melting models often appear in the literatures: One is the uniformly-mixed model where the water fraction is constant throughout the particle, and another is concentric-sphere model where the water is confined to the outer shell and snow to the inner core. However, many observations [1] suggest that melting of the snowflake starts at its surface and gradually develops towards the center. It therefore becomes more realistic to model a melting snowflake as non-uniform mixture. To compute the scattering properties of such non-uniform melting particles, the stratified-sphere (or multi-layer sphere) scattering model is used, in which a uniform mixture is assumed within each layer with a water fraction that varies with radius. The advantage of using the stratified-sphere model is not only that the melting snowflake can be more realistically prescribed, but its analytical solution exists [2][3]. Having described the stratified-sphere model in Section II, the simulations of the radar bright-band profiles for the cases of TRMM PR and dual-wavelength airborne radar are made in Section III. The results reveal that the simulated profiles agree reasonably well with the measurements.

## II. MELTING SNOWFLAKES

As mentioned previously, the stratified sphere provides a great flexibility to model non-uniform snow-water mixtures in which the fractional water content is given as a function of

the radius. The stratified-sphere melting model, used in this study, is composed of 100 equal-thickness layers, and an exponential equation is employed to describe the distribution of the fractional water content of melting snow. In Fig.1 examples are shown of melting particles with the water fractions of 0.2 (left) and 0.4 (right). The gray levels represent the values of water fractions within the particle. The effective dielectric constant of the uniform mixture, applied in each layer of the stratified sphere, is derived from the internal electric fields of the mixture by use of a conjugate gradient-fast Fourier transform (CGFFT) numerical method [4]. The snow density used is uniform within the particle, whereas some measurements indicate that the snow density decreases with increase of radius. However, studies have demonstrated that the difference of the effective dielectric constants between the uniform snow density and non-uniform snow density with the same average density as the uniform case are negligible small [5].

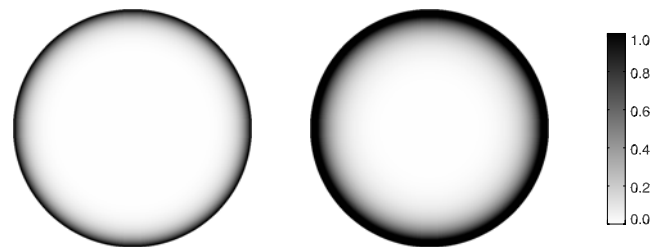


Fig.1. Examples of stratified-sphere model for the melting snowflakes for the overall water fractions of 0.2 (left) and 0.4 (right). The gray levels represents the fractional water contents.

## IV. SUMMARY

To use a more realistic melting model, the melting snowflake is modeled as a stratified sphere where the fractional water content is given as a function of the radius. Using this model the simulations of the radar reflectivity profiles associated with the melting layer are made for the cases of the TRMM PR and the dual-wavelength airborne radar. The raindrop size distributions, as input parameters of the melting model, are determined by matching the simulated and measured reflectivity in rain. For TRMM PR the Marshall-Palmer drop size distribution is used, while the 2-parameter exponential form of size distribution is applied for the airborne radar. In the simulations the same melting model is applied for TRMM PR and dual-wavelength airborne radar in the sense that the distributions of the fractional water contents within the melting snowflakes are treated the exactly same. The simulated bright-band profiles are in good agreement with the measured ones.

**NASA/TM-2002-210005**

## **SIMBIOS Project 2001 Annual Report**

Giulietta S. Fargion, Science Applications International Corporation, Maryland  
Charles R. McClain, Goddard Space Flight Center, Greenbelt, Maryland

National Aeronautics and  
Space Administration

**Goddard Space Flight Center**  
Greenbelt, Maryland 20771

March 2002

## Chapter 1

# An Overview of SIMBIOS Project Activities and Accomplishments During FY01

Charles R. McClain

*NASA Goddard Space Flight Center, Greenbelt, Maryland*

Giulietta S. Fargion

*Science Applications International Corporation (SAIC), Beltsville, Maryland*

In FY01, the SIMBIOS Project brought a number of activities to fruition and laid the groundwork for FY02 initiatives. With SeaWiFS continuing to perform well, the Terra platform and MODIS launched in December 1999, and several other global missions scheduled for launch (e.g., the Aqua platform with MODIS in 2002, the ENVISAT mission with MERIS in 2002, and ADEOS-II with GLI and POLDER in 2002), the first real opportunities to merge global data sets can be pursued. NASA HQ approved a three-year continuation of the science team (2001-2003) under an NRA and the Project Office. As it is taking some time for the MODIS team to work through the initial on-orbit processing issues, data merger-related activities within the Project Office have been in the development of data merging algorithms and software to read MODIS, development of capabilities for working with multiple global data sets in the future (i.e., OCTS-GAC reprocessing) and supporting the characterization of OSMI. These activities and accomplishments are described below.

### *SIMBIOS Science Team Support*

- a. The fifth science team meeting was held in Baltimore in January 2002 with a substantial US (SIMBIOS and MODIS PIs) and international participation, with official representation from OCTS, POLDER-I and II, MOS, MERIS, GLI, and VIIRS missions. During the meeting the team addressed atmospheric correction and bio-optical algorithms, a MODIS data merging plan for 2002, uncertainty budget and sources from in situ observation, SeaWiFS re-processing, protocols updates and international collaborations. The agenda, presentations, minutes and recommendations are posted at <http://simbios.gsfc.nasa.gov/Info/>
- b. Under a SIMBIOS NRA released in late 1999, a new science team was selected and has been funded under contracts or interagency agreements (2000-2003). The initial team consists of 19 U.S. and 12 international

investigations with additional international investigations to be added as post-NRA proposals are received and accepted (i.e., Australian and Korean proposals). Agreements with the international team members were initiated by NASA/HQ in Fall 2000 and most of them have now been signed.

In October 2001 the SIMBIOS Project management conducted team performance evaluations on all investigations. Formal evaluations of investigations funded through contracts are required by the NASA Procurement Office. All investigations, with the exclusion of one, were renewed for the second year (2002).

### *Satellite Data Characterization*

- a. KOMPSAT/OSMI characterization work was done in collaboration with KARI. Joint scientific papers were presented at the Fall AGU meeting in San Francisco (Franz and Kim, 2002; Kim et al. 2002). In addition, KARI requested assistance from the Project to identify a schedule to record onboard OSMI data. Our recommendation is now implemented.
- b. The Project is hosting a NASDA representative (Mr. Tanaka) for one year (June 2001-June 2002) at NASA Goddard Space Flight Center to assist in the GLI preparations. The Project worked on a document entitled "Instrument characterization of the GLI", delivered at the GLI science team meeting in Tokyo (November 2001).

### *Satellite Data Analyses*

- a. OCTS GAC data reprocessing was completed. This was a very productive collaboration effort with NASDA and Japanese scientists. A scientific presentation was given at the Fall 2001 AGU meeting in San Francisco (Tanaka et al. 2001). OCTS-GAC data is available through the GSFC DAAC, the SIMBIOS Project and NASDA.

**American Geophysical  
Union (AGU)**

**2002 Spring Meeting  
Washington  
Convention Center  
Washington, DC**

**May 28-31, 2002  
(Tuesday – Friday)**

## **Monitoring the Radiometric Stability of the SeaWiFS Transfer Radiometer II**

Authors: Gerhard Meister<sup>1</sup>, Giulietta Fargion<sup>2</sup>, Charles McClain<sup>3</sup>

<sup>1</sup>: Futuretech Corp., SIMBIOS Project, Goddard Space Flight Center, Greenbelt, MD, USA

<sup>2</sup>: Science Applications International Corporation, SIMBIOS Project, Goddard Space Flight Center, Greenbelt, MD, USA

<sup>3</sup>: NASA, Goddard Space Flight Center, Greenbelt, MD, USA

The SIMBIOS (Sensor Intercomparison and Merger for Biological and Interdisciplinary Oceanic Studies) Project Office conducts calibration round-robin intercomparison experiments on a yearly basis. The core instrument is the SeaWiFS Transfer Radiometer II (SXR-II) designed by the National Institute of Standards and Technology (NIST). This filter radiometer measures the radiances produced in the participating laboratories in six wavelength channels from 411 nm to 777 nm. These measured radiances are compared to the radiances expected by the laboratories. The SXR-II is calibrated once a year at the SIRCUS (Spectral Irradiance and Radiance Calibration with Uniform Sources) facility at the NIST.

The radiometric stability of the SXR-II is one of the largest contributions to the combined standard uncertainty of the SXR-II. The latter is estimated to be about 0.8 %. The calibration coefficients of the six SXR-II channels between the NIST calibrations from December 2000 and December 2001 changed between 0.3 % and 1.6 %. The SIMBIOS Project monitors the radiometric stability of the SXR-II with commercially available portable light sources called SeaWiFS

Quality Monitors (SQM) on a monthly basis. This contribution discusses the monitoring results from 2001, which were done with an SQM-II from Satlantic Inc. These results showed that a linear interpolation between the two NIST calibrations describes the evolution of the SXR-II calibration coefficients to within  $\pm 0.5$  %, except for channel 1. We also present preliminary results from 2002 with an SQM (OCS-5002) from Yankee Environmental Systems, Inc.



# 2002 IEEE International Geoscience and Remote Sensing Symposium and the 24<sup>th</sup> Canadian Symposium on Remote Sensing



REMOTE SENSING:  
Integrating Our  
View of the Planet



June 24-28, 2002  
Toronto Canada

# IGARSS 2002

# Integral Equations for a dual-wavelength radar

Robert Meneghini, Code 975, NASA/GSFC, Greenbelt, MD, 20071

Liang Liao, Caelum Research Corp, Code 975

Toshio Iguchi, Communications Research Laboratory, Tokyo, 184-8795, Japan

## I. INTRODUCTION

A dual-wavelength spaceborne weather radar is expected to be one of the primary instruments on the proposed Global Precipitation Mission, GPM, satellite. In addition, airborne dual-wavelength weather radar data at (13.6, 35 GHz), (10, 35 GHz), (10, 94 GHz) have been or will be acquired within the next several years. The objective of the paper is to outline some of the techniques for analyzing such data with a focus on an approach that uses integral equations that describe the change in the DSD parameters with radar range.

## II. DUAL-WAVELENGTH METHODS

Although dual-wavelength radar techniques for ground-based weather radars have been superseded by polarimetric methods, the dual-wavelength radar offers perhaps the best opportunity for accurate measurements of rain and drop size distribution parameters from airborne and spaceborne platforms. From space, a near-nadir viewing geometry for weather radar is dictated by the need to obtain precipitation measurements uncontaminated by the surface. However, at near-nadir incidence, polarimetric techniques such as  $Z_{DR}$  or  $\kappa_{DP}$  that depend on the oblate shape of the raindrops and near-vertical alignment can no longer be used.

Dual-wavelength techniques for rain estimation can be classified into two types. The first comprises methods that estimate the attenuation or differential attenuation followed by a conversion of attenuation into meteorological quantities such as rain rate,  $R$ , or liquid water content,  $M$ . An advantage of using the specific attenuation,  $k$ , rather than the radar reflectivity factor,  $Z$ , to infer  $R$  and  $M$  is that  $k$ ,  $M$ , and  $R$  are approximately equal to the third or fourth moment of the drop size distribution. As a consequence, the estimation of  $M$  or  $R$  from  $k$  is fairly insensitive to the exact form of the drop size distribution, DSD.

The best-known approach of this first type is the standard dual-wavelength method where the frequency difference in radar return powers at range  $r_2$  is subtracted from the same frequency difference at range  $r_1$ . It can be shown from the radar equation that if the scattering is Rayleigh at  $r_1$  and  $r_2$  (i.e., the individual backscattering cross sections of the raindrops within the scattering volumes are proportional to diameter<sup>6</sup> and frequency<sup>4</sup>) this difference of differences is proportional to differential path attenuation in the interval  $[r_1, r_2]$ . The technique is simple to apply. Moreover, if differential attenuation can be estimated accurately, it serves as an accurate estimator of  $M$  and  $R$  because of the insensitivity of the  $k$ - $R$ ,  $k$ - $M$  relations to the DSD. However, the assumption of Rayleigh scattering used in the method is problematic at higher frequencies and higher rain rates where

significant non-Rayleigh scattering can occur. Another disadvantage is that the fractional standard deviation, FSD, in the estimate tends to be large because of the finite sampling of the radar and the relatively small differential signal. Although the FSD can be decreased by choosing a larger interval over which the technique is applied, this degrades the resolution. Although the standard dual-wavelength technique is questionable for high resolution estimates for the (13.6, 35 GHz) combination proposed for GPM, it may be well suited for estimating the differential attenuation over the full path, thereby serving as a constraint for the backward recursion solution described below.

In the second approach, the radar reflectivity factors are corrected for attenuation and the information on the size distribution is inferred from the non-Rayleigh backscattering characteristics of the hydrometeors. The equations can take the form either of two coupled Volterra integral equations or two coupled non-linear first order differential equations for the parameters of the DSD [1-3]. Only the first formulation will be considered here. Note that in the standard method, Rayleigh scattering is assumed whereas in this approach, the signal that we wish to extract is the non-Rayleigh scattering signal. Moreover, the objective of the second approach is to estimate parameters of the DSD and then proceed to the  $R$  and  $M$  estimates whereas the first approach proceeds from the attenuation directly to  $R$  and  $M$ . The solution to the integral or differential equations, however, is unstable if it is carried out in the forward direction from the storm top toward the surface. This is similar to the instability in the Hitschfeld-Bordan solution in the presence of moderate attenuation in the case of single attenuating-wavelength radar data. The solution can be made more stable by reformulating the equations so that the solution proceeds from the surface to the storm top. This can be done, however, only if estimates of the path integrated attenuation, PIA, at both frequencies can be obtained. We discuss several possibilities below.

In the surface reference technique, SRT, the 2-way PIA is approximated by the difference in the radar return powers from the surface in the presence and absence of rain. The technique can be applied at each frequency so the path attenuations at frequencies 1 and 2 are available. We denote the specific attenuations (dB/km) at  $f_1$  and  $f_2$  by  $k(f_1)$  and  $k(f_2)$ . An alternative is to estimate the differential path attenuation by forming the frequency difference of the surface return powers outside and inside the rain and then taking a difference of these differences. To obtain  $k(f_1)$  and  $k(f_2)$  from the specific differential attenuation,  $k_{f_1-f_2}$ , we can use measured DSD data and Mie scattering calculations to obtain linear fits of the form:  $k(f) = \alpha_i + \beta_i k_{f_1-f_2}$ ,  $f_i = f_1$  or  $f_2$ . For example, at  $T = 10$  C, with  $f_1 = 35$  GHz and  $f_2 = 13.6$  GHz we obtain  $\alpha_1 = 0.117$ ,  $\beta_1 = 1.04$ ,  $\alpha_2 = 0.117$ ,  $\beta_2 = 0.042$ .

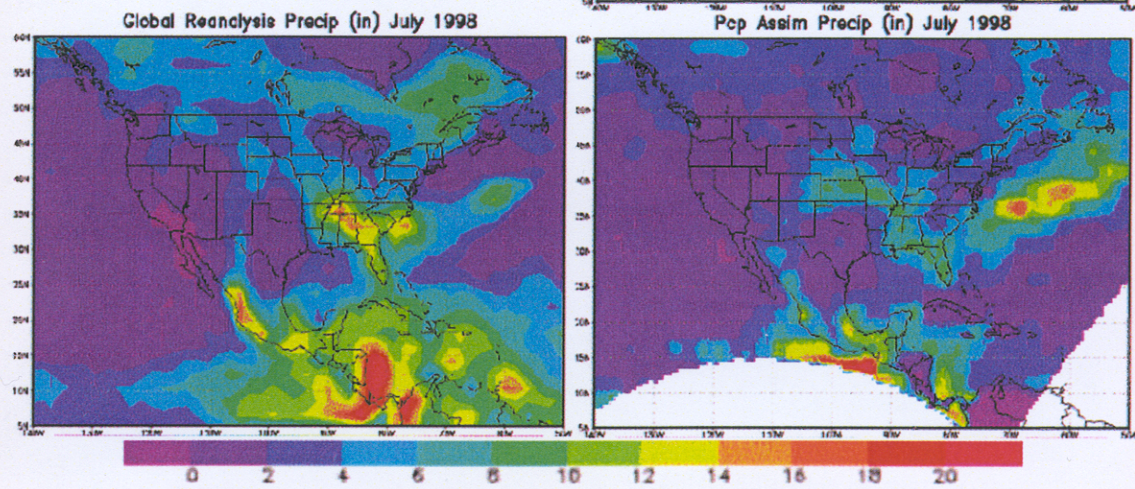


# 16th Conference on Hydrology



**13–17 January 2002**  
**Orlando, Florida**

## **NCEP Regional Reanalysis Result for July 1998**



AMERICAN METEOROLOGICAL SOCIETY



## J1.1 REDUCING NEAR-SURFACE COOL/MOIST BIASES OVER SNOWPACK AND EARLY SPRING WET SOILS IN NCEP ETA MODEL FORECASTS VIA LAND SURFACE MODEL UPGRADES

K. Mitchell<sup>1</sup>, M. Ek<sup>1,2</sup>, D. Lohmann<sup>1,2</sup>, V. Koren<sup>3</sup>, J. Schaake<sup>3</sup>,  
Q. Duan<sup>3</sup>, P. Grunmann<sup>1,2</sup>, G. Gayno<sup>5</sup>, Y. Lin<sup>1</sup>, E. Rogers<sup>1</sup>, D. Tarpley<sup>4</sup>, C. Peters-Lidard<sup>6</sup>

<sup>1</sup>NOAA/NWS/National Centers for Environmental Prediction/Environmental Modeling Center

<sup>2</sup>University Corporation for Atmospheric Research/Visiting Scientist Program

<sup>3</sup>NOAA/NWS/Office of Hydrologic Development

<sup>4</sup>NOAA/National Environmental Satellite, Data, and Information Service/Office of Res. & Applications

<sup>5</sup>USAF Air Force Weather Agency

<sup>6</sup>NASA/GSFC Hydrological Sciences Branch

### 1. INTRODUCTION

Since 1996, a series of NOAA GAPP/GCIP-sponsored land-surface related advances have been implemented in the NCEP mesoscale Eta model and its Eta-based data assimilation system (EDAS). This began with the introduction in January 1996 of a multi-layer soil-vegetation-snow land-surface model originally developed at Oregon State University (Mahrt and Pan, 1984), and modified for use in the Eta model (Chen et al 1996). At that time, the Eta model used initial soil moisture and temperature from the NCEP global model data assimilation system (GDAS), which employs soil moisture nudging to a fixed, annual-cycle soil moisture climatology.

Over the following 2-3 years, subsequent advances to the Eta model land-surface treatment included the use of the NESDIS, high-resolution, NDVI-based vegetation greenness fraction database, adjustments to the initial global model soil moisture, an increase from two to four soil layers, and the use of the NESDIS operational daily 23-km North American snow cover and sea ice analysis. This late 90's period of Eta land-surface improvements culminated in June 1998 with the introduction of continuous self-cycling of Eta soil moisture and soil temperature in the Eta 4-D Data Assimilation System (EDAS). The latter employs no soil moisture nudging. Since then and up to the present (over three years), the Eta model's initial soil moisture and soil temperature have been sole products of the continuous cycling of these two land states in the coupled land-atmosphere EDAS.

Between June 1998 and July 2001, no further significant changes were implemented to the operational Eta/EDAS land-surface package. Section 2 presents examples of the validation of Eta model performance during that period. Simultaneously during that period, off-line development focused on our next generation of land-surface improvements, to include frozen soil processes, plus substantial advances to the snowpack physics and ground heat flux physics.

This phase of significant upgrades, in collaboration with our GAPP/GCIP and other partners, led us to coin the name "NOAH" to designate our new LSM. Section 3 describes these LSM upgrades and Section 4 presents some results from the successful testing of these upgrades in the coupled Eta/EDAS, which culminated in their operational implementation on 24 July 2001.

### 4. COUPLED ETA MODEL TESTING

Pre-implementation testing of the upgraded NOAH LSM in the coupled Eta model spanned 1) a summer month (12 Aug - 12 Sep 2000), 2) a winter month (01 Feb - 01 Mar 2001), and a spring month (24 Apr - 24 May 2001). Over these three periods we continuously executed the cycled EDAS and launched twice-daily 60-h Eta forecasts (one each from the 00Z and 12Z initial times) for both A) the control configuration (then operational suite) and B) the test configuration with the NOAH LSM encompassing the land-surface changes summarized in the previous section. The next two sub-sections present two examples of model bias reduction in the test case.

#### 4.1 *Spring case*

The Eta model control case (i.e. as operational prior to the 24 Jul 2001) exhibits a near-surface cool (moist) bias in forecasts of air temperature (dewpoint) throughout the U.S. north central plains in spring, when the near-surface soil is typically moist from spring rains and the recent snowmelt season, and before substantial green vegetation has emerged. Inspection of Fig. 4 of the 60-h Eta forecast, valid at 00Z on 30 Apr 2001, of the dew point temperature in the lower boundary layer reveals that the test (right frame) is substantially less moist than the control (left frame).

# **NASA/TM-2002-210004/Rev3-Vol1**

**James L. Mueller<sup>1</sup> and Giulietta S. Fargion<sup>2</sup>**  
**Editors**

<sup>1</sup> *CHORS, San Diego State University, San Diego, California*

<sup>2</sup> *Science Applications International Corporation, Beltsville, Maryland*

## **Ocean Optics Protocols For Satellite Ocean Color Sensor Validation, Revision 3, Volume 1**

J. L. Mueller, C. Pietras, S. B. Hooker, D. K. Clark, A. Morel, R. Frouin, B.G. Mitchell,  
R. R. Bidigare, C. Trees, J. Werdell, G. S. Fargion, R. Arnone, R. W. Austin, S. Bailey,  
W. Broenkow, S. W. Brown, K. Carder, C. Davis, J. Dore, M. Feinholz, S. Flora, Z.P.  
Lee, B. Holben, B. C. Johnson, M. Kahru, D. M. Karl, Y. S Kim, K. D. Knobelspiesse, C.  
R. McClain, S. McLean, M. Miller, C. D. Mobley, J. Porter, R.G. Steward, M. Stramska,  
L. Van Heukelem, K. Voss, J. Wieland, M. A. Yarbrough and M. Yuen.

National Aeronautical and  
Space administration

**Goddard Space Flight Space Center**  
Greenbelt, Maryland 20771

**February 2002**

## Chapter 1

# Ocean Color Radiometry and Bio-Optics

James L. Mueller<sup>1</sup>, Roswell W. Austin<sup>1</sup>, Giulietta S. Fargion<sup>2</sup> and Charles R. McClain<sup>3</sup>

<sup>1</sup>*Center for Hydro-Optics and Remote Sensing, San Diego State University, California*

<sup>2</sup>*Science Applications International Corporation, Beltsville, Maryland*

<sup>3</sup>*NASA, Goddard Space Flight Center, Greenbelt, Maryland*

## 1.1 INTRODUCTION

During the period from *circa* 1985 to 1991, the National Aeronautics and Space Administration (NASA) charged a series of successive science working groups with the task of recommending guidelines, goals and mission design criteria for future satellite ocean color remote sensors. The deliberations of these working groups were based on the ocean color science community's experiences with the Nimbus-7 Coastal Zone Color Scanner (CZCS). On the one hand, the highly successful CZCS mission firmly established ocean color remote sensing as a powerful tool for monitoring and studying the bio-optical properties of the global ocean. On the other hand, the radiometric responsivities of the CZCS channels declined progressively with time throughout its 8-year operating life, which just as firmly established the need to independently verify a satellite sensor's performance using *in situ* measurements of the ocean and atmosphere. From those two general perspectives, the principal recommendations of these NASA Ocean Color Science Working Groups (collectively) included:

1. **Baseline satellite ocean color products** should include
  - a. Normalized water-leaving radiances  $L_{\text{WN}}(\lambda)$  (Gordon and Clark, 1981),
  - b. Aerosol radiances  $L_a(\lambda)$ ,
  - c. Chlorophyll *a* concentration  $Chl$  [ $\text{mg m}^{-3}$ ],
  - d. The diffuse attenuation coefficient  $K(490)$  at a wavelength of 490 nm, and
  - e. Calibrated radiances  $L_t(\lambda)$  observed at the satellite.
2. **Principal goals for product uncertainties** should be
  - a. Less than **5 % uncertainty** in  $L_{\text{WN}}(\lambda)$  and
  - b. Less than **35 % uncertainty** in  $Chl$ .
3. An **ongoing satellite ocean color sensor system validation program** is necessary, using *in situ* measurements of ocean radiometric and bio-optical properties, and of atmospheric optical properties, to verify system performance - including algorithms - immediately after launch and throughout a satellite ocean color sensor's operating lifetime.

These and other recommendations of the earlier working groups were endorsed by the Sea-viewing Wide Field-of-view Sensor (SeaWiFS) Science Team and accepted by NASA. Of particular significance in the present context, the SeaWiFS Project Office moved immediately to implement a SeaWiFS Validation Plan designed to assure a best effort to achieve the above product uncertainty goals (McClain *et al.* 1992). A critical aspect of the validation plan was that *in situ* radiometric, optical and bio-optical measurements of uniformly high quality and accuracy be obtained for verifying SeaWiFS system performance and product uncertainties. Therefore, in 1991 the SeaWiFS Project Office sponsored a workshop to recommend appropriate measurements, instrument specifications, and protocols specifying methods of calibration, field measurements, and data analysis necessary to support SeaWiFS validation, leading to the first publication of *Ocean Optics Protocols for SeaWiFS Validation* (Mueller and Austin 1992). Continued discourse within the ocean color research community led to Revisions 1 (Mueller and Austin 1995) and 2 (Fargion and Mueller 2000) of these protocols.

# **NASA/TM-2002-210004/Rev3-Vol1**

**James L. Mueller<sup>1</sup> and Giulietta S. Fargion<sup>2</sup>**  
**Editors**

<sup>1</sup> *CHORS, San Diego State University, San Diego, California*

<sup>2</sup> *Science Applications International Corporation, Beltsville, Maryland*

## **Ocean Optics Protocols For Satellite Ocean Color Sensor Validation, Revision 3, Volume 1**

J. L. Mueller, C. Pietras, S. B. Hooker, D. K. Clark, A. Morel, R. Frouin, B.G. Mitchell,  
R. R. Bidigare, C. Trees, J. Werdell, G. S. Fargion, R. Arnone, R. W. Austin, S. Bailey,  
W. Broenkow, S. W. Brown, K. Carder, C. Davis, J. Dore, M. Feinholz, S. Flora, Z.P.  
Lee, B. Holben, B. C. Johnson, M. Kahru, D. M. Karl, Y. S Kim, K. D. Knobelspiesse, C.  
R. McClain, S. McLean, M. Miller, C. D. Mobley, J. Porter, R.G. Steward, M. Stramska,  
L. Van Heukelem, K. Voss, J. Wieland, M. A. Yarbrough and M. Yuen.

National Aeronautical and  
Space administration

**Goddard Space Flight Space Center**  
Greenbelt, Maryland 20771

**February 2002**



## Chapter 3

# Data Requirements for Ocean Color Algorithms and Validation

James L. Mueller<sup>1</sup>, Giulietta S. Fargion<sup>2</sup> and Charles R. McClain<sup>3</sup>

<sup>1</sup>*Center for Hydro-Optics and Remote Sensing, San Diego State University, California*

<sup>2</sup>*Science Applications International Corporation, Beltsville, Maryland*

<sup>3</sup>*NASA, Goddard Space Flight Center, Greenbelt, Maryland*

### 3.1 INTRODUCTION

The principal *in situ* variables to be measured, or derived from measurements, for satellite ocean color sensor validation, and algorithm development and validation, are listed in Table 3.1. The variables are grouped, in Table 3.1, into four related groups: Radiometric Quantities (both oceanic and atmospheric), Inherent Optical Properties (IOP) of sea water, Biogeochemical and Bio-Optical Properties of sea water, and Ancillary Data and Metadata required to support the use, analysis, interpretation, and quality assessment of the other data. Those *in situ* variables that are measured are classified into three categories of descending priority.

The first category of measurements, flagged “Required” in Table 3.1, is the minimum subset required for validating a satellite sensor’s radiometric performance, exact normalized water-leaving radiances (Chapter 13), and fundamental derived products, including chlorophyll *a* concentration, aerosol optical thickness, and *K*(490), and for associated algorithm development and validation.

The second category, flagged “Highly Desired” in Table 3.1, are measurements that supplement the minimum subset and are needed for investigations focused on atmospheric correction algorithms and aerosols, relationships between IOP and remote sensing reflectance, and/or Case 3 algorithms.

The third category, flagged “Specialized Measurement” in Table 3.1, are measurements which either address aspects of ocean bio-optics that are secondary to satellite remote sensing, or require highly specialized equipment that is not readily available to the community at large.

A fourth category, flagged as “Derived”, comprises key quantities that are either calculated from the *in situ* measurements, or are derived from models. The above set of variables is also listed in Table 3.2, to identify the satellite ocean color sensor application for which each measurement is needed. Table 3.2 also provides an index of the protocol chapters addressing each *in situ* measurement.

### 3.2 RADIOMETRIC QUANTITIES

Surface incident spectral irradiance in air,  $E_s(\lambda) \equiv E_d(0^+, \lambda)$ , downwelled spectral irradiance,  $E_d(z, \lambda)$ , and upwelled spectral radiance,  $L_u(z, \lambda)$ , are the fundamental measurable quantities needed to derive normalized water-leaving radiances (or equivalently remote sensing reflectance) in most circumstances. Other radiometric properties listed in Table 3.1, including sky radiance and normal solar irradiance, are also important *in situ* measurements in the SIMBIOS ocean color validation program. Also listed are critical radiometric quantities that are calculated, or derived, from *in situ* measurements. In some cases, listed radiometric quantities may be derived, wholly or in part, from other non-radiometric measurements listed in the table. For example, remote sensing reflectance may either be calculated directly as the ratio of water-leaving radiance  $L_w(\lambda)$  to incident irradiance,  $L_w(\lambda):E_s(\lambda)$ , or it may be modeled as a function of the IOP ratio of the backscattering to absorption coefficients,  $b_b(\lambda):a(\lambda)$ , and the Bidirectional Reflectance Distribution Function (BRDF) (Chapter 13).

# **NASA/TM-2002-210004/Rev3-Vol1**

**James L. Mueller<sup>1</sup> and Giulietta S. Fargion<sup>2</sup>**  
**Editors**

<sup>1</sup> *CHORS, San Diego State University, San Diego, California*

<sup>2</sup> *Science Applications International Corporation, Beltsville, Maryland*

## **Ocean Optics Protocols For Satellite Ocean Color Sensor Validation, Revision 3, Volume 1**

J. L. Mueller, C. Pietras, S. B. Hooker, D. K. Clark, A. Morel, R. Frouin, B.G. Mitchell, R. R. Bidigare, C. Trees, J. Werdell, G. S. Fargion, R. Arnone, R. W. Austin, S. Bailey, W. Broenkow, S. W. Brown, K. Carder, C. Davis, J. Dore, M. Feinholz, S. Flora, Z.P. Lee, B. Holben, B. C. Johnson, M. Kahru, D. M. Karl, Y. S Kim, K. D. Knobelspiesse, C. R. McClain, S. McLean, M. Miller, C. D. Mobley, J. Porter, R.G. Steward, M. Stramska, L. Van Heukelem, K. Voss, J. Wieland, M. A. Yarbrough and M. Yuen.

National Aeronautical and  
Space administration

**Goddard Space Flight Space Center**  
Greenbelt, Maryland 20771

**February 2002**

## Preface

This document stipulates protocols for measuring bio-optical and radiometric data for the Sensor Intercomparison and Merger for Biological and Interdisciplinary Oceanic Studies (SIMBIOS) Project activities and algorithm development. This document supersedes the earlier version (Fargion and Mueller 2000) and is organized into four parts:

- *Introductory Background:* The initial part covers perspectives on ocean color research and validation (Chapter 1), fundamental definitions, terminology, relationships and conventions used throughout the protocol document (Chapter 2), and requirements for specific *in situ* observations (Chapter 3).
- *Instrument Characteristics:* This group of chapters begins with a review of instrument performance characteristics required for *in situ* observations to support validation (Chapter 4), and the subsequent chapters cover detailed instrument specifications and underlying rationale (Chapter 5) and protocols for instrument calibration and characterization standards and methods (Chapters 6 through 8).
- *Field Measurements and Data Analysis:* The methods used in the field to make the *in situ* measurements needed for ocean color validation, together with methods of analyzing the data, are briefly, but comprehensively, reviewed in Chapter 9. The remaining chapters of this part provide detailed measurement and data analysis protocols for in-water radiometric profiles (Chapter 10), the Marine Optical Buoy (MOBY) radiometric observatory for vicarious calibration of satellite ocean color sensors (Chapter 11), above water measurements of remote sensing reflectance (Chapter 12), determinations of exact normalized water-leaving radiance (Chapter 13), atmospheric radiometric measurements to determine aerosol optical thickness and sky radiance distributions (Chapter 14), determination of absorption spectra from water samples (Chapter 15), and determination of phytoplankton pigment concentrations using HPLC (Chapter 16) and fluorometric (Chapter 17) methods.
- *Data Reporting and Archival:* Chapter 18 describes the methods and procedures for data archival, data synthesis and merging, and quality control applicable to the SeaWiFS Bio-optical Archive and Storage System (SeaBASS), which is maintained to support ocean color validation for the SeaWiFS, SIMBIOS and other cooperating satellite sensor projects. Current SeaBASS file content and formatting requirements are given in Appendix B.

What is new in Revision 3 to the ocean optics protocol document, as compared to Revision 2 (Fargion and Mueller 2000). The most obvious changes are the insertion of 3 new chapters into the document, and the renumbering of the other chapters to accommodate them. The new chapters are:

1. Chapter 2, *Fundamental Definitions, Relationships and Conventions*, introduces the radiometric quantities, inherent optical properties, fundamental concepts and terminology underlying the *in situ* measurement and analysis protocols discussed throughout the document. The chapter also discusses the scales adopted in these protocols for such quantities as extraterrestrial solar irradiance, and the absorption and scattering coefficients of pure water.
2. Chapter 11, *MOBY, A Radiometric Buoy for Performance Monitoring and Vicarious Calibration of Satellite Ocean Color Sensors: Measurement and Data Analysis Protocols*, documents the specific measurement and data analysis protocols used in the operation of this critical radiometric observatory. The MOBY normalized water-leaving radiance time series has provided the principal, common basis for vicarious calibration of every satellite ocean color sensor in operation since 1996.
3. Chapter 13, *Normalized Water-Leaving Radiance and Remote Sensing Reflectance: Bidirectional Reflectance and Other Factors*, develops the physical basis underlying the bidirectional aspects of the ocean's reflectance, and presents methods for removing this effect to determine *exact normalized water-leaving radiance*, the only form of water-leaving radiance suitable for comparisons between determinations based on satellite and *in situ* measurements.

Aside from renumbering, several of the chapters carried over from Revision 2 have been revisited and significantly revised, while others have been modified only slightly. The two chapters providing overviews of Instrument Characteristics (Chapter 4) and Field Measurements and Data Analysis (Chapter 9) have been revised to reflect the changed content of those two major parts of the document.

# **NASA/TM-2002-210004/Rev3-Vol2**

**James L. Mueller<sup>1</sup> and Giulietta S. Fargion<sup>2</sup>**  
**Editors**

<sup>1</sup> *CHORS, San Diego State University, San Diego, California*

<sup>2</sup> *Science Applications International Corporation, Beltsville, Maryland*

## **Ocean Optics Protocols For Satellite Ocean Color Sensor Validation, Revision 3, Volume 2**

J. L. Mueller, C. Pietras, S. B. Hooker, D. K. Clark, A. Morel, R. Frouin, B.G. Mitchell,  
R. R. Bidigare, C. Trees, J. Werdell, G. S. Fargion, R. Arnone, R. W. Austin, S. Bailey,  
W. Broenkow, S. W. Brown, K. Carder, C. Davis, J. Dore, M. Feinholz, S. Flora, Z.P.  
Lee, B. Holben, B. C. Johnson, M. Kahru, D. M. Karl, Y. S Kim, K. D. Knobelspiesse, C.  
R. McClain, S. McLean, M. Miller, C. D. Mobley, J. Porter, R.G. Steward, M. Stramska,  
L. Van Heukelem, K. Voss, J. Wieland, M. A. Yarbrough and M. Yuen.

National Aeronautical and  
Space administration

**Goddard Space Flight Space Center**  
Greenbelt, Maryland 20771

**February 2002**

## Chapter 12

# Above-Water Radiance and Remote Sensing Reflectance Measurement and Analysis Protocols

James L. Mueller<sup>1</sup>, Curtiss Davis<sup>2</sup>, Robert Arnone<sup>3</sup>, Robert Frouin<sup>4</sup>, Kendall Carder<sup>5</sup>, Z.P. Lee<sup>5</sup>, R.G. Steward<sup>5</sup>, Stanford Hooker<sup>6</sup>, Curtis D. Mobley<sup>7</sup> and Scott McLean<sup>8</sup>

<sup>1</sup>*Center for Hydro-Optics and Remote Sensing, San Diego State University, California*

<sup>2</sup>*Naval Research Laboratory, Washington, District of Columbia*

<sup>3</sup>*Naval Research Laboratory, Stennis Space Center, Mississippi*

<sup>4</sup>*Scripps Institution of Oceanography, University of California, San Diego, California*

<sup>5</sup>*University of South Florida, St. Petersburg, Florida*

<sup>6</sup>*NASA, Goddard Space Flight Center, Greenbelt, Maryland*

<sup>7</sup>*Sequoia Scientific Inc., Redmond, Washington*

<sup>8</sup>*Satlantic Inc., Halifax, Nova Scotia, Canada*

## 12.1 INTRODUCTION

As an alternative to the in-water methods of Chapters 10 and 11, water-leaving radiance can be measured from the deck of a ship. A shipboard radiometer is used to measure radiance  $L_{\text{sf}}(\lambda, \theta, \phi \in \Omega_{\text{FOV}}; \theta_o)$  emanating from the sea surface at zenith angle  $\theta$  (usually chosen between  $30^\circ$  and  $50^\circ$ ) and azimuth angle  $\phi$  (usually chosen between  $90^\circ$  and  $180^\circ$  away the sun's azimuth  $\phi_o$ ). In the convention used here, azimuth angles  $\phi$  are measured relative to the sun's azimuth, *i.e.*  $\phi_o = 0$ .

The surface radiance measured with a radiometer having a solid-angle field of view (FOV) of  $\Omega_{\text{FOV}}$  sr may be expressed, following Mobley (1999), as

$$L_{\text{sf}}(\lambda, \theta, \phi \in \Omega_{\text{FOV}}; \theta_o) = L_{\text{w}}(\lambda, \theta, \phi \in \Omega_{\text{FOV}}; \theta_o) + \rho L_{\text{sky}}(\lambda, \theta_{\text{sky}}, \phi_{\text{sky}} \in \Omega'_{\text{FOV}}; \theta_o). \quad (12.1)$$

$L_{\text{w}}(\lambda, \theta, \phi \in \Omega_{\text{FOV}}; \theta_o)$  is water-leaving radiance centered at angles  $(\theta, \phi)$  and averaged over  $\Omega_{\text{FOV}}$  [as weighted by the radiometer's directional response function (see Chapter 5)].  $L_{\text{sky}}(\lambda, \theta_{\text{sky}}, \phi_{\text{sky}} \in \Omega'_{\text{FOV}}; \theta_o)$  is sky radiance measured with the radiometer looking upward at angles  $(\theta_{\text{sky}}, \phi_{\text{sky}})$ . In practice,  $\theta$  and  $\theta_{\text{sky}}$  are numerically equal angles in the nadir and zenith directions, respectively, and the sea and sky viewing azimuths  $\phi = \phi_{\text{sky}}$ . The reflectance factor  $\rho$  is operationally defined as the total skylight actually reflected from the wave-roughened sea surface into direction  $(\theta, \phi)$  divided by sky radiance measured with the radiometer from direction  $(\theta_{\text{sky}}, \phi_{\text{sky}})$ , both quantities being averaged over  $\Omega_{\text{FOV}}$  (Mobley 1999). Remote sensing reflectance is then determined, using water-leaving radiance calculated from (12.1), as

$$R_{\text{RS}}(\lambda, \theta, \phi \in \Omega_{\text{FOV}}; \theta_o) = \frac{L_{\text{w}}(\lambda, \theta, \phi \in \Omega_{\text{FOV}}; \theta_o)}{E_{\text{s}}(\lambda; \theta_o)}, \quad (12.2)$$

where  $E_{\text{s}}(\lambda; \theta_o)$  is incident spectral irradiance measured above the sea surface. All of the above variables vary with solar zenith angle  $\theta_o$ .

A simplified notation is used in Chapters 10 and 11 (and elsewhere in the protocols) when discussing water leaving radiance  $L_{\text{w}}(\lambda)$  and remote sensing reflectance  $R_{\text{RS}}(\lambda)$  derived from in-water profile measurements of  $L_{\text{u}}(z, \lambda)$ . Because  $L_{\text{u}}(z, \lambda)$  is measured viewing the nadir direction,  $L_{\text{w}}(\lambda)$  represents radiance leaving the surface in the zenith direction  $(\theta, \phi) = (0^\circ, 0^\circ)$ . Therefore,  $L_{\text{w}}(\lambda)$  in Chapter 11 corresponds to  $L(\lambda, 0, 0 \in \Omega; \theta)$ , and  $R_{\text{RS}}(\lambda)$  to  $R(\lambda, 0, 0 \in \Omega; \theta)$ , in the present notation.

# **NASA/TM-2002-210004/Rev3-Vol2**

**James L. Mueller<sup>1</sup> and Giulietta S. Fargion<sup>2</sup>**  
**Editors**

<sup>1</sup> *CHORS, San Diego State University, San Diego, California*

<sup>2</sup> *Science Applications International Corporation, Beltsville, Maryland*

## **Ocean Optics Protocols For Satellite Ocean Color Sensor Validation, Revision 3, Volume 2**

J. L. Mueller, C. Pietras, S. B. Hooker, D. K. Clark, A. Morel, R. Frouin, B.G. Mitchell,  
R. R. Bidigare, C. Trees, J. Werdell, G. S. Fargion, R. Arnone, R. W. Austin, S. Bailey,  
W. Broenkow, S. W. Brown, K. Carder, C. Davis, J. Dore, M. Feinholz, S. Flora, Z.P.  
Lee, B. Holben, B. C. Johnson, M. Kahru, D. M. Karl, Y. S Kim, K. D. Knobelspiesse, C.  
R. McClain, S. McLean, M. Miller, C. D. Mobley, J. Porter, R.G. Steward, M. Stramska,  
L. Van Heukelem, K. Voss, J. Wieland, M. A. Yarbrough and M. Yuen.

National Aeronautical and  
Space administration

**Goddard Space Flight Space Center**  
Greenbelt, Maryland 20771

**February 2002**



## Preface

This document stipulates protocols for measuring bio-optical and radiometric data for the Sensor Intercomparison and Merger for Biological and Interdisciplinary Oceanic Studies (SIMBIOS) Project activities and algorithm development. This document supersedes the earlier version (Fargion and Mueller 2000) and is organized into four parts:

- *Introductory Background:* The initial part covers perspectives on ocean color research and validation (Chapter 1), fundamental definitions, terminology, relationships and conventions used throughout the protocol document (Chapter 2), and requirements for specific *in situ* observations (Chapter 3).
- *Instrument Characteristics:* This group of chapters begins with a review of instrument performance characteristics required for *in situ* observations to support validation (Chapter 4), and the subsequent chapters cover detailed instrument specifications and underlying rationale (Chapter 5) and protocols for instrument calibration and characterization standards and methods (Chapters 6 through 8).
- *Field Measurements and Data Analysis:* The methods used in the field to make the *in situ* measurements needed for ocean color validation, together with methods of analyzing the data, are briefly, but comprehensively, reviewed in Chapter 9. The remaining chapters of this part provide detailed measurement and data analysis protocols for in-water radiometric profiles (Chapter 10), the Marine Optical Buoy (MOBY) radiometric observatory for vicarious calibration of satellite ocean color sensors (Chapter 11), above water measurements of remote sensing reflectance (Chapter 12), determinations of exact normalized water-leaving radiance (Chapter 13), atmospheric radiometric measurements to determine aerosol optical thickness and sky radiance distributions (Chapter 14), determination of absorption spectra from water samples (Chapter 15), and determination of phytoplankton pigment concentrations using HPLC (Chapter 16) and fluorometric (Chapter 17) methods.
- *Data Reporting and Archival:* Chapter 18 describes the methods and procedures for data archival, data synthesis and merging, and quality control applicable to the SeaWiFS Bio-optical Archive and Storage System (SeaBASS), which is maintained to support ocean color validation for the SeaWiFS, SIMBIOS and other cooperating satellite sensor projects. Current SeaBASS file content and formatting requirements are given in Appendix B.

What is new in Revision 3 to the ocean optics protocol document, as compared to Revision 2 (Fargion and Mueller 2000). The most obvious changes are the insertion of 3 new chapters into the document, and the renumbering of the other chapters to accommodate them. The new chapters are:

1. Chapter 2, *Fundamental Definitions, Relationships and Conventions*, introduces the radiometric quantities, inherent optical properties, fundamental concepts and terminology underlying the *in situ* measurement and analysis protocols discussed throughout the document. The chapter also discusses the scales adopted in these protocols for such quantities as extraterrestrial solar irradiance, and the absorption and scattering coefficients of pure water.
2. Chapter 11, *MOBY, A Radiometric Buoy for Performance Monitoring and Vicarious Calibration of Satellite Ocean Color Sensors: Measurement and Data Analysis Protocols*, documents the specific measurement and data analysis protocols used in the operation of this critical radiometric observatory. The MOBY normalized water-leaving radiance time series has provided the principal, common basis for vicarious calibration of every satellite ocean color sensor in operation since 1996.
3. Chapter 13, *Normalized Water-Leaving Radiance and Remote Sensing Reflectance: Bidirectional Reflectance and Other Factors*, develops the physical basis underlying the bidirectional aspects of the ocean's reflectance, and presents methods for removing this effect to determine *exact normalized water-leaving radiance*, the only form of water-leaving radiance suitable for comparisons between determinations based on satellite and *in situ* measurements.

Aside from renumbering, several of the chapters carried over from Revision 2 have been revisited and significantly revised, while others have been modified only slightly.



PROCEEDINGS OF SPIE  
SPIE—The International Society for Optical Engineering

# ***Remote Sensing for Agriculture, Ecosystems, and Hydrology III***

**Manfred Owe  
Guido D'Urso**  
*Chairs/Editors*

**17–19 September 2001  
Toulouse, France**

*Sponsored and Published by*  
SPIE—The International Society for Optical Engineering

*Cooperating Organizations*  
EOS—European Optical Society  
CNES—Centre National d'Etudes Spatiales (France)  
NASA—National Aeronautic and Space Administration (USA)



**Volume 4542**

SPIE is an international technical society dedicated to advancing engineering and scientific applications of optical, photonic, imaging, electronic, and optoelectronic technologies.

# Recent advances in microwave sensing of soil moisture

Manfred Owe<sup>a</sup>, Richard A.M. de Jeu<sup>b</sup>

<sup>a</sup>NASA/Goddard Space Flight Center, Greenbelt, MD 20771;

<sup>b</sup>Faculty of Earth Sciences, Vrije Universiteit Amsterdam, The Netherlands

## ABSTRACT

A new approach for retrieving surface soil moisture from satellite microwave brightness temperature is described. The approach uses radiative transfer theory together with a non-linear optimization routine to partition the observed microwave signal into its soil and vegetation components. Vegetation optical depth is derived directly from the microwave polarization difference index, while the soil component is solved in terms of the soil dielectric constant. A global data base of soil physical properties is then used to derive soil moisture from the soil dielectric constant. The approach is tested with historical SMMR data to produce time series of surface soil moisture over several global test sites. Comparisons with ground observations of soil moisture are made. Preliminary results over several global test sites are provided.

**Keywords:** Remote sensing, microwave brightness temperature, soil moisture, radiative transfer

## 1. INTRODUCTION

Satellite remote sensing offers potentially the greatest single contribution to large-scale monitoring of the Earth's surface. While ground measurements typically provide the greatest accuracy, they are manpower-intensive, costly, and time consuming. In addition, they are still point measurements, and are usually difficult to aggregate to provide reliable spatial averages. Satellite systems can offer the spatial, temporal, and spectral resolution necessary for consistent and continuous uninterrupted coverage of the whole Earth environment and its surrounding atmosphere. Such detailed observations are necessary in order to detect often-subtle environmental changes. Microwave remote sensing is unique, in that it is the only technology which responds directly to the absolute volume of water which is present in the environment. Radiometric temperature readings in the microwave region have been shown to yield information on soil moisture, precipitable water in clouds, precipitation, and snow. Remote sensing technology is central to the integration of the many interrelated but highly variable point scale phenomena to more useful, regionally-oriented land surface processes. Soil moisture retrieval by microwave is the only remote sensing technique that provides a direct measure of the absolute volume of water in the top soil layer. While the physics of modelling soil emission is relatively straight-forward, accounting for the effects of the overlying vegetation has always presented a more difficult challenge. The signal which emanates from the soil, results from the natural thermal emission in the microwave region, the magnitude of which is determined by the dielectric properties of the combined soil water mixture. However, a vegetation canopy will influence this signal, both by attenuating the soil emission, and by contributing a signal of its own. Emission characteristics of the vegetation are a function of the vegetation dielectric properties. The signal that is subsequently observed by a microwave sensor is highly complex, and must be partitioned into its source components before any soil moisture information can be extracted. Several new approaches for retrieving surface soil moisture from satellite radiometer data have been developed recently <sup>1</sup>. The approach presented here uses radiative transfer theory to solve for surface moisture and the vegetation optical depth. The methodology is somewhat unique, in that it does not require any field observations of soil moisture or canopy biophysical properties for calibration purposes and may be applied at any wavelength. The procedure is being tested with historical 6.6 GHz brightness temperature observations from the Scanning Multichannel Microwave Radiometer (SMMR) <sup>2</sup>. Some microwave theory is presented, along with some preliminary results from several validation studies. Comparisons are made to in-situ observations of soil moisture from several global test sites.



PROCEEDINGS OF SPIE  
SPIE—The International Society for Optical Engineering

# ***Remote Sensing for Agriculture, Ecosystems, and Hydrology III***

**Manfred Owe  
Guido D'Urso**  
*Chairs/Editors*

**17–19 September 2001  
Toulouse, France**

*Sponsored and Published by*  
SPIE—The International Society for Optical Engineering

*Cooperating Organizations*  
EOS—European Optical Society  
CNES—Centre National d'Etudes Spatiales (France)  
NASA—National Aeronautic and Space Administration (USA)



**Volume 4542**

SPIE is an international technical society dedicated to advancing engineering and scientific applications of optical, photonic, imaging, electronic, and optoelectronic technologies.



# Aqua

## MONITORING THE EARTH'S WATER CYCLE AND ASSOCIATED VARIABLES FROM THE VANTAGE OF SPACE

### Aqua Overview

Issues of climate and climate change have considerable relevance to all species of life on Earth. Furthermore, they have received much publicity over the past many years, particularly because of the realization that humans could be having unintended and perhaps detrimental impacts. Nonetheless, the understanding of the Earth/atmosphere system remains inadequate to sort out with certainty human from non-human impacts on long-term climate or to predict with high confidence the likely course of climate changes over the next several decades.

Aqua is a satellite mission aimed at improving our understanding of the Earth/atmosphere system, along with changes occurring within it, through the monitoring and analysis of dozens of Earth variables from a space-based platform orbiting the Earth. Aqua is part of the Earth Observing System (EOS), an international Earth-focused satellite program centered at the United States (U.S.) National Aeronautics and Space Administration (NASA).

“Aqua” being Latin for “water”, the Aqua mission is named for the large amount of information it will collect about the Earth’s water cycle, including ocean surface water, evaporation from the oceans, water vapor in the atmosphere, clouds, precipitation, soil moisture, sea ice, land ice, and snow cover on the land and ice. Additional variables also being measured by Aqua include radiative energy fluxes, atmospheric aerosols, vegetation cover on the land, phytoplankton and dissolved organic matter in the oceans, and air, land, and water temperatures. One particularly exciting benefit anticipated from Aqua is an improvement in weather forecasting resulting from the Aqua atmospheric temperature and water vapor profiles.



Photos of the Aqua spacecraft at TRW in Redondo Beach, California, with all instruments on board. After launch, the solar array will be unfurled, instrument doors will be opened, and antennas will be deployed, with the resulting configuration indicated in the line drawing on p. 2. (Photos courtesy of TRW.)

### Brochure credits:

Author:	Claire L. Parkinson
Designer:	Winnie Humberson
Reviewers:	Moustafa Chahine Mike Gunson Michael D. King Elena Lobl Vincent Salomonson Akira Shibata Roy Spencer Bruce A. Wielicki





The Aqua spacecraft will carry six major Earth-observing instruments and will be launched from Vandenberg Air Force Base in California, on board a Delta II 7920 - 10L launch vehicle. The launch is scheduled for no earlier than April 18, 2002. Once the spacecraft is launched, it will be maneuvered into a near-polar orbit at an altitude of 705 kilometers, with the satellite orbiting the Earth every 98.8 minutes and crossing the equator on its northward journey at 1:30 p.m. local time and on its southward journey at 1:30 a.m. local time. This will allow collection of afternoon data (as well as 1:30 a.m. data), complementary to the collection of morning data (about 10:30 a.m.) by the EOS Terra satellite launched in December 1999. In order to emphasize the afternoon/morning contrast, the Aqua and Terra missions were originally named EOS-PM and EOS-AM, respectively.

The six Earth-observing instruments on Aqua are:

- ◆ Atmospheric Infrared Sounder (AIRS)
- ◆ Advanced Microwave Scanning Radiometer for EOS (AMSR-E)
- ◆ Advanced Microwave Sounding Unit (AMSU)
- ◆ Clouds and the Earth's Radiant Energy System (CERES)
- ◆ Humidity Sounder for Brazil (HSB)
- ◆ Moderate Resolution Imaging Spectroradiometer (MODIS)

Technically, the spacecraft will be carrying eight Earth-observing instruments, as it has two identical copies of the CERES and the AMSU consists of two physically separate units, the AMSU-A1 and AMSU-A2. Also, Aqua carries several additional instruments, to run the spacecraft, format and store the data, and send the data to the ground. Using standard satellite terminology, however, the Aqua spacecraft is generally said to have six instruments, as listed above. Of these, the AMSR-E is provided by Japan, the HSB is provided by Brazil, and the other four instruments plus the spacecraft, the launch vehicle, and the launch are provided by the United States.

Schematic of the Aqua orbit, with nine consecutive passes over the equator labeled sequentially. Aqua will orbit the Earth at an altitude of 705 km and will approach but not pass directly over the North and South Poles. As the satellite passes northward across the equator, it will do so at 1:30 p.m. local time, then, 49.4 minutes later, as it passes southward across the equator on the opposite side of the Earth, it will do so at 1:30 a.m. local time. (Schematic by Jesse Allen.)

# Satellite Imagery for Environment Reporting

Journalists can use these images and data to report and illustrate stories.

By Claire Parkinson

**D**uring the past several decades, satellite technology has provided an amazing new ability to observe the earth-atmosphere system. With satellites, the most remote regions of the globe can be viewed as readily as the least remote regions, and data can be collected globally within a few days. Some instruments can obtain surface data even in the presence of a substantial cloud cover, while other instruments can provide the data to produce three-dimensional visualizations of the structure of such atmospheric phenomena as hurricanes and thunderstorms.

Satellites collect data relevant to a wide range of environmental topics, from the ozone hole and low-level pollution in the atmosphere, to deforestation and glacier retreats on the land, to algae blooms and El Niño-signaling temperature patterns in the oceans, to biomass burning and shrinking lakes or eroding coastlines. In each of these cases, and many others, the amount of information that the satellites can provide is enormous. By carefully selecting satellite imagery, these pictures can be used quite effectively by reporters to illustrate many points. For example, journalists who might be reporting on the shrinking of the Aral Sea (caused largely by the diversion of inflowing waters for such purposes as irrigation) can vividly portray this shrinkage by presenting side-by-side, identically geolocated images from different decades.

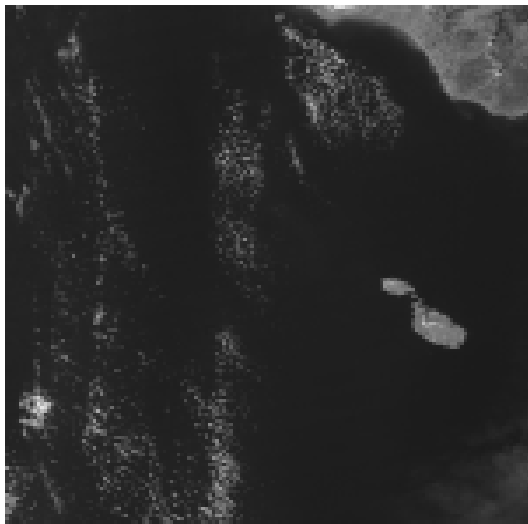
## Types of Satellite Data

Satellite data come in different types, but a common factor is that all satellite instruments measure radiation and only radiation. Some sensors measure various wavelengths of visible radiation, all of which our eyes can see, and other sensors measure ultraviolet, infrared, microwave or other types of radiation, none of which our eyes can

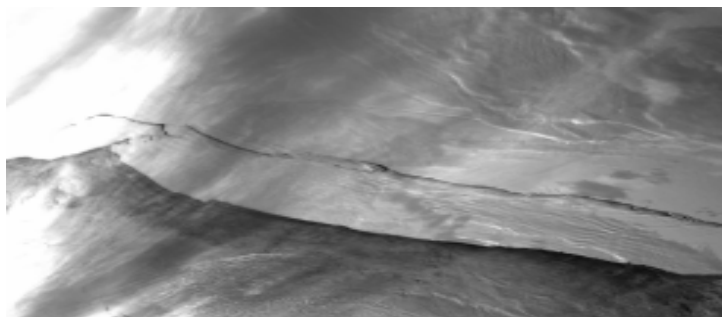
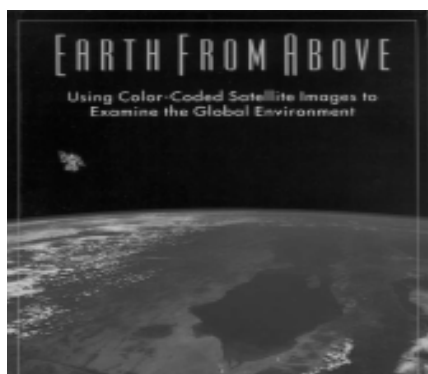
see. In any event, no matter what the topic of ultimate application, what's measured directly is exclusively radiation.

Satellite images constructed from visible data have one inherent gigantic advantage, which is that the images are generally readily understood just by looking at them: Clouds look like clouds, sea ice floes look like sea ice floes, land/sea boundaries are readily identified, etc. Furthermore, the value of some visible imagery has been clear since the first earth-observing satellites were launched decades ago. A prime example of this utility is provided by the visible imagery of hurricanes. Hurricanes form over warm ocean areas, fed by evaporation from the ocean beneath. In view of their oceanic origin, prior to satellites hurricanes were often not observed until just hours before landfall. Now they are readily recognizable in satellite visible images, often days before landfall, thereby enabling what can be lifesaving warnings to the communities along their paths.

Visible radiation is often ideal for observing hurricanes, clouds or, under clear conditions, many phenomena at the earth's surface. Satellite instruments measuring only visible radiation, however, have the same limitations that our eyes have.



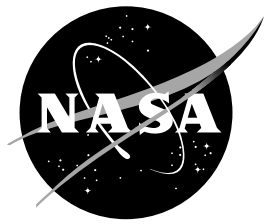
Eruption of Mount Etna, in Sicily, as viewed from NASA's Aqua satellite on October 30, 2002, using data from the Moderate Resolution Imaging Spectroradiometer (MODIS) instrument. *Original image in color, courtesy of the MODIS Science Team.*



Calving of a major iceberg off the coast of Antarctica, as viewed from NASA's Terra satellite on March 28, 2000, using data from the MODIS instrument. This iceberg is twice the size of Delaware and broke off from Antarctica's Ross Ice Shelf, necessitating remapping of the coastal boundaries. *Original image in color, courtesy of Jacques Descloitres and the MODIS Science Team.*

# NASA Facts

National Aeronautics and  
Space Administration



**Goddard Space Flight Center**  
Greenbelt, Maryland 20771  
<http://www.gsfc.nasa.gov>

February 2002

FS-2002-1-028-GSFC

## The Earth Observing System Aqua Series Claire Parkinson

*These articles focus on the overarching science priorities of the EOS Aqua mission.*  
<http://aqua.nasa.gov>

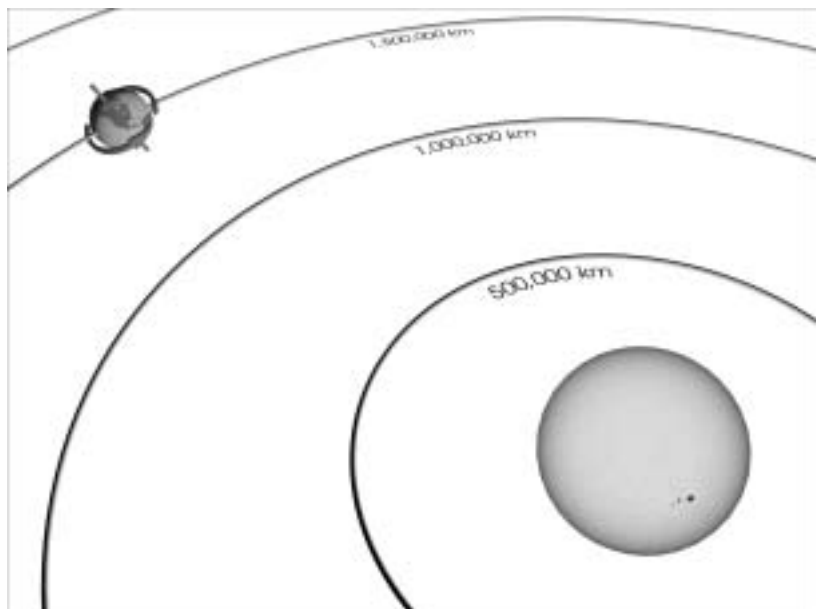
# Weather Forecasting Through the Ages

### Introduction

Imagine a rotating sphere that is 12,800 kilometers (8000 miles) in diameter, has a bumpy surface, is surrounded by a 40-kilometer-deep mixture of different gases whose concentrations vary both spatially and over time, and is heated, along with its surrounding gases, by a nuclear reactor 150 million kilometers (93 million miles) away. Imagine also that this sphere is revolving around the nuclear reactor and that some locations are heated more during one part of the revolution and others during another part of the revolution. And imagine that this mixture of gases continually receives inputs from the surface below, generally calmly but sometimes through violent and highly localized injections. Then, imagine that after watching the gaseous mixture, you are expected to predict its state at one location on the sphere one, two, or more days into the future. This is essentially the task encountered day by day by a weather forecaster (Ryan, Bulletin of the American Meteorological Society, 1982).

### Early History

The art of weather forecasting began with early civilizations using reoccurring astronomical and meteorological events to help them monitor seasonal changes in the weather. Around 650 B.C., the Babylonians tried to predict short-term weather changes based on the appearance of clouds and optical



Earth rotates on its axis once every 23 hours, 56 minutes, and completes one revolution around the sun every 365.25 days.

phenomena such as haloes. By 300 B.C., Chinese astronomers had developed a calendar that divided the year into 24 festivals, each festival associated with a different type of weather.

Around 340 B.C., the Greek philosopher Aristotle wrote *Meteorologica*, a philosophical treatise that included theories about the formation of rain, clouds, hail, wind, thunder, lightning, and hurricanes. In addition, topics such



Aristotle, as sculpted by the Greek sculptor Lysippos.

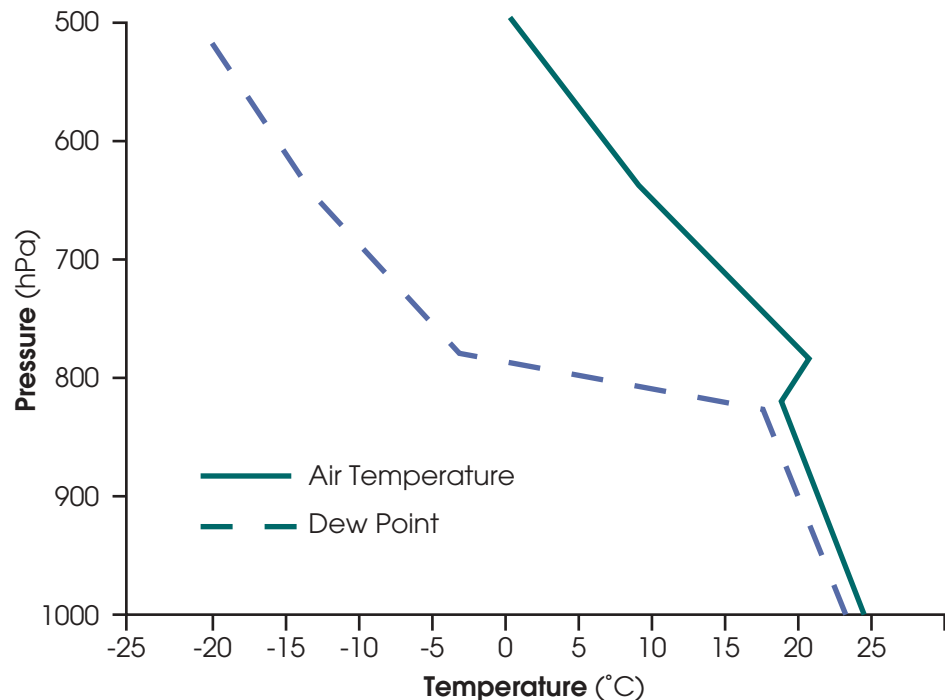
for almost 2000 years. Although many of Aristotle's claims were erroneous, it was not until about the 17th century that many of his ideas were overthrown.

as astronomy, geography and chemistry were also addressed. Aristotle made some remarkably acute observations concerning the weather, along with some significant errors, and his four-volume text was considered by many to be the authority on weather theory

invented the barometer for measuring atmospheric pressure in 1643.

While these meteorological instruments were being refined during the seventeenth through nineteenth centuries, other related observational, theoretical, and technological developments also contributed to our knowledge of the atmosphere; and individuals at scattered locations began to make and record atmospheric measurements. The invention of the telegraph and the emergence of telegraph networks in the mid-nineteenth century allowed the routine transmission of weather observations to and from observers and compilers. Using these data, crude weather maps were drawn and surface wind patterns and storm systems could be identified and studied. Weather-observing stations began appearing all across the globe, eventually spawning the birth of synoptic weather forecasting, based on the compilation and analysis of many observations taken simultaneously over a wide area, in the 1860s.

Throughout the centuries, attempts have been made to produce forecasts based on weather lore and personal observations. However, by the end of the Renaissance, it had become increasingly evident that the speculations of the natural philosophers were inadequate and that greater knowledge was necessary to further our understanding of the atmosphere. In order to do this, instruments were needed to measure the properties of the atmosphere, such as moisture, temperature, and pressure. The first known design in western civilization for a hygrometer, an instrument to measure the humidity of air, was described by Nicholas Cusa (c.1401-1464, German) in the mid-fifteenth century. Galileo Galilei (1564-1642, Italian) invented an early thermometer in 1592 or shortly thereafter; and Evangelista Torricelli (1608-1647, Italian)



A schematic sounding of air temperature and dewpoint derived from radiosonde data. This sample schematic sounding includes a temperature "inversion" (temperatures increasing with height) at about 800 hPa and reflects atmospheric conditions that frequently precede the development of severe thunderstorms and possibly tornadoes. [1 hectoPascal (hPa) = 1 millibar (mb).]

## Closing

Only fifty years ago, weather forecasting was an art, derived from the inspired interpretation of data from a loose array of land-based observing stations, balloons, and aircraft. Since then it has evolved substantially, based on an array of satellite and other observations and sophisticated computer models simulating the atmosphere and sometimes additional elements of the

Earth's climate system. All this has been made possible by advances in satellite technology, a sweeping acceleration in worldwide communications, and overwhelming increases in computing power. Aqua's AIRS/AMSU/HSB combination should further these advances, enabling more accurate predictions over longer periods.

# **Report to NASA on a Workshop on Sea Ice Data Assimilation**

Held at the

**Naval Academy,  
Annapolis, MD**

On

**July 23-24, 2002**

Report Edited by  
Kim Partington, Ronald Lindsay, Jinro Ukita

September 2002



# 1 Executive Summary

NASA's Earth Science Enterprise (ESE) aims to understand the Earth system including the effects of humans on the environment. The value of data assimilation (DA) to operational weather forecasting is well recognized, but it has only been comparatively recently that its application to climate research has been initiated. Within this context, a number of DA projects with specific application to sea ice are now under way. This workshop on sea ice DA was organized to assess overall progress made by these projects and to help to address recommendations in a joint effort to enhance the productivity of this area of research.

The workshop objectives, key strategic areas, priority recommendations, and metrics are summarized below. This is followed by background section. The main body of this report consists of three sections: issues and strategies, recommendations and metrics. Information on the agenda of the meeting, the list of attendees and the summary of presentations may be found in the appendices.

The following objectives were set out for this meeting:

- To provide recommendations to NASA on how to improve the collective productivity of data assimilation projects both current and future, including:
  - Collaborations and links between projects and expert groups
  - Generic and specific improvements to NASA datasets
- To generate informal links between related projects that can help to address the complexities of data assimilation. This community is one in which mutual support may be particularly useful given that the projects are pilot projects.
- To agree on the key technical issues that need to be addressed to make progress with data assimilation. In particular, to agree on a consensus approach, if appropriate (building on, or modifying the approach recommended by NSIDC at their workshop as reported in Weaver et al., 2000).
- To consider how progress may be assessed with data assimilation: milestones, evaluation criteria, and priorities.

In order to build sound strategies the workshop identified five essential areas in the DA procedures as:

- Formulating science questions to be answered,
- Preparation for assimilation
  - Selecting and constructing a model and DA methods and determining their error characteristics,
  - Selecting forcing and assimilation data and determining their errors,
- Performing model simulations with DA, and
- Evaluating the model results with respect to the questions posed.

## SeaWiFS Postlaunch Technical Report Series

Stanford B. Hooker, Editor

*NASA Goddard Space Flight Center  
Greenbelt, Maryland*

Elaine R. Firestone, Senior Scientific Technical Editor

*Science Applications International Corporation  
Beltsville, Maryland*

## Volume 16, Navigation Algorithms for the SeaWiFS Mission

Frederick S. Patt

*Science Applications International Corporation  
Beltsville, Maryland*

## ABSTRACT

The navigation algorithms for the Sea-viewing Wide Field-of-view Sensor (SeaWiFS) were designed to meet the requirement of 1-pixel accuracy—a standard deviation ( $\sigma$ ) of 2. The objective has been to extract the best possible accuracy from the spacecraft telemetry and avoid the need for costly manual renavigation or geometric rectification. The requirement is addressed by postprocessing of both the Global Positioning System (GPS) receiver and Attitude Control System (ACS) data in the spacecraft telemetry stream. The navigation algorithms described are separated into four areas: orbit processing, attitude sensor processing, attitude determination, and final navigation processing. There has been substantial modification during the mission of the attitude determination and attitude sensor processing algorithms. For the former, the basic approach was completely changed during the first year of the mission, from a single-frame deterministic method to a Kalman smoother. This was done for several reasons: a) to improve the overall accuracy of the attitude determination, particularly near the sub-solar point; b) to reduce discontinuities; c) to support the single-ACS-string spacecraft operation that was started after the first mission year, which causes gaps in attitude sensor coverage; and d) to handle data quality problems (which became evident after launch) in the direct-broadcast data. The changes to the attitude sensor processing algorithms primarily involved the development of a model for the Earth horizon height, also needed for single-string operation; the incorporation of improved sensor calibration data; and improved data quality checking and smoothing to handle the data quality issues. The attitude sensor alignments have also been revised multiple times, generally in conjunction with the other changes. The orbit and final navigation processing algorithms have remained largely unchanged during the mission, aside from refinements to data quality checking. Although further improvements are certainly possible, future evolution of the algorithms is expected to be limited to refinements of the methods presented here, and no substantial changes are anticipated.

## 1. INTRODUCTION

The navigation processing for the Sea-viewing Wide Field-of-view Sensor (SeaWiFS) data is performed as part of the level-0 to -1a conversion. The level-0 to -1a software extracts and converts the required telemetry from the data stream and passes it to the navigation code, which produces per-scan-line spacecraft position and instrument pointing information. The output of navigation is stored in the level-1a data products for use by downstream processing.

The navigation code is composed of two, largely independent subsystems: orbit processing, which filters the data from the onboard global positioning system (GPS) receiver to produce orbit vectors; and attitude processing, which filters the spacecraft attitude control system (ACS) telemetry and instrument tilt telemetry to determine the SeaWiFS sensor orientation.

The remainder of this section defines constants, reference frames, and transformations which are used in the algorithm descriptions.

### 1.1 Constants

The following constants are defined here for later use:

- $R_E$ , Earth equatorial radius (6,378.137 km);
- $R_M$ , Earth mean radius (6,371 km);
- $f$ , dimensionless Earth flattening factor ( $1/298.257$ );
- $\omega_E$ , Earth rotation rate ( $7.29211585494 \times 10^{-5} \text{ s}^{-1}$ );

- $\omega_O$ , nominal Orbit angular rate ( $2\pi/5940$ );
- $G_m$ , Earth gravitational constant ( $398600.5 \text{ km}^3 \text{ s}^{-2}$ ); and
- $J_2$ , dimensionless Earth gravity field perturbation term ( $1.08263 \times 10^{-3}$ ).

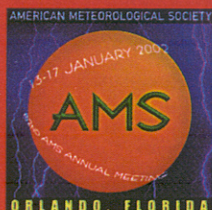
### 1.2 Reference Frames

In order to describe the navigation algorithms, several basic reference frames (all frames have orthonormal axes) are defined below.

- a. *Earth-Centered Inertial (ECI)*: This reference frame has its origin at the Earth's center and is inertially fixed. The axes are defined as:  $x$  on the equator at the vernal equinox;  $z$  at the North Pole;  $y$  orthogonal to  $z$  and  $x$  in the right-hand sense.
- b. *Earth-Centered Earth-Fixed (ECEF)*: This reference frame also has its origin at the Earth's center and rotates with the Earth. The axes are defined as:  $x$  at  $0^\circ$  latitude and longitude (Greenwich meridian at the equator);  $y$  at  $0^\circ$  latitude and  $90^\circ$  longitude; and  $z$  at the North Pole (also known as Earth-Centered Rotating, or ECR).
- c. *Orbital*: This frame has its origin at the spacecraft position and is defined as:  $x$ -axis along the geodetic nadir vector;  $y$ -axis perpendicular to  $x$  and opposite the spacecraft velocity vector; and  $z$ -axis toward the orbit normal.



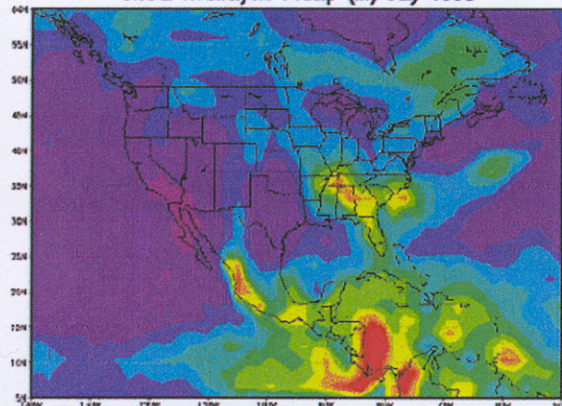
# 16th Conference on Hydrology



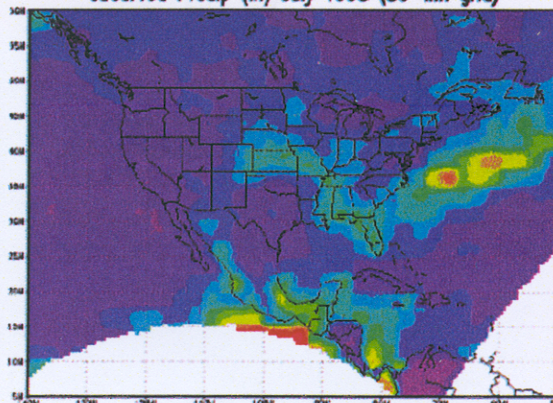
**13–17 January 2002**  
**Orlando, Florida**

## **NCEP Regional Reanalysis Result for July 1998**

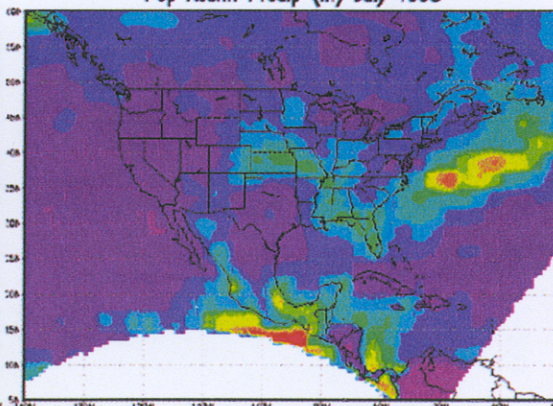
Global Reanalysis Precip (in) July 1998



Observed Precip (in) July 1998 (80-km grid)



Pop Assim Precip (in) July 1998



AMERICAN METEOROLOGICAL SOCIETY



C. D. Peters-Lidard\*<sup>1</sup>  
 Hydrological Sciences Branch, Code 974  
 NASA/Goddard Space Flight Center  
 Greenbelt, MD 20771

## 1. INTRODUCTION

Topographic effects on runoff generation have been documented observationally (e.g., Dunne and Black, 1970) and are the subject of the physically based rainfall-runoff model TOPMODEL (Beven and Kirkby, 1979; Beven, 1986a;b) and its extensions, which incorporate variable soil transmissivity effects (Sivapalan et al, 1987; Wood et al., 1988; 1990). These effects have been shown to exert significant control over the spatial distribution of runoff, soil moisture and evapotranspiration, and by extension, the latent and sensible heat fluxes (Famiglietti et al., 1992; Famiglietti and Wood, 1994a; b; Peters-Lidard et al, 1999).

The objective of this research is to investigate and demonstrate the impact of topographic control of runoff production and lateral soil water redistribution on the water and energy balance as simulated by the NCEP NOAH land surface model (Mahrt and Ek, 1984; Mahrt and Pan, 1984; Pan and Mahrt, 1987; Chen et al., 1996; Schaake et al, 1996; Chen et al., 1997; Mitchell, 1999). Currently, the NOAH model solves the Richards equation for 1-D vertical soil water transport in each land surface model grid, which corresponds to the atmospheric model horizontal grid. There is no provision for lateral soil water redistribution or for explicit subgrid soil moisture heterogeneity. Several modifications to NOAH have been incorporated which parameterize the effects of subgrid variability in topography and/or soil moisture, including:

- infiltration/runoff generation parameter "REFKDT" (Schaake et al., 1996). REFKDT is a tuneable parameter that significantly impacts surface infiltration and hence the partitioning of total runoff into surface and subsurface runoff. Increasing REFKDT decreases surface runoff.
- non-linear soil moisture stress function for stomatal resistance (Chen et al., 1996). The non-linearity in this function represents the ability of wetter portions of the grid to transpire even when the grid-averaged soil moisture is near the wilting point, as well as the dryer portions of the grid which may be stressed when the grid-averaged soil moisture is near field capacity.
- drainage parameter "SLOPE" (Schaake et al., 1996). SLOPE is a coefficient between 0.1-1.0 that modifies the drainage out the bottom of the bottom soil layer. A larger surface slope implies larger drainage.

TOPMODEL provides a physically-based approach to represent subgrid topography and soil effects on the runoff production, the soil moisture distribution and drainage, via a drainage index which can be estimated directly from digital topographic and soils data. In the

current project, the three parameterizations above are being replaced with a subgrid distribution of the TOPMODEL drainage index to explicitly represent the subgrid distribution of water table depth and soil moisture. The effect of this subgrid distribution on lateral soil water redistribution, runoff generation and surface fluxes will be modeled statistically in the manner of Famiglietti and Wood (1994a) and Peters-Lidard et al. (1997). We are demonstrating the NOAH model in both its original and new forms in the Arkansas-Red River basin using all other input parameters as specified in the LDAS project. By incorporating topographic effects into the existing NOAH model while all other processes remain the same, the effects of this representation on runoff, soil moisture and energy fluxes can be isolated. All simulations are being run off-line and in a retrospective mode for this test period.

## 4. CONCLUSIONS

The work to date suggests the following three conclusions:

TO 1. The baseflow predicted by the PMODEL equation seems to behave more smoothly and realistically than the original formulation, which has a peak in the summertime.

2. The baseflow predictions, as with other aspects of TOPMODEL, are highly sensitive to parameters related to the Topographic index distribution and the decay of saturated hydraulic conductivity with depth.

3. In order to be useful as an LDAS model, the TOPMODEL parameters must be available for the CONUS and beyond, and therefore, an understanding of the effects of DEM resolution on the parameter estimation is essential.

More results and detailed discussion will be presented at the conference.



# Proceedings of the Twelfth

## PSU/NCAR Mesocale Model Users' Workshop



June 24-25, 2002  
Boulder, CO



C. D. Peters-Lidard<sup>\*1</sup>, J. N. McHenry<sup>2</sup> C. J. Coats<sup>2</sup>

<sup>1\*</sup> NASA's Goddard Space Flight Center  
Hydrological Sciences Branch, Code 974  
Greenbelt, MD

<sup>2</sup>Environmental Modeling Center  
MCNC-North Carolina Supercomputing Center  
Research Triangle Park, NC

## 1. INTRODUCTION

Phase II of the Advanced Texas Air Quality Model (ATAQM) has been implemented for the Texas Natural Resources Conservation Commission (TNRCC) to support simulations of the August 25-31, 1998 ozone-exceedance episode in the 8-county Houston-Galveston Non-Attainment Area. ATAQM is a new, state-of-science modeling system that should significantly improve upon recognized deficiencies in current meteorological modeling systems used to drive air quality models in support of State Implementation Planning. ATAQM Phase II consists of the Fifth-Generation PSU/NCAR Mesoscale Model Version 3 (MM5v3); the TOPMODEL-based Land Atmosphere Transfer Scheme (TOPLATS; Famiglietti and Wood, 1994; Peters-Lidard et al, 1997) land surface hydrology model; and a Sea-Surface Atmosphere Transfer Scheme (SSATS). The TOPLATS model is driven with both in situ and remotely sensed estimates of key meteorological variables, including solar radiation and precipitation, and the SSATS model is driven with observed Sea Surface Temperature (SST) data from a combination of in situ (NOAA PORTS) and remotely sensed (CoastWatch AVHRR products) sources. This modeling system is fully documented at [http://www.emc.mcnc.org/projects/TNRCC-projects/tnrcc\\_public.html](http://www.emc.mcnc.org/projects/TNRCC-projects/tnrcc_public.html). Below, we discuss the model configuration and results for the episode.

## 2. APPROACH

### 2.1. TOPLATS Configuration

The TOPLATS Study Domain (TSD) for this project was set by mosaicking 8-Digit Hydrologic Unit Code watersheds provided by the National Hydrography Dataset (NHD) (USGS, 2001). This domain was chosen to include all watersheds that contain areas of Harris County (Houston), Texas as well as all counties that border Harris. Using this one-county buffer region as a guideline, the domain to model for TOPLATS was set as a large portion of the Eastern Coastal Plains of Texas with an area of approximately 96,000 square kilometers. The region covers an expanse from Matagorda Bay in the most southern point (28.07 N) to near Waco, Texas in the north (31.81 N), and from Lake Charles, Louisiana

in the east (93.01 W) to the suburbs of Austin, Texas at the westernmost location (97.37 W)(Figure 1).

The region chosen for this project is much larger than those typically used in previous TOPLATS studies, and is only possible due to the parallel techniques and high performance I/O that have been implemented as part of this research (Coats et al., 1999; Peters-Lidard et al., 1999). The TOPMODEL concept assumes that base flow is the same throughout the watershed of interest, and when the watershed is much larger than 500 square kilometers in area, this assumption may be invalid. Therefore for a large region such as the HGA study requires, the domain is subdivided into smaller watersheds suitable for TOPLATS. In total the region has been divided into 173 watersheds (Figure 2), each of which has watershed-specific parameters required for TOPLATS.

Parameters for TOPLATS were estimated using readily available Digital Elevation Model (DEM), landcover and soils databases. TOPLATS was then "spun-up" for the period January 1-August 24, prior to coupling, using observed forcing data, including NEXRAD WSR88D precipitation, observed solar radiation, and observed surface-station meteorology including wind-speed, temperature, relative humidity, etc. More details about the TOPLATS databases and spin-up are available online at:

[http://www.emc.mcnc.org/projects/TNRCC-projects/ATAQM/ataqmlI\\_report1.pdf](http://www.emc.mcnc.org/projects/TNRCC-projects/ATAQM/ataqmlI_report1.pdf)



Figure 1. Houston-Galveston study region.



**Second Annual  
Earth Science Technology  
Conference (ESTC-2)**

**Pasadena, CA  
June 11-13, 2002**

# Synthetic Thinned Aperture Radiometry (STAR) Technologies Enabling 10-km Soil Moisture Remote Sensing from Space

J.R. Piepmeier<sup>1</sup>, F.A. Pellerano<sup>1</sup>, P. O'Neill<sup>2</sup>, D. LeVine<sup>3</sup>, E. Kim<sup>3</sup>, T. Doiron<sup>1</sup>

NASA's Goddard Space Flight Center

<sup>1</sup>Microwave Instrument Technology Branch/555

<sup>2</sup>Hydrological Sciences Branch/974

<sup>3</sup>Microwave Sensors Branch/975

Greenbelt, MD 20771

**Abstract - Remote sensing of soil moisture at 1.4 GHz at 10-km spatial resolution from space requires the use of very large radiometer apertures (>20 m). Synthetic thinned aperture radiometry (STAR) is a viable solution to the large aperture problem, and several technologies are being developed to enable a spaceflight STAR instrument. The primary motivation for the development is a reduction in power and size, which is achieved by using low power microelectronics, including silicon germanium (SiGe) and ultra low power (ULP) CMOS. STAR system architecture, SiGe microwave radiometer receivers, ULP digital correlators, and calibration are discussed.**

## I. INTRODUCTION

NASA's Earth Science Enterprise and the hydrology community are focused on achieving a 10-km spatial resolution global soil moisture mission towards the end of the decade. This type of resolution represents a significant technological challenge. Observation of soil moisture is based on relatively low frequency thermal microwave emission at L-band (1.4 GHz). The long wavelengths at this frequency coupled with the high spatial and radiometric resolutions required necessitates the use of very large apertures (>20 m) [1, 2].

An engineering trade study was completed by NASA Goddard Space Flight Center (GSFC) to determine alternative system configurations that could achieve the science requirements and to identify the most appropriate technology investments and development path for NASA to pursue in order to bring about such a mission [1]. The conclusion of this study was that Synthetic Thinned Aperture Radiometry (STAR) is the most promising technology to enable these very large non-rotating apertures in space. In this technique, the coherent product (correlation) of the signal from pairs of antennas is measured at different antenna-pair spacings (baselines). These products yield sample points in the Fourier transform of the brightness temperature map of the scene, and the scene itself is reconstructed by inverting the sampled transform [3]. The reconstructed image includes all of the pixels in the entire field-of-view of the antennas.

The main advantage of the STAR architecture is that it requires no mechanical scanning of the antenna. Using a static antenna simplifies the spacecraft dynamics and improves the time-bandwidth product of the radiometer. Furthermore, aperture thinning reduces the overall volume and mass of the instru-

ment. A disadvantage is the reduction of radiometric sensitivity (or increase in rms noise) of the image due to a decrease in signal-to-noise for each measurement compared to a filled aperture. Pixel averaging is required for good radiometric sensitivity.

In essence, we are trading a nearly intractable mechanical problem for a tractable electrical one. Because a large STAR radiometer uses many receivers and correlators, the primary objective of our technology development has been to drive down electrical power dissipation, volume and mass. We accomplish this goal through the innovative use of low power microelectronics, including silicon germanium (SiGe) and ultra low power CMOS (ULP CMOS), for microwave receivers, analog-to-digital converters, and digital correlators. In addition, we are studying system architecture issues such as correlated calibration sources and signal distribution.

## II. SYSTEM TECHNOLOGY

Technology development for the 10-km soil moisture remote sensing problem began with two investigations. First, a concept was developed for a space-based instrument through a science-driven architecture study [1]. From this study, engineering constraints were derived that motivated several component technology developments. Second, an aircraft instrument was developed to validate the two-dimensional STAR technique for soil moisture remote sensing [4]. The instrument is a research tool that will be used to address remote sensing and instrument systems engineering issues associated with development of a spaceflight STAR instrument.

## IV. FUTURE TECHNOLOGY AND SUMMARY

Several technologies motivated by science-driven system studies for 10-km soil moisture remote sensing from space have been presented. The primary developmental drivers are low power and size requirements, which are met using state-of-the-art microelectronics and sensible system design. The next steps needed to advance towards a flight instrument have been proposed and include an integrated panel of SiGe receivers and antennas, the study of a fully integrated SiGe RF-digital receiver-on-a-chip, and the appropriate demonstration of a deployable STAR arm either on the ground or in space. These developments are on-track for a soil moisture mission launch in ~2008.

# 2002 IEEE International Geoscience and Remote Sensing Symposium and the 24<sup>th</sup> Canadian Symposium on Remote Sensing



REMOTE SENSING:  
Integrating Our  
View of the Planet



June 24-28, 2002  
Toronto Canada

# IGARSS 2002



# The Airborne Conical Scanning Millimeter-wave Imaging Radiometer (CoSMIR)

J.R. Piepmeier, P. Racette, W. Manning<sup>1</sup>, J.R. Wang

NASA's Goddard Space Flight Center  
Greenbelt, MD 20771

<sup>1</sup>Joint Center for Earth Systems Technology  
Baltimore, MD 21250

**Abstract - Results of the first science flight of the airborne Conical Scanning Millimeter-wave Imaging Radiometer (CoSMIR) for high-altitude observations from the NASA ER-2 is discussed. Imagery collected from the flight demonstrates CoSMIR's unique conical/cross-track imaging mode and provides comparison of CoSMIR measurements to those of the SSM/T-2 satellite radiometer.**

## INTRODUCTION

The airborne Conical Scanning Millimeter-wave Imaging Radiometer (CoSMIR) will provide measurements useful for atmospheric studies and satellite calibration and validation. Designed to match the tropospheric sounding channels of the Defense Meteorological Satellite Program (DMSP) Special Sensor Microwave Imager/Sounder (SSMIS), the CoSMIR consists of four radiometers operating at 50-54 (3 channels - 50.3, 52.8, and 53.6), 91.655 (dual polarization), 150.0, and 183.31 (3 channels -  $\pm 1$ ,  $\pm 3$ , and  $\pm 6.6$ ) GHz. For a detailed description of the instrument see [1]. In February, 2002, CoSMIR successfully completed an engineering check flight and its first science flight on the NASA ER-2 high-altitude research aircraft. Imagery was collected using CoSMIR's unique combined conical and cross-track scan mode. Results from this flight are discussed below.

## COSMIR IMAGERY

Demonstration of CoSMIR's unique combined conical/cross-track imaging mode can be seen in Fig. 1 for the 50.3 GHz channel. The top two maps contain the forward-conical and aft-conical images over and near the San Francisco Bay area of California; the Bay itself is located slightly above and left of the center of the map. The Pacific coast is seen in the top left portion of the map and the wetland areas contained within and near the San Luis National Wildlife Refuge are located in the lower right section of the maps. The increase in atmospheric path length is noticeable between the conical and cross-track images at 50.3 GHz, which is located near the molecular oxygen 60 GHz absorption complex. An increase in path length leads to an increase in molecular oxygen within the path. This increase produces the higher

brightness temperature values seen in the conical-scan images, with incidence angles of  $53.6^\circ$ , compared to the cross-track image with incidence angles less than those of the conically scanned images.

A comparison between the three double-sideband CoSMIR and Special Sensor Microwave/Temperature-2 (SSM/T-2) channel frequencies centered on the 183.31 GHz water vapor band is shown in Fig. 2. The map area is located over the Pacific Ocean southwest of San Francisco. The aircraft flight line followed the sub-satellite track so the CoSMIR cross-track brightness temperatures near nadir (at the center of the swath) are comparable to the underlying cross-track SSM/T-2 brightness temperatures. Comparisons of the  $183.31 \pm 1.0$  GHz channels and the  $183.31 \pm 3.0$  GHz channels are shown in the top-left and middle-left images, respectively. Excellent agreement can be seen in the imagery. The bottom-left image is a comparison of the CoSMIR  $183.31 \pm 6.6$  GHz channel and the SSM/T-2  $183.31 \pm 7.0$  GHz channel. Precipitable water amounts increase along the descending flight line in the southwest direction. Observed brightness temperature differences at  $183 \pm 6.6/7.0$  GHz between the CoSMIR and the SSM/T-2 can be attributed to differences in the passband characteristics of the two instruments. The CoSMIR forward and aft viewing conical scans are shown in the middle and right column, respectively. The channel frequencies and color bars are applicable for the three images contained in each row. The small (+) symbols signify the center beam locations for the SSM/T-2 brightness temperature data.

This development was supported by the Defense Meteorological Satellite Program and the NASA Goddard Space Flight Center.

# **NASA/TM-2002-21004/Rev3-Vol1**

**James L. Mueller<sup>1</sup> and Giulietta S. Fargion<sup>2</sup>**  
**Editors**

<sup>1</sup> *CHORS, San Diego State University, San Diego, California*

<sup>2</sup> *Science Applications International Corporation, Beltsville, Maryland*

## **Ocean Optics Protocols For Satellite Ocean Color Sensor Validation, Revision 3, Volume 1**

J. L. Mueller, C. Pietras, S. B. Hooker, D. K. Clark, A. Morel, R. Frouin, B.G. Mitchell,  
R. R. Bidigare, C. Trees, J. Werdell, G. S. Fargion, R. Arnone, R. W. Austin, S. Bailey,  
W. Broenkow, S. W. Brown, K. Carder, C. Davis, J. Dore, M. Feinholz, S. Flora, Z.P.  
Lee, B. Holben, B. C. Johnson, M. Kahru, D. M. Karl, Y. S Kim, K. D. Knobelspiesse, C.  
R. McClain, S. McLean, M. Miller, C. D. Mobley, J. Porter, R.G. Steward, M. Stramska,  
L. Van Heukelem, K. Voss, J. Wieland, M. A. Yarbrough and M. Yuen.

National Aeronautical and  
Space administration

**Goddard Space Flight Space Center**  
Greenbelt, Maryland 20771

**February 2002**



## Chapter 7

# Calibration of Sun Photometers and Sky Radiance Sensors

Christophe Pietras<sup>1</sup>, Mark Miller<sup>2</sup>, Kirk D. Knobelspiesse<sup>3</sup>, Robert Frouin<sup>4</sup>, Brent Holben<sup>5</sup> and Ken Voss<sup>6</sup>

<sup>1</sup>*Science Applications International Corporation, Beltsville, Maryland*

<sup>2</sup>*Department of Applied Science, Brookhaven National Laboratory, Upton, New York*

<sup>3</sup>*Science Systems and Applications, Inc., Greenbelt, Maryland*

<sup>4</sup>*Scripps Institution of Oceanography, University of California, San Diego, California*

<sup>5</sup>*Biospheric Sciences Branch, NASA Goddard Space Flight Center, Greenbelt, Maryland*

<sup>6</sup>*Physics Department, University of Miami, Florida*

## 7.1 INTRODUCTION

Atmospheric sensors are designed to measure direct solar signals and sky radiances in order to retrieve the radiative properties of the atmosphere. There are two major types of instruments in use to perform these measurements: sun photometers and sky radiance scanning systems including fast rotating shadow-band radiometers.

Sun photometers capture photometric intensity of the direct solar beam. Their fields of view are small, typically between 1° and 3°, in order to minimize contamination of the transmitted solar signal by scattered skylight. Some photometers are manually aimed at the sun using sun-sighting optics, while other types of photometers are fixed in place and are equipped with automatic sun-tracking mechanisms.

MicroTops II (Morys *et al.* 1998; Porter *et al.* 1999) and SIMBAD (Deschamps *et al.* 2000; Fougnie *et al.* 1999a, 1999b) are two examples of hand-held sun photometers. The fields of view (FOV) of hand-held sun photometers are typically between 2° and 3°, which is generally larger than the FOVs of the automatic sun-tracking photometers (Table 7.1). The wider FOV allows the user to manually aim the instrument at the sun from the rolling deck of a ship. The even wider field of view of SIMBAD (Table 7.1) is intended to measure marine reflectance as well as the solar signal. An improved version, called SIMBADA, has been recently developed and is available since 2001. SIMBADA new features are an integrated GPS and 11 channels.

Examples of fixed, automated tracking sun photometers include the CIMEL (Holben *et al.*, 1998) and the PREDE (Nakajima *et al.*, 1996). The design of a particular sun tracking mechanism is dependent on whether it is to be used on a moving platform (e.g., PREDE POM-01 Mark II), or on a stable station (e.g., CIMEL, PREDE POM-01L). CIMEL and PREDE instruments perform both sun photometric and sky radiance measurements. In sky radiance mode, these instruments measure sky radiances within 3° of the sun in the aureole, and also scan the sky radiance distribution in the principal solar plane. The FOV of the CIMEL and PREDE instruments are less than 1.5° and the instruments are equipped with collimators for stray light rejection (O'Neill *et al.*, 1984; Holben *et al.* 1998; Nakajima *et al.* 1996).

Fast rotating shadow-band radiometers measure solar intensity values indirectly from diffuse and global upper hemispheric irradiance. They have a 2 $\pi$  FOV and are equipped with a solar occulting apparatus. Finally, electronic camera systems equipped with “fisheye” lenses may be used to measure the full sky radiance distribution (Voss *et al.* 1989).

Sun photometers and sky radiometers commonly have several channels from 300 nm to 1020 nm and narrow bandwidths (approximately 10 nm). Their characteristics are summarized in Table 7.1. This chapter will describe calibration techniques, and uncertainties of the sun photometers and sky radiometers. Measurement and data analysis protocols and procedures are discussed in Chapter 14.

# 2002 IEEE International Geoscience and Remote Sensing Symposium and the 24<sup>th</sup> Canadian Symposium on Remote Sensing



REMOTE SENSING:  
Integrating Our  
View of the Planet



June 24-28, 2002  
Toronto Canada

# IGARSS 2002

# STUDY OF THE VARIABILITY IN THE RAIN DROP SIZE DISTRIBUTION OVER A 2.3 KM PATH

Rafael F. Rincon<sup>\*1</sup>, Roger Lang<sup>1</sup>, Robert Meneghini<sup>2</sup>, Steven Bidwell<sup>2</sup>, and Ali Tokay<sup>3</sup>

<sup>1</sup>The George Washington University, Washington, DC

<sup>2</sup>NASA/GSFC, Greenbelt, MD

<sup>3</sup>JCET, UMBC, Baltimore, MD

**Abstract-** In an effort to study the drop size distribution (DSD) a state-of-the-art instrument arrangement was deployed on Wallops Island, VA. The instrumentation consisted of a 2.3-km multi-frequency microwave link, three impact disdrometers, and a network of optical and tipping bucket raingauges. A dual-frequency inversion technique was implemented with the link measurements of attenuations at 25 GHz and 38 GHz to estimate the path-average DSD. Concurrently, an X-band, dual-polarization radar, located in the vicinity, collected polarization and reflectivity measurements over the link path. The evaluation of the estimates and measurements generated some preliminary results.

## I. INTRODUCTION

An accurate estimation of the drop size distribution (DSD) is essential in the retrieval of rainfall parameters from microwave measurements and in the modeling of microwave propagation through rain. The DSD is characterized by a high temporal and spatial variability that affects both microwave measurements and ground validation. To study the temporal and spatial variation of drop size distributions a state-of-the-art instrument arrangement was deployed on Wallops Island, VA. The instrumentation consisted of a 2.3-km multi-frequency microwave link, three impact (Joss-Waldvogel) disdrometers, and a network of optical and tipping bucket raingauges. Concurrently, NOAA's ground base X-band radar, located in the vicinity of the link during the March 2001 rain event, collected polarization and reflectivity measurements. The radar operates at 9.34 GHz at horizontal and vertical polarizations.

In this work inversion techniques implemented with the link measurements provided DSD estimates over the path for a highly convective event on March 21, 2001. The estimates were evaluated in conjunction with the measurements from the three disdrometers located directly under the microwave path. The results were evaluated with the radar measurements aloft. Additionally, the estimated DSD and the disdrometer measurements were used to

compute path-average rain rates and rainfall accumulation. These results were compared to path-average measurements from the network of optical and tipping bucket rain gauges.

## III. CONCLUSION

The link attenuation measurements at 25 and 38 GHz and the implementation of dual-frequency inversion technique yielded a path average DSDs based on an analytical Gamma model. The technique was applied during a highly convective rain event with maximum rain rates of nearly 120 mm/hr. The results showed the potential of the link DSD estimates as a validation tool as well as an accurate estimator of microwave and rainfall parameters.

The rain event presented exhibited high DSD variability over the path, affecting the agreement between the averaged point measurements. The underestimation observed with the disdrometer may also be attributed to the limited measurable drop range from 0.3 to 5 mm.

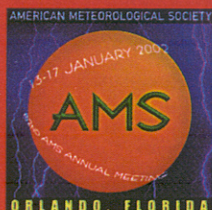
A more detailed study of the DSD variability and its effects on the rainfall retrievals is under way. The results will be presented at the conference.

---

\* NASA/GSFC/ 975, Bldg. 33, Rm. B409  
Greenbelt, MD 20771  
Phone: (301) 614-5725, Fax: (301) 614-5558  
E-mail: rafael@priam.gsfc.nasa.gov



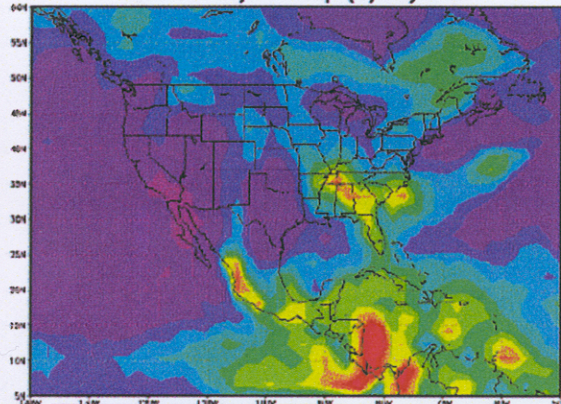
# 16th Conference on Hydrology



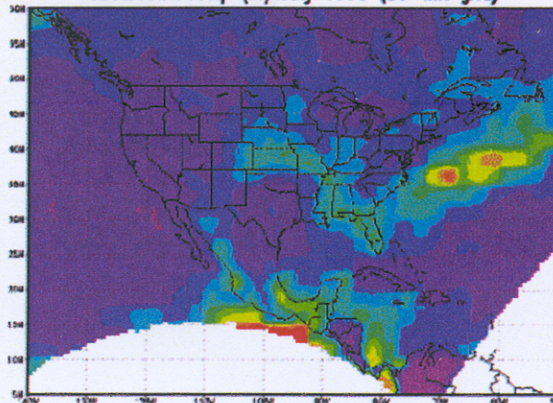
**13–17 January 2002**  
**Orlando, Florida**

## **NCEP Regional Reanalysis Result for July 1998**

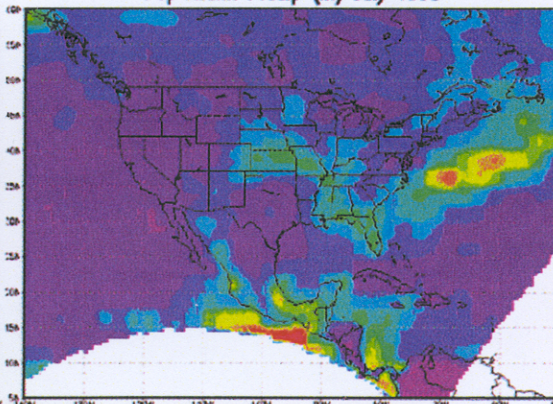
Global Reanalysis Precip (in) July 1998



Observed Precip (in) July 1998 (80-km grid)



Pop Assim Precip (in) July 1998



AMERICAN METEOROLOGICAL SOCIETY



Matthew Rodell<sup>1\*</sup>, P. R. Houser<sup>1</sup>, U. Jambor<sup>1</sup>, J. Gottschalck<sup>1</sup>,  
J. Radakovich<sup>1</sup>, K. Arsenault<sup>1</sup>, C.-J. Meng<sup>2</sup>, and K. E. Mitchell<sup>2</sup>  
<sup>1</sup>NASA GSFC, Greenbelt, Maryland <sup>2</sup>NOAA NCEP, Camp Springs, Maryland

## 1. Introduction

Satellite remote sensing of hydrometeorological states and fluxes has improved steadily over the past two decades. At the same time, increases in supercomputing power and affordability have allowed atmospheric and land surface models to gain complexity and resolution. These models have the ability to fill in observational gaps, so that incorporating data from advanced observing systems into models as forcings and constraints maximizes our knowledge of the processes and resulting states of the Earth system.

The Global Land Data Assimilation System (GLDAS), which is being developed jointly at NASA's Goddard Space Flight Center and NOAA's National Centers for Environmental Prediction, enables users to run multiple, state-of-the-art land surface models (LSMs) using a combination of modeled and observation-based forcing fields (Houser et al., 2001). Drivers have been installed for Mosaic (Koster and Suarez, 1992), the Common Land Model (Dai et al., 2001), the Catchment LSM (Koster, et al., 2000), and NOAA's Noah LSM. The primary goal of GLDAS is to produce global, high resolution (0.25°), near-real time fields of land surface states and fluxes. These will be used to initialize weather and climate prediction models and to facilitate flood and drought prediction, agricultural productivity forecasting, water resources decision-making, and a variety of studies in the Earth sciences.

By utilizing data from advanced observing systems, GLDAS can avoid systematic biases which arise in atmospheric model-based precipitation and radiation forcing fields and accumulate in land surface moisture and temperature states. GLDAS is enhanced further by the capability of running the one dimensional LSMs on subgrid tiles, which are based on a 1 km global vegetation dataset, an elevation correction based on the GTOPO30 global digital elevation model, and a soil parameterization based on Reynolds, Jackson, and Rawls (1999) 5' global soils information. Future enhancements will include satellite observation-based vegetation updates, a runoff routing scheme, and assimilation of satellite-derived snow (MODIS), soil temperature and moisture (AMSR), and terrestrial water storage (GRACE) observations.

## 2. Methods

GLDAS began running in near-real time on 1 March 2001, with Mosaic as the operational LSM. The spatial resolution was set to 0.25°, with one vegetation tile per grid square, 30 minutes was the length of each time step, and Mosaic's original soil scheme was used. Surface state variables were initialized based on fields from NOAA's global, 4DDA, real time meteorological

modeling system (GDAS). GDAS also provided all of the forcing data. By 30 July 2001 the time step had been shortened to 15 minutes and the primary source of forcing data had been changed to NASA's GEOS 3.24 global, 4DDA, real time meteorological modeling system. Temporal and spatial interpolation has been required to derive forcing from the GDAS and GEOS files, which are produced every three hours at 0.7° and 1.0° resolutions, respectively.

Since 31 July 2001, geostationary satellite infrared (IR) and TRMM / SSM/I microwave-based, 0.25°, 6-hourly mean rain rate fields from the U.S. Naval Research Laboratory (NRL) have been incorporated into the forcing. NRL does not generate precipitation estimates poleward of 60°, and TRMM / SSM/I coverage is incomplete at 6-hourly resolution. Therefore GLDAS uses GEOS precipitation as a base, overlays NRL IR-based rain, and overlays the result with NRL microwave-based rain.

A restart file was used to initiate a run of GLDAS which paralleled the operational run between 31 July and 31 August 2001. All parameters were identical in the two runs, except that NRL observation-based rain was not used in the test run. The hypothesis was that using observation-based precipitation forcing has a positive effect on the modeled state of the land surface.

## 4. Discussion

A major theme of the GLDAS project is the utilization of observation-based fields for forcing and constraining land surface models. The results of this investigation support the feasibility of that approach by demonstrating that 1) observation-based develop similar large scale patterns of precipitation accumulation over the course of a month, and 2) believable patterns of soil moisture develop when the observation-based precipitation fields are used as forcing. Furthermore, the small scale heterogeneity seen in the observation-based precipitation fields and resultant soil moisture output fields is likely to be more realistic than the spatial uniformity produced by the modeled forcing. When GLDAS output fields of land surface states are used to reinitialize global coupled meteorological models, the small scale heterogeneity in soil moisture, to which the atmosphere is sensitive, may feed back to have a positive effect on those model simulations.

During the period of study, TRMM / SSM/I rain was not available for 108 non-consecutive hours and IR rain was not available for 114 non-consecutive hours. These data gaps overlapped for 90 hours, during which time GLDAS relied on GEOS forcing exclusively. Therefore the observed precipitation field in Figure 1 (and likewise the output in Figure 2) might be slightly more similar to GEOS field than it otherwise would be. Data gaps are likely to be unavoidable when modeling in near-real time, so the results shown here can be considered representative of GLDAS.

For more results and a detailed description of the GLDAS project, please visit <http://ldas.gsfc.nasa.gov>.

\* **Corresponding author address:** Matthew Rodell, Hydrological Sciences Branch, Code 974.1, NASA Goddard Space Flight Center, Greenbelt, MD 20771; e-mail: mattro@dao.gsfc.nasa.gov.

# 2002 IEEE International Geoscience and Remote Sensing Symposium and the 24<sup>th</sup> Canadian Symposium on Remote Sensing



REMOTE SENSING:  
Integrating Our  
View of the Planet



June 24-28, 2002  
Toronto Canada

# IGARSS 2002



# **An Overview of the Earth Observing System MODIS Instrument and Associated Data Systems Performance**

by

Vincent V. Salomonson, William Barnes, Jack Xiong, Steve Kempfer and Ed Masuoka

NASA/Goddard Space Flight Center

Greenbelt, Maryland

***Abstract-* The MODIS instrument on the EOS Terra Mission has completed over 2 years of successful operation. Excellent data products have been developed and a full year or more of these products are now available. Validation of these products is continuing and efforts to improve product availability and access are underway. The MODIS on the EOS Aqua satellite is projected to become operational in the late spring/early summer of 2002.**

## **I. INTRODUCTION**

The Moderate Resolution Imaging Spectroradiometer (MODIS) on the Earth Observing System (EOS) Terra Mission began to produce data in February 2000. Now a little over 2 years from that time, the instrument continues to produce good data. Nearly 40 land, oceans, and atmospheres products are achieving maturity for science and applications studies. This paper summarizes the status of the instrument and the status of processing, archiving and dissemination of MODIS products

## **II. MODIS INSTRUMENT STATUS**

The MODIS instrument has performed well overall. The first several months from launch to October 31, 2000 saw a lot of different adjustments in instrument parameters to reduce electronic noise, striping in some bands, band-to-band crosstalk, etc. On October 31, 2000 a stable configuration, including the operation of the instrument on the "B-side" electronics, was finalized. The instrument operated in that configuration from November 1, 2000 to June 15, 2001. On June 15, 2001 the instrument went out of operation due to a high energy proton event and stayed out of operation until July 2, 2001. Instrument operations were resumed operating on the "A-side" electronics. It was decided, based on performance, that the instrument would remain in that configuration until other factors indicated differently. Up through early March of 2002, the instrument

continues to operate on the A-side. Furthermore, this configuration shows no significant differences relative to instrument performance on the B-side during November 2000 to June 2001.

During the period November 2000 to the present, the instrument shows performance at or above specifications in terms of signal-to-noise in all reflected solar bands (1-19, and 26) [1]. The noise-equivalent-delta-temperature (NEDT) performance in thermal infrared bands (20-25, 27-35) also show at or better than specification performance except for occasional channels within a band. Some striping, electronic noise, crosstalk, etc. can still be observed, particularly in short-wave infrared bands and the 1.38 micrometer band (band 26). For the most part, however, all bands provide scientifically useful performance and the Level 1 data from the instrument is considered to be validated for scientific use for the period November 2000 to the present (early March 2002 when this paper was written).

## **VI. SUMMARY AND CONCLUSIONS**

The Terra MODIS instrument is performing well. Over 40 data products have been developed by the MODIS Science Team that are scientifically useful. These data products have been processed and a relatively complete time series completed extending from November 1, 2000 to the present. These products are distributed among the three DAAC's handling MODIS products. Substantial efforts are ongoing at the Earth Sciences Data and Information System (ESDIS) Project and DAAC's to improve the user access and interfaces to make the acquisition of MODIS products as user-friendly as possible. The launch of the EOS Aqua spacecraft with a second MODIS on it is eagerly anticipated because it will complement the Terra MODIS by providing afternoon (1:30 P.M. local equator crossing time) observations. The launch date planned at the writing of this paper is April 18, 2002.

# 2002 IEEE International Geoscience and Remote Sensing Symposium and the 24<sup>th</sup> Canadian Symposium on Remote Sensing



REMOTE SENSING:  
Integrating Our  
View of the Planet



June 24-28, 2002  
Toronto Canada

# IGARSS 2002

# Estimation of Soil Moisture change with PALS's L-band Radiometer

Jiancheng Shi<sup>1</sup>, E. G. Njoku<sup>2</sup>, K. S. Chen<sup>3</sup>, T. Jackson<sup>4</sup>, P. O'Neill<sup>5</sup>

<sup>1</sup>Institute for Computational Earth System Science

University of California, Santa Barbara

Tel: 805-893-2309, Fax: 805-893-2578, E-mail: [shi@icess.ucsb.edu](mailto:shi@icess.ucsb.edu)

<sup>2</sup>NASA/JPL, <sup>3</sup>National Central University Taiwan, <sup>4</sup>USDA/ARS, <sup>5</sup>NASA/GSFC

**Abstract – This study demonstrates the capability of estimating the relative soil moisture change using repeat-pass L-band radiometer. It shows 1) evaluation of the effects of the surface roughness and vegetation in the repeat-pass measurements, 2) development of a technique to estimate the relative soil moisture change, and 3) validation with the ground soil moisture measurements from SGP99 experiment.**

## I. INTRODUCTION

It is understood that the emission from vegetated areas is a function of water content and its spatial distribution as determined by vegetation structure and underlying surface conditions – roughness and soil moisture. Even through these effects can be modeled if the ground measurements are available, it is quite difficult to take into account these effects in the inversion process for soil moisture estimation.

One of the advantages in the satellite passive microwave measurements is the quick repeat-time. They are capable to re-visit or measure surface conditions within a few days. The general characteristics of temporal variability of nature surfaces – the properties that affect the emission signals are:

- Surface soil moisture varies constantly over the time and has a significant diurnal circle during a day until it reaches a very dry condition.
- Vegetation water content has also diurnal variability but it may have no significant change at the same time during a day unless there is a precipitation event. Most of vegetation growth or microstructure in terms of scatter size, shape, and orientation has a longer time scale (days – week) to be considered having a significant change.
- Surface roughness, in general, can be considered as a constant for a long time period (weeks) except some man-made or weather events such as rainfall and agriculture activities.

Therefore, some variables such as surface roughness and vegetation can be considered as a constant between two or three data acquisitions. The changes between the data acquisitions will be mainly resulted from surface soil moisture change. These characteristics make it possible to develop a technique to estimate surface soil moisture change with vegetated surfaces.

In this study, we evaluate the effect of the surface roughness and vegetation cover on estimating the relative soil moisture change. Based on these characteristics, we demonstrate a technique that uses L-band radiometer to estimate the relative soil moisture change from repeat-pass

measurements and its validation of PALS instrument derived soil moisture change with the ground measurements from SGP99 experiment.

## II. EFFECTS OF THE SURFACE ROUGHNESS IN REPEAT-PASS MEASUREMENTS

To evaluate the effect of the surface roughness on estimating the relative soil moisture change, we first simulated a bare surface emissivity database at 1.41 GHz. This database covers the most possible soil moisture and roughness conditions and the incidence angle from 20° to 70°. Then, we developed a simplified model using this database. It is written as:

$$R_p^e = 1 - E_p = A_p \cdot r_p^{B_p} \quad (1)$$

where  $E_p$  is emissivity and  $p$  indicates the polarization.  $R^e$  is the effective reflectance that includes the effect of the surface roughness.  $A_p$  and  $B_p$  are the roughness parameters depending on the polarization, incidence angle, surface RMS height, correlation length and the type of the correlation function. They represent an overall effect of the surface roughness.  $r_p$  is the flat surface reflectivity.

Under change detection concept, the relationships in terms of the ratio between any two measurements are evaluated with assumption of no surface roughness change. The signal change between two measurements is resulted only from surface soil moisture change. By varying all possible combination of soil moistures, we simulated the effective reflectivity ratio. That is:

$$R_{p2}^e / R_{p1}^e = (1 - E_{p2}) / (1 - E_{p1}) \quad (2)$$

## V. SUMMARY

One advantage of the passive microwave sensors is the quick repeat-time within a few days. Except soil moisture, most of natural surface characteristics, such as surface roughness and vegetation properties, can be reasonable assumed that there is no-change between the repeat measurements (same time during a day) between the data acquisitions. Based on this concept, we demonstrated the relative soil moisture change in terms of the ratio can be directly estimated from the repeat-pass measurements for both bare and vegetated surfaces when the small albedo assumption is valid. The advantage of this technique is that it does not require the surface information – we do not need to know if the pixel is a bare, vegetated, or fractionally vegetated, and vegetation information as long as the small albedo assumption is valid.



# 2002 IEEE International Geoscience and Remote Sensing Symposium and the 24<sup>th</sup> Canadian Symposium on Remote Sensing



REMOTE SENSING:  
Integrating Our  
View of the Planet



June 24-28, 2002  
Toronto Canada

# IGARSS 2002

# Observation of Snowfall over Land by Microwave Radiometry from Space

G. M. Skofronick-Jackson

University of Maryland, Baltimore County, GEST Center

NASA Goddard/Code 975

Greenbelt, MD 20771

301-614-5720, FAX 301-614-5558, gailsjackson@ieee.org

J. A. Weinman

NASA Goddard/Code 975

Greenbelt, MD 20771

D.-E. Chang

Forecast Research Laboratory, Meteorological Research Institute

Korea Meteorological Administration,

Seoul, 156-720, Korea

**Abstract** - High frequency ( $\nu > 100$  GHz) observations from AMSU-B during the March 5-6, 2001 New England blizzard are used to investigate the detection of snowfall over land. The AMSU-B data are compared to NEXRAD reflectivities. The radiative effects of a snow model are compared with observations. Low altitude water vapor is shown to obscure emission from the underlying ground at high frequencies, but at high altitudes water vapor also reduces the impact of scattering by snow particles.

## 1. INTRODUCTION

Although most global precipitation occurs as rainfall, snowfall plays a significant role in the extra-tropical hydrological cycle. Snow serves as a reservoir of water that can be released later in the year to support agriculture and hydroelectric activities. Beside the economic and recreational value of snow, snow storms can be hazardous for transportation and other economic activities. One of the important challenges for future satellites is to detect these snow storms from space.

Because snow accumulation on land affects the emission properties of the surface, the measurement of snowfall within the atmosphere has been difficult with radiometers that operate at frequencies less than 100 GHz. Water vapor absorption at frequencies greater than 100 GHz can screen the emission from snow covered surfaces. The Advanced Microwave Sounding Units (AMSU-B) radiometers on the NOAA 15 and 16 spacecraft [1] provide observations at 89, 150 and  $183 \pm 1, \pm 3, \pm 7$  GHz. This study will demonstrate that radiation at those higher frequencies can be used to measure snowfall over land because water vapor screening obscures the underlying snow-covered surface.

The AMSU-B radiometer on NOAA-15 initially encountered radio frequency interference from on-board transmitters that were ultimately shut down in the autumn of 1999. Modifications were implemented on the NOAA-16 AMSU-B so that reliable spaceborne data at frequencies greater 100 GHz were available by the winter of 2000-01.

## 2. CASE STUDY

The Nor'easter of March 5-6, 2001 presented a unique opportunity to observe intense snowfall over land with the NOAA-16 AMSU-B. That blizzard was one of the more in-

tense snow storms of the season, depositing on the order of 50 cm of snow on much of VT, NH and northeastern NY with several stations reporting deposits of 75 cm. Wet snow and sleet were reported along the New England coast, but the mean temperatures encountered in NH and VT remained around  $-5$  C, and reported maxima were only  $-2$  C, so that melting could be disregarded over inland regions throughout the entire day.

Fig. 1 shows a composite of the National Weather Service (NWS) operational weather radar reflectivity,  $Z_{\text{eff}}$  (dBZ) obtained over the Northeastern U.S. on March 5, 2001 at 23:00 UTC. The snowfall was greatest over CT, MA, VT, and NH. Although the NWS operational radar data have well known limitations, in the absence of a preplanned field observation campaign, they provide readily available data to compare to snowfall derived from microwave brightness temperatures.

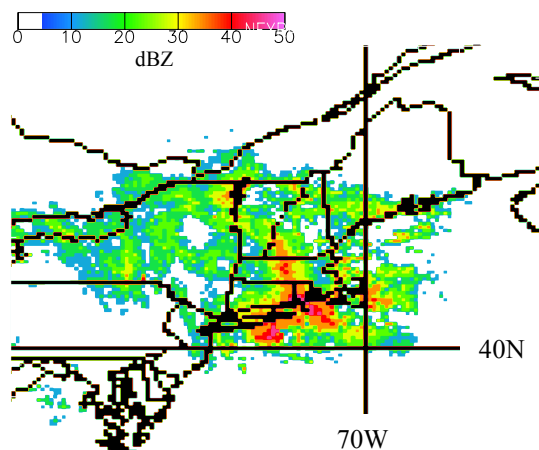


Figure 1: NWS NEXRAD reflectivities for March 5, 2001 2300 UTC.

## 4. SUMMARY

In summary, the NEXRAD and AMSU-B 150 and 183 GHz channels were found to be qualitatively related to the coincident NEXRAD radar data. Furthermore, an appropriate snow particle model was found to match attenuation measurements of snow and the issues surrounding surface emissivity were addressed. A process is underway to more fully characterize the relationships between the higher frequency brightness temperatures and the snow in the cloud profile.



# **Report to NASA on a Workshop on Sea Ice Data Assimilation**

Held at the

**Naval Academy,  
Annapolis, MD**

On

**July 23-24, 2002**

Report Edited by  
Kim Partington, Ronald Lindsay, Jinro Ukita

September 2002

## 9.7 Representation of Antarctic Coastal Polynyas in Ocean Climate Models: A Justification for Assimilation of Ice Concentration?

Achim Stoessel

Department of Oceanography  
Texas A&M University, College Station

Thorsten Markus

NASA Goddard Space Flight Center  
Greenbelt, Maryland

### Abstract

The representation of Antarctic coastal polynyas in global ocean general circulation models (OGCMs) have a profound impact on long-term deep-ocean properties. Compared to maximum ranges in magnitude of ambient conditions such as wind velocity and air temperature, the extent of coastal polynyas play the most decisive role in determining the rate of Antarctic Bottom Water formation, through the process of sea-ice formation, brine release, and formation of High Salinity Shelf Water. This study investigates the local, regional and high-frequency behaviour of the model representation of coastal polynyas with the aid of daily ice concentration derived from satellite passive microwave data using the "NASA Team 2" algorithm. Large regional and temporal discrepancies arise that are primarily related to the type of convection parameterization used in the model. Arguing that the empirical "thermodynamic lead closing" parameter is the weakest part in the sea-ice component of the OGCM, ice is being redistributed within a model grid cell by assimilating NT2 ice concentration. This measure yields potentially more reliable estimates on the impact of critical high-latitude processes on long-term deep-ocean properties. On the other hand, there are still various issues to be solved, e.g. whether the presented assimilation strategy is useful for the entire ice pack, how to properly deal with coastline mismatch between data and model, and how much assimilation of daily data interferes with daily winds that drive the sea-ice model. Besides the assimilation, this paper has revealed major short-time scale discrepancies between modelled and satellite-derived ice concentration, suggesting that much work is still needed to improve subgrid-scale high-latitude processes in global OGCMs.

# **Report to NASA on a Workshop on Sea Ice Data Assimilation**

Held at the

**Naval Academy,  
Annapolis, MD**

On

**July 23-24, 2002**

Report Edited by  
Kim Partington, Ronald Lindsay, Jinro Ukita

September 2002

## 9.8 Spatial and Temporal Characteristics of Arctic Sea-ice Deformation and its Implication in Data Assimilation

Jinro Ukita, Antony Liu, and Yunhe Zhao

NASA-Goddard Flight Space Center  
Code 971  
Greenbelt, MD 20771

On interannual to decadal timescales atmospheric circulation exhibits strong modal structures, in which coherent and recursive patterns such as ones defined by NAO and AO emerge. These modes and their associated phases have Arctic manifestations as evidenced by different modes in ice motion. Given this background questions arise as to how these variations in ice motion lead to varying modes of ice deformation, how these modes in deformation modify the way in which sea ice mass is redistributed, how this is compared to possible influence on the mass balance by other oceanic and thermodynamic processes, e.g. more oceanic heat flux, higher air temperature, or more snow precipitation etc., and how this ultimately modifies the sea ice mass balance and eventually the regional freshwater balance. These questions can be more effectively answered through an optimal use of model outputs and data – data assimilation. The first and important step in this effort is to make a critical assessment on data so as to identify relevant spatial and temporal scales for assimilation analysis.

The process most directly responsible for the redistribution of sea-ice mass is uniaxial closing (contraction), e.g. a ice flow against the coast. Yet it is a rare class of events as on the average Arctic ice motion is close to being non-divergent. This requires a careful analysis on how to extract information characterizing this process. Our results based on merged ice motion data constructed from satellite and buoy observations indicate that the relevant timescale for this process likely falls in the range of month to season. Over this temporal scale the emerged spatial pattern on the frequency of uniaxial-contraction events resembles to observed and simulated patterns in ice thickness. These results suggest that within this framework roughly speaking daily to synoptic timescale is a required temporal resolution for assimilation analysis to be both valid and meaningful. They also suggest an effectiveness of a 100 km resolution.

On the basis of this assessment work is under way to construct a simple forward and adjoint ice dynamic model.

# 2002 IEEE International Geoscience and Remote Sensing Symposium and the 24<sup>th</sup> Canadian Symposium on Remote Sensing



REMOTE SENSING:  
Integrating Our  
View of the Planet



June 24-28, 2002  
Toronto Canada

# IGARSS 2002



# Rain Rate Measurement with an Airborne Scanning Radar Altimeter

E. J. Walsh\*, C. W. Wright, D. Vandemark, L. F. Bliven  
NASA/GSFC/Wallops Flight Facility, Wallops Island, VA 23337

E. Uhlhorn, P. G. Black, F. D. Marks, Jr.  
NOAA/AOML/Hurricane Research Division, Miami, FL 33149-1097

## I. INTRODUCTION

The NASA Scanning Radar Altimeter (SRA) sweeps a radar beam of  $1^\circ$  half-power width (two-way) across the aircraft ground track within  $\pm 22^\circ$  of nadir, simultaneously measuring the backscattered power at its 36 GHz (8.3 mm) operating frequency and the range to the sea surface at 64 points spaced across the swath at  $0.7^\circ$  incidence angle intervals. The measurement geometry is shown in Fig. 1 with the specific numbers referring to the flights made into Hurricane Humberto on 23 and 24 September 2001, aboard a WP-3D hurricane research aircraft of the NOAA Aircraft Operations Center. The ranges produce raster lines of sea surface topography at a 10 Hz rate. The SRA was primarily designed to produce sea surface directional wave spectra, but the backscattered power measurements can be used to determine path integrated rain rate below the aircraft.

## II. HURRICANE HUMBERTO

Hurricane Humberto strengthened to Category 2 during the first flight, then diminished to Category 1 for the second flight. The SRA aircraft flight pattern, shown in Fig. 2 for 24 September 2001, was the same on both days. It featured three radial passes through the eye, connected by downwind legs, and was coordinated with three other aircraft in the Coordinated Observations of Vortex Evolution and Structure (COVES) experiment.

The surface wind speed measured by the NOAA AOML Hurricane Research Division (HRD) Stepped Frequency Microwave Radiometer (SFMR) along the flight track is shown in top panel of Fig. 3. The closest approach to the center of the eye on the three radial passes is indicated by the wind speed minimums at 2124 and 2254 UTC on 24 September and 0032 UTC on 25 September 2001. Rain rate measured by the SFMR along the aircraft ground track is shown in the bottom panel.

## III. SRA RAIN MEASUREMENT TECHNIQUE

Calculations based on the Marshall-Palmer distribution indicate that the attenuation (dB/km) of a 36 GHz radar signal is approximately linearly related to rain rate [1]. At 1.8 km height, the SRA signal suffers a 1 dB attenuation for each mm/hr of rain rate. If the sea surface radar backscatter coefficient is constant as one transitions into a region of rain, the loss of signal will determine the rain rate to an accuracy of a fraction of a mm/hr. In general, changes in the backscatter coefficient at nadir are small compared to the rain absorption in the hurricane high wind

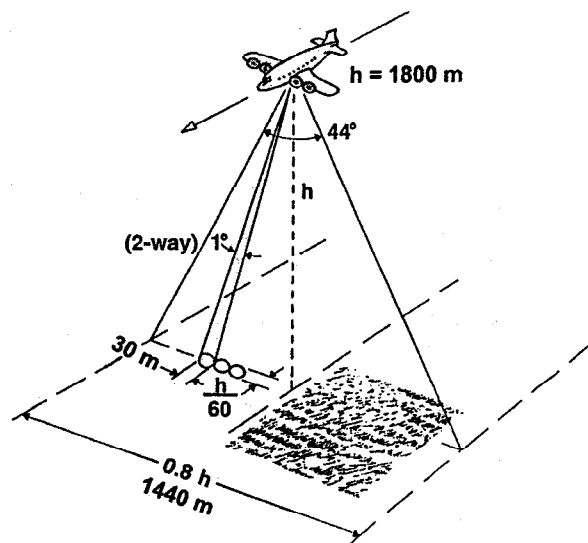


Fig. 1. Scanning Radar Altimeter measurement geometry.

environment and can be differentiated from changes in rain absorption by examining the variation of backscattered power with incidence angle.

Figure 4 shows the variation of the backscattered power at (a)  $37.43^\circ\text{N}$ ,  $66.69^\circ\text{W}$ , near the beginning of the southeast pass through the eye, and at (b)  $37.04^\circ\text{N}$ ,  $65.71^\circ\text{W}$ . The first observation was during a SFMR data gap, but the SRA data

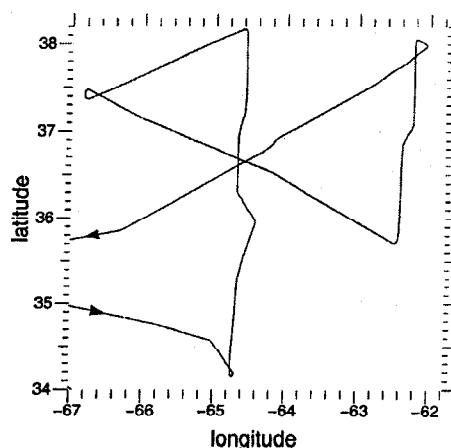


Fig. 2. NOAA aircraft flight track on 24 September 2001.

\*presently on assignment at NOAA Environmental Technology Laboratory, 325 Broadway, Boulder, CO 80305-3328.

**NASA/TM-2002-210005**

## **SIMBIOS Project 2001 Annual Report**

Giulietta S. Fargion, Science Applications International Corporation, Maryland  
Charles R. McClain, Goddard Space Flight Center, Greenbelt, Maryland

National Aeronautics and  
Space Administration

**Goddard Space Flight Center**  
Greenbelt, Maryland 20771

March 2002

## Chapter 20

# Assessment, Validation, and Refinement of the Atmospheric Correction Algorithm for the Ocean Color Sensors

Menghua Wang

*University of Maryland, Baltimore County, Baltimore, Maryland*

### 20.1 INTRODUCTION

The primary focus of this proposed research is for the *atmospheric correction algorithms evaluation and development and satellite sensor calibration and characterization*. It is well known that the atmospheric correction, which removes more than 90% of sensor-measured signals contributed from atmosphere in the visible, is the key procedure in the ocean color remote sensing (Gordon and Wang, 1994). The accuracy and effectiveness of the atmospheric correction directly affect the remotely retrieved ocean bio-optical products. On the other hand, for ocean color remote sensing, in order to obtain the required accuracy in the derived water-leaving signals from satellite measurements, an on-orbit vicarious calibration of the whole system, i.e., sensor and algorithms, is necessary. In addition, it is important to address issues of (i) cross-calibration of two or more sensors and (ii) in-orbit vicarious calibration of the sensor-atmosphere system. The goal of these researches is to develop methods for meaningful comparison and possible merging of data products from multiple ocean color missions. With support and collaboration from the SIMBIOS project office, much efforts have been on studying and comparing the ocean color data derived from the Japanese Ocean Color and Temperature Scanner (OCTS) and the French Polarization and Directionality of the Earth's Reflectances (POLDER). OCTS and POLDER were both on board Japan's Sun-synchronous Advanced Earth Observing Satellite (ADEOS) from August 1996 to June 1997, collecting about 10 months of global ocean color data.

This provides a unique opportunity for developing methods and strategies for the merging of ocean color data from multiple ocean color sensors. In this report, I will very briefly discuss other research activities, but mainly focus on describe collective efforts (with SIMBIOS project office) in the OCTS and POLDER comparison study.

### 20.2 RESEARCH ACTIVITIES

- (a) Studies have been carried out to understand various effects on the performance of the SeaWiFS atmospheric correction algorithm for the ocean color and atmospheric aerosols: (i) the solar and viewing geometry effects, in particular, for cases of the large solar and viewing zenith angles; (ii) the Earth curvature effects, i.e., the spherical-shell atmosphere (SSA) vs. the plane-parallel atmosphere (PPA) (Ding and Gordon, 1994); (iii) effects of the sun glint contaminations on the derived SeaWiFS ocean and atmospheric products (Wang and Bailey, 2001); (iv) the effects of ocean surface wind speed on the SeaWiFS derived aerosol optical thickness; and (v) the effects of polarization in the aerosol lookup tables on the SeaWiFS derived ocean color and atmosphere products. These research works (except item (iii)) are still on going. Some preliminary results, however, show importance and necessary to account for some of these effects.
- (b) I have been working on activities for the International Ocean-Color Coordinating Group (IOCCG) atmospheric correction working group. The main objective of the working group is to quantify the performance of the various exiting atmospheric correction algorithms used for the various ocean color missions. Therefore, the derived ocean color products from various ocean color missions can be meaningfully compared and possibly merged. As the atmospheric correction is a key procedure in the ocean color remote sensing, we want to answer question such as how can derived ocean color products from one sensor be best compared with those from others. We want to quantify the differences among the performance of the atmospheric correction algorithms. The core working group members are from OCTS/GLI (Japan), SeaWiFS (US), MODIS (US), POLDER (France), and MERIS (Europe). I am currently serving as the working group leader.
- (c) In collaboration with A. Isaacman, B. Franz, and C. McClain and the SIMBIOS project office, we have studied and compared the ocean color data derived the OCTS and POLDER.

# **The SeaWiFS Bio-Optical Archive and Storage System (SeaBASS): Current Architecture and Implementation**

## *Editors*

Giulietta S. Fargion, Science Applications International Corporation, Beltsville, Maryland  
Charles R. McClain, Goddard Space Flight Center, Greenbelt, Maryland

## *Authors*

P. Jeremy Werdell, Science System and Applications Inc., Lanham, Maryland  
Sean W. Bailey, Futuretech Corporation, Greenbelt, Maryland

National Aeronautics and  
Space Administration

**Goddard Space Flight Center**  
Greenbelt, Maryland 20771

September 2002

## Chapter 1

### Introduction

#### 1.1 Motivation and Philosophy

Experiences with past and present satellite ocean color missions, such as the Coastal Zone Color Scanner (CZCS) and Sea-viewing Wide Field-of-view Sensor (SeaWiFS), demonstrate the need for high quality *in situ* measurements for bio-optical algorithm development and satellite data product validation (Gordon et al. 1983, Evans and Gordon 1994, McClain et al. 1998, Hooker and McClain 2000). The National Aeronautics and Space Administration (NASA) SeaWiFS Project, for example, is tasked with producing normalized water-leaving radiances with an absolute accuracy of 5% (Hooker and Esaias 1993), which requires comparative, globally distributed *in situ* radiometric measurements with accuracy finer than 5%. The advent of additional missions, such as the Moderate Resolution Imaging Spectroradiometer (MODIS) and the Medium Resolution Imaging Spectrometer (MERIS), and the approach of future missions, including the Global Imager (GLI) and the second Polarization and Directionality of the Earth's Reflectances (POLDER-2) instrument, further underline the need for accurate, temporally and geographically diverse samples of oceanographic and atmospheric data.

Historically, the amount of data suitable for algorithm development and satellite validation activities has been limited due to a paucity of simultaneous observations and the difficulty associated with obtaining globally distributed sampling (O'Reilly et al. 1998, Bailey et al. 2000). With regards to the latter, spatial biases are often undesirable for satellite missions with continuous global coverage. Due to their required accuracy, these data are additionally limited by biases introduced by varying measurement and data processing techniques (Hooker and Maritorena 2000, Hooker et al. 2001). As such, global, high quality, *in situ* data

sets are invaluable and prerequisite to advance the field of ocean color.

To facilitate the assembly of a global bio-optical data set, the SeaWiFS Project developed the SeaWiFS Bio-optical Archive and Storage System (SeaBASS), a local repository for *in situ* radiometric and phytoplankton pigment data used regularly in their scientific analyses (Hooker et al. 1994). The system has since been expanded to contain oceanographic and atmospheric data sets collected by the NASA Sensor Intercomparison and Merger for Interdisciplinary Biological and Oceanic Studies (SIMBIOS) Project (McClain et al. 2002), as part of NASA Research Announcements (NRA) NRA-96-MTPE-04 and NRA-99-OES-99, which has aided considerably in minimizing spatial bias and maximizing data acquisition rates (McClain and Fargion 1999a and 1999b, Fargion and McClain 2001 and 2002). The SeaWiFS and SIMBIOS Project Offices (SPO) currently share responsibility for the maintenance of SeaBASS, including all design modification and construction.

To develop consistency across multiple data contributors and institutions, the SPO has defined and documented a series of *in situ* data requirements and sampling strategies that ensure that any particular set of measurements will be acceptable for bio-optical and atmospheric correction algorithm development and ocean color sensor validation (Mueller and Austin 1995, Fargion et al. 2001, Mueller et al. 2002a and 2002b). In addition, the SPO has sponsored a series of round-robin activities to establish and advance the state of instrument calibration, protocols, and traceability to radiometric standards (Mueller 1993, Meister et al. 2002). Data prepared using these techniques are suitable for both verifying the radiometric precision and stability of satellite-borne ocean color sensors and validating the algorithms used to relate the radiances to other geophysical parameters.



# **NASA/TM-2002-210004/Rev3-Vol2**

**James L. Mueller<sup>1</sup> and Giulietta S. Fargion<sup>2</sup>**  
**Editors**

<sup>1</sup> *CHORS, San Diego State University, San Diego, California*

<sup>2</sup> *Science Applications International Corporation, Beltsville, Maryland*

## **Ocean Optics Protocols For Satellite Ocean Color Sensor Validation, Revision 3, Volume 2**

J. L. Mueller, C. Pietras, S. B. Hooker, D. K. Clark, A. Morel, R. Frouin, B.G. Mitchell,  
R. R. Bidigare, C. Trees, J. Werdell, G. S. Fargion, R. Arnone, R. W. Austin, S. Bailey,  
W. Broenkow, S. W. Brown, K. Carder, C. Davis, J. Dore, M. Feinholz, S. Flora, Z.P.  
Lee, B. Holben, B. C. Johnson, M. Kahru, D. M. Karl, Y. S Kim, K. D. Knobelspiesse, C.  
R. McClain, S. McLean, M. Miller, C. D. Mobley, J. Porter, R.G. Steward, M. Stramska,  
L. Van Heukelem, K. Voss, J. Wieland, M. A. Yarbrough and M. Yuen.

National Aeronautical and  
Space administration

**Goddard Space Flight Space Center**  
Greenbelt, Maryland 20771

**February 2002**

## Chapter 18

### SeaBASS Data Protocols and Policy

P. Jeremy Werdell<sup>1</sup>, Sean Bailey<sup>2</sup>, and Giulietta S. Fargion<sup>3</sup>

<sup>1</sup>*Science Systems and Applications Inc., Lanham, Maryland*

<sup>2</sup>*Futuretech Corporation, Greenbelt, Maryland*

<sup>3</sup>*Science Applications International Corporation, Beltsville, Maryland*

#### 18.1 INTRODUCTION

The SeaWiFS Project developed the SeaWiFS Bio-optical Archive and Storage System (SeaBASS) to be a local repository for *in situ* optical and pigment data products regularly used in a variety of scientific analyses. Information on the original SeaBASS design is provided in Hooker et al. (1994), and has since been expanded to contain data sets collected by participants of the SIMBIOS Project. A detailed description of the SeaBASS system is available via the World Wide Web:

<<http://seabass.gsfc.nasa.gov>>.

Both the SeaWiFS and SIMBIOS Projects use *in situ* bio-optical data for the validation of SeaWiFS and other satellite (e.g., OCTS and POLDER) data products, and for the development of new ocean color algorithms. In addition, SeaBASS supports international protocol workshops, data merger studies, and time-series studies. Archived data include measurements of water-leaving radiance, chlorophyll *a*, and other related optical and pigment parameters. When available, additional oceanographic and atmospheric data (given in Table 2.1) are also archived in SeaBASS. Data are collected by a number of different instrument packages, such as profilers, buoys, and above-water measurement devices, on a variety of platforms, including ships, moorings, and drifters. The contents of SeaBASS are made readily available to the SIMBIOS and MODIS Science Team Members, and to other approved individuals (e.g., members of other ocean color instrument teams, volunteer-contributing researchers, etc.) on a case-by-case basis. Access to the database and data archive is available to authorized users through the SeaBASS Web page.

As SIMBIOS US Science Team members are contractually obligated to provide data to SeaBASS, the volume of archived data is rapidly increasing (McClain and Fargion 1999a and 1999b). With the launch of MODIS, as well as a number of present and upcoming international missions (e.g., GLI, POLDER-2, MERIS, OCI, OCM, etc.), the use of the SeaBASS data archive is expected to increase dramatically as these missions begin to require validation data.

#### 18.2 SeaBASS DATA FORMAT

SeaBASS presently contains over 22,000 bio-optical data files, encompassing more than 650 separate experiments. In addition, its historical pigment database holds over 286,000 records of phytoplankton pigment data. To account for the continuous growth of the data archive, the Project believed it essential to develop efficient data ingestion and storage techniques. Such ingestion procedures and protocols were designed to be as straightforward and effortless as possible on the part of the contributing investigators, while still offering a useful format for internal analysis efforts. The Project considered the following to be the most important in the design of the system:

1. Simple data format, easily read and updated;
2. Global portability across multiple computer platforms; and
3. Web accessible data holdings.

# 2002 IEEE International Geoscience and Remote Sensing Symposium and the 24<sup>th</sup> Canadian Symposium on Remote Sensing



REMOTE SENSING:  
Integrating Our  
View of the Planet



June 24-28, 2002  
Toronto Canada

IGARSS  
2002

# Realtime Storm Surge Measurement with a Scanning Radar Altimeter

C. W. Wright, E. J. Walsh<sup>1</sup>, W. B. Krabill, D. Vandemark

NASA/Goddard Space Flight Center, Code 972, Wallops Flight Facility, Wallops Island, VA 23337

A. W. Garcia

U.S. Army Engineer Research and Development Center, 3909 Halls Ferry Road, Vicksburg, MS 39180-6199

P. G. Black, F. D. Marks, Jr.

NOAA/AOML/Hurricane Research Division, 4301 Rickenbacker Causeway, Miami, FL 33149-1097

R. A. Luetlich, Jr.

University of North Carolina at Chapel Hill, Institute of Marine Sciences, 3431 Arendell Street, Morehead City, NC 28557

<sup>1</sup>presently on assignment at NOAA Environmental Technology Laboratory, 325 Broadway, Boulder, CO 80305-3328

## I. INTRODUCTION

The NASA Scanning Radar Altimeter (SRA) was designed primarily to measure the energetic portion of the directional wave spectrum by generating a topographic map of the sea surface [1]. The SRA measurement geometry is shown in Fig. 1. The specific numbers refer to the Hurricane Bonnie landfall flight to be described shortly.

The SRA sweeps a radar beam of 1° (two-way) half-power width across the aircraft ground track over a swath equal to 0.8 of the aircraft height, simultaneously measuring the backscattered power at its 36 GHz (8.3 mm) operating frequency and the range to the sea surface at 64 positions at 0.7° incidence angle intervals. The maximum scan rate was 8 Hz during the Hurricane Bonnie flights, but it is presently 10 Hz. In realtime, the slant ranges are multiplied by the cosine of the off-nadir incidence angles (including the effect of aircraft roll attitude) to determine the vertical distances from the aircraft to the sea surface. These distances are subtracted from the aircraft height to produce a sea-surface elevation map which is displayed on a monitor in the aircraft to enable realtime assessments of data quality and wave properties.

On 24 August 1998, the SRA, aboard a NOAA hurricane research aircraft, provided the first documentation of the directional wave spectrum throughout a hurricane in open water when Hurricane Bonnie was about 400 km east of Abaco Island, Bahamas [2]. On 26 August 1998, the SRA provided the first documentation of the directional wave spectrum throughout a hurricane making landfall as Bonnie was approaching Wilmington, NC [3].

## II. SRA WAVE TOPOGRAPHY MEASUREMENTS

Figure 2 shows a gray-scale-coded topographic map produced from about 700 SRA scan lines as the aircraft crossed Cape Lookout (34.58°N, 76.53°W) during the landfall flight. The aircraft flight direction was from right to left in Fig. 3. The wave topography shows a dramatic spatial variation in the wave field with the waves propagating toward the northwest on the

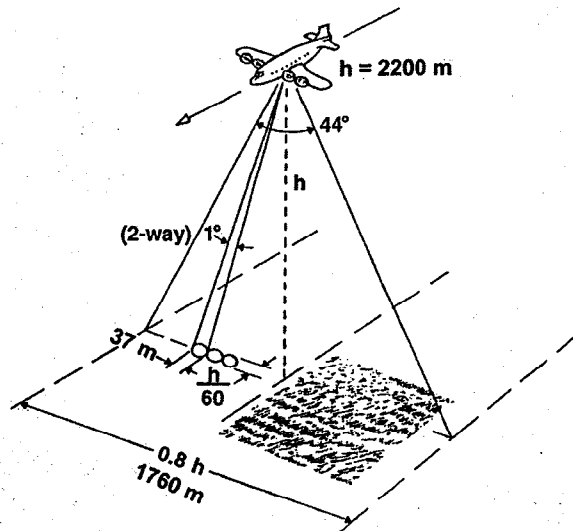


Fig. 1. Scanning Radar Altimeter measurement geometry.

east side of Cape Lookout, and toward the north on the west side.

Figure 3 shows five contiguous 10-km segments of SRA gray-scale coded topography on a different flight line as the NOAA aircraft headed north toward Cape Hatteras (35.27°N, 75.44°W). The waves were just starting to “feel” the ocean floor at the beginning of this data set, and the water depth decreased along the track. The waves were initially propagating toward about 335°. As the waves approached the shore, the wavelength shortened, the amplitude decreased, and the propagation direction turned toward the north and finally northeast. The surf zone began at about 6.3 km up from the bottom of the right 10 km segment. The tip of Cape Hatteras is apparent at the top of the same segment.

All the analysis described so far does not require an absolute determination of the height of the aircraft. The swath is wide enough that each scan line can be processed independently and its mean elevation set to zero.

NASA Technical Memorandum 2002–206892, Volume 21

## SeaWiFS Postlaunch Technical Report Series

Stanford B. Hooker, Editor

*NASA Goddard Space Flight Center  
Greenbelt, Maryland*

Elaine R. Firestone, Senior Scientific Technical Editor

*Science Applications International Corporation  
Beltsville, Maryland*

## Volume 21, The Eighth SeaWiFS Intercalibration Round-Robin Experiment (SIRREX-8), September–December 2001

Giuseppe Zibordi

Davide D’Alimonte

Dirk van der Linde

Jean-François Berthon

*JRC/Institute for Environment and Sustainability  
Ispra, Italy*

Stanford B. Hooker

*NASA/Goddard Space Flight Center  
Greenbelt, Maryland*

James L. Mueller

*SDSU/Center for Hydro-Optics and Remote Sensing  
San Diego, California*

Gordana Lazin

Scott McLean

*Satlantic, Inc.  
Halifax, Canada*



## ABSTRACT

This report documents the scientific activities during the eighth SeaWiFS Intercalibration Round-Robin Experiment (SIRREX-8) held at the Center for Hydro-Optics and Remote Sensing (CHORS), the Joint Research Centre (JRC), and Satlantic, Inc. The objectives of SIRREX-8 were to a) quantify the uncertainties associated with measuring the immersion factor with a standard protocol, b) establish if instrument-to-instrument variability prevents the assignment of a set of immersion factors for an entire series of sensors, c) compare average immersion factors obtained from sample OCI-200 radiometers with those provided by Satlantic for the same series of instruments, and d) measure the cosine response of one sensor at CHORS and Satlantic. An overview of SIRREX-8 is given in Chapt. 1, the immersion factor methods used by the participating laboratories are presented in Chapt. 2–4, and the data processing code is documented in Chapt. 5. The cosine response methods and results are presented in Chapt. 6, along with an analysis of the data. A synthesis of the immersion factor results is presented in Chapt. 7 and includes a discussion and conclusion of the effort with respect to the objectives.

## Prologue

The purpose of the Sea-viewing Wide Field-of-view Sensor (SeaWiFS) Project at the National Aeronautics and Space Administration (NASA) Goddard Space Flight Center (GSFC) is to obtain valid ocean color data of the world ocean for a five-year period, to process that data in conjunction with ancillary data to meaningful biological parameters, and to make that data readily available to researchers (Hooker et al. 1992). The success of the SeaWiFS mission will be determined by the quality of the ocean color data set and its availability. The culmination of properly executing this responsibility is achieving a radiometric accuracy to within 5% absolute and 1% relative, water-leaving radiances to within 5% absolute, and chlorophyll *a* concentration to within 35% over a range of 0.05–50.0 mg m<sup>-3</sup> (Hooker and Esaias 1993).

The type and quality of supporting *in situ* optical measurements and analytical protocols for SeaWiFS calibration and validation were drafted at a SeaWiFS workshop in 1990. A central perspective of the workshop was that the significant expense of field work dictates *in situ* observations will accrue over several years from a variety of sources, using different instruments and approaches. These data must be internally consistent, of known and documented accuracy (but within SeaWiFS requirements), and in a form readily accessible for analysis by ocean color scientists. The findings and recommendations of the workshop were presented by Mueller and Austin (1992) and were immediately adopted as the SeaWiFS Ocean Optics Protocols (SOOP).

Although the immediate concerns of the SOOP were the SeaWiFS mission, the capabilities of other potential ocean color sensors were also recognized, with the intent of developing databases that are relevant to long-term future needs. The importance of the SOOP and the accuracy requirements contained therein is well recognized by the

broader scientific and commercial ocean color community, as evidenced by the considerable expansion of the original document to accommodate a broader range of measurements, techniques, and sampling considerations (Mueller and Austin 1995, Mueller 2000, and Mueller et al. 2001).

Ensuring the SeaWiFS calibration and validation field data sets are of uniform quality and have an uncertainty less than 5% requires a continuing commitment to quantifying the uncertainties associated with the spaceborne and *in situ* instrumentation. The uncertainties associated with the satellite sensor are not considered here, although it is important to remember that half of the total uncertainty budget is apportioned to the satellite sensor. Assuming the uncertainties combine in quadrature (the square root of the sum of the squares), the allowed uncertainty in the remote and *in situ* optical data is approximately 3.5% for each ( $\sqrt{5^2/2}$ ).

The sources of uncertainty for the ground truth part of the total uncertainty budget have a variety of sources:

1. The measurement protocols used in the field;
2. The environmental conditions encountered during data collection;
3. The absolute calibration of the field radiometers, which must also be traceable to the National Institute of Standards and Technology (NIST);
4. The conversion of the light signals to geophysical units in a data processing scheme; and
5. The stability of the radiometers in the harsh environment they are subjected to during transport and use.

The first step in the process of controlling uncertainties in field data was establishing and publishing the SOOP. The proper application of the SOOP also reduces any unnecessary contributions from environmental effects, but it does not completely remove them—as environmental conditions worsen, which may be unavoidable, uncertainties inexorably increase.

NASA Technical Memorandum 2002–206892, Volume 21

## SeaWiFS Postlaunch Technical Report Series

Stanford B. Hooker, Editor

*NASA Goddard Space Flight Center  
Greenbelt, Maryland*

Elaine R. Firestone, Senior Scientific Technical Editor

*Science Applications International Corporation  
Beltsville, Maryland*

## Volume 21, The Eighth SeaWiFS Intercalibration Round-Robin Experiment (SIRREX-8), September–December 2001

Giuseppe Zibordi

Davide D’Alimonte

Dirk van der Linde

Jean-François Berthon

*JRC/Institute for Environment and Sustainability  
Ispra, Italy*

Stanford B. Hooker

*NASA/Goddard Space Flight Center  
Greenbelt, Maryland*

James L. Mueller

*SDSU/Center for Hydro-Optics and Remote Sensing  
San Diego, California*

Gordana Lazin

Scott McLean

*Satlantic, Inc.  
Halifax, Canada*

---

## Chapter 7

---

### SIRREX-8 Results, Discussion, and Conclusions

GIUSEPPE ZIBORDI

DAVIDE D’ALIMONTE

*JRC/IES/Inland and Marine Waters*

*Ispira, Italy*

STANFORD B. HOOKER

*NASA/Goddard Space Flight Center*

*Greenbelt, Maryland*

JAMES L. MUELLER

*SDSU/Center for Hydro-Optics and Remote Sensing*

*San Diego, California*

SCOTT MCLEAN

GORDANA LAZIN

*Satlantic, Inc.*

*Halifax, Canada*

#### ABSTRACT

The SIRREX-8 experiment for comparing immersion factors involved nine OCI-200 sensors which were all characterized at three different facilities—CHORS, JRC, and Satlantic—using similar laboratory protocols. One of the radiometers,  $E_u$  S/N 130, was selected as a so-called *reference* sensor and was measured more frequently than the other eight. The analysis of the SIRREX-8 data showed intralaboratory measurement uncertainties, evaluated through multiple characterizations of the reference radiometer and defined by two standard deviations, ranging from 0.28% for Satlantic, and up to 0.49% and 0.60% for JRC and CHORS, respectively. Interlaboratory uncertainties, evaluated with data from the nine common radiometers, showed average UPDs lower than  $\pm 0.6\%$ . The analysis of  $I_f(\lambda)$  variability across radiometers of the same series showed average values of approximately 2%, with maximum values of up to 5%, for all three laboratories. Typical  $I_f(\lambda)$  values for the OCI-200 series of radiometers were produced with  $I_f(\lambda)$  data from measurements taken from the three laboratories.

---

## 7.1 INTRODUCTION

The data collected at the three laboratories involved in the SIRREX-8 immersion coefficient intercomparison experiment were analyzed (after quality assurance) to investigate the following:

1. Intralaboratory uncertainties derived from the multiple measurements of the reference radiometer, and
2. Interlaboratory uncertainties derived from the common set of nine radiometers.

Additional objectives of the data analysis were: a) determining the average immersion factors; b) quantifying the variability across the OCI-200 series of radiometers (widely used in ocean color calibration and validation activities); and c) proposing a set of so-called *typical* spectral values for the considered series of radiometers.

## 7.2 THE DATA SET

The SIRREX-8 data set included the measurements made at CHORS, JRC, and Satlantic for nine OCI-200 radiometers. The methods used at each laboratory followed the protocol described in Mueller and Austin (1995) for the characterization of immersion factors, although there were differences between the published and practiced procedures. Table 12 presents the number of measurement sequences included in the data set. Filtering of measurement sequences affected by perturbations, like poor water quality or radiometer-to-source misalignment, was implemented in near-real time just after each measurement sequence by processing the data with the code described in Chapt. 5. One quality-assured measurement sequence per instrument per laboratory was considered acceptable for comparing data among the three different laboratories.

NASA Technical Memorandum 2002–206892, Volume 21

## SeaWiFS Postlaunch Technical Report Series

Stanford B. Hooker, Editor

*NASA Goddard Space Flight Center  
Greenbelt, Maryland*

Elaine R. Firestone, Senior Scientific Technical Editor

*Science Applications International Corporation  
Beltsville, Maryland*

## Volume 21, The Eighth SeaWiFS Intercalibration Round-Robin Experiment (SIRREX-8), September–December 2001

Giuseppe Zibordi

Davide D’Alimonte

Dirk van der Linde

Jean-François Berthon

*JRC/Institute for Environment and Sustainability  
Ispra, Italy*

Stanford B. Hooker

*NASA/Goddard Space Flight Center  
Greenbelt, Maryland*

James L. Mueller

*SDSU/Center for Hydro-Optics and Remote Sensing  
San Diego, California*

Gordana Lazin

Scott McLean

*Satlantic, Inc.  
Halifax, Canada*

---

## Chapter 6

---

### Cosine Response Measurements

GIUSEPPE ZIBORDI

*JRC/IES/Inland and Marine Waters Unit  
Ispra, Italy*

STANFORD B. HOOKER

*NASA/Goddard Space Flight Center  
Greenbelt, Maryland*

JAMES L. MUELLER

*SDSU/Center for Hydro-Optics and Remote Sensing  
San Diego, California*

SCOTT MCLEAN

*GORDANA LAZIN  
Satlantic, Inc.  
Halifax, Canada*

#### ABSTRACT

In addition to the immersion factor characterizations, the cosine response was measured for one irradiance sensor at CHORS and Satlantic (motivated by some preliminary measurements at the JRC). The angular response of an OCI-200 in-water radiometer was characterized by CHORS and by Satlantic using a similar methodology, although the former relied on a point source with a horizontal rotation of the sensor, and the latter relied on a collimated source and a vertical rotation. Results from the analysis of the data from Satlantic show deviations from the ideal cosine response for most of the collectors within, or very close to, the limits suggested by the SeaWiFS Ocean Optics Protocols (i.e., 2% between 0–65° and 10% above 65°). Results obtained from the analysis of the CHORS data show deviations from the ideal cosine response within the suggested limits for the OCI-200 central collector, but consistently higher deviations for the six collectors symmetrically located around the centermost one. The latter result is primarily explained by the use of different sources at the two laboratories (i.e., a lamp at CHORS and a lamp plus a collimator at Satlantic).

---

### 6.1 INTRODUCTION

The calibration of irradiance sensors takes place in air with light arriving normal to the plane of the cosine collector faceplate. To properly measure all irradiance arriving at the collector plane, the response should follow a cosine function, such that

$$E_{\theta} = E_0 \cos \theta, \quad (7)$$

where  $E_{\theta}$  is the measured irradiance in response to the light flux arriving at angle  $\theta$  with respect to the normal of the collector plane, and  $E_0$  is the measured irradiance the same light flux would produce if it were measured normal to the collector plane. Irradiance sensors have a field of view that extends over the hemisphere normal to the sensor faceplate, which is usually separated into two 90° halves, i.e., during a characterization,  $-90^{\circ} < \theta < +90^{\circ}$ .

If (7) is satisfied, an on-axis calibration can be used, and the device will correctly measure the irradiance arriving at the collector plane (regardless of the directional origin of the light). Of course, for an in-water sensor to correctly measure irradiance, there is the added requirement that the immersion factor must be correctly characterized. For in-water irradiance sensors, which were the only ones considered in SIRREX-8, the cosine response must be made with the radiometer under water.

### 6.2 PRELIMINARY INQUIRIES

A continuing philosophy of the entire SIRREX activity has been to incrementally investigate the sources of uncertainty in radiometric calibrations and measurements. The primary reason for this approach has been the difficulty of assembling the needed resources (personnel, equipment,